CAPITAL UNIVERSITY OF SCIENCE AND
TECHNOLOGY, ISLAMABAD

Experimental and Computational Analysis of Rooftop Solar PV Mounting Structure Subject to Wind Load

by

Arhaam Mubarak

A thesis submitted in partial fulfillment for the
degree of Master of Science

in the

Faculty of Engineering
Department of Mechanical Engineering

2023

This thesis is dedicated to the priceless assets of my life.

My Beloved Parents

My father, Dr. Mubarak Hussain Haider, my mother Ms. Asma Mubarak, and also my grandmother Naziran BiBi have not only been a source of motivation and inspiration for me but also bestowed my self-confidence and trust in Allah. My all hardships became opportunities for me due to their endless prayers, love, support, guidance, sacrifices, and encouragement to complete my thesis.

My Dearest Siblings

My sisters despite their busy schedules of study were always there with me through every daunting challenge. I will never forget their unprecedented help in the completion of my landmark achievement. A sincere gratitude to them for being my best supporters.

CERTIFICATE OF APPROVAL

Experimental and Computational Analysis of Rooftop Solar PV Mounting Structure Subject to Wind Load

by

Arhaaam Mubarak

(MME201002)

THESIS EXAMINING COMMITTEE

S. No.	Examiner	Name	Organization
(a)	External Examiner	Dr. Naseem Ahmad	IST, Islamabad
(b)	Internal Examiner	Dr. Muhammad Irfan	CUST, Islamabad
(c)	Supervisor	Prof. Mohammad Javed Hyder	CUST, Islamabad

Prof. Mohammad Javed Hyder
Thesis Supervisor
April, 2023

Dr. Muhammad Mahabat Khan
Head
Dept. of Mechanical Engineering
April, 2023

Dr. Imtiaz Ahmad Taj
Dean
Faculty of Engineering
April, 2023

Author's Declaration

I, **Arhaam Mubarak** hereby state that my MS thesis titled "**Experimental and Computational Analysis of Rooftop Solar PV Mounting Structure Subject to Wind Load**" is my own work and has not been submitted previously by me for taking any degree from Capital University of Science and Technology, Islamabad or anywhere else in the country/abroad.

At any time if my statement is found to be incorrect even after my graduation, the University has the right to withdraw my MS Degree.

(Arhaam Mubarak)
Registration No: MME201002

Plagiarism Undertaking

I solemnly declare that research work presented in this thesis titled "**Experimental and Computational Analysis of Rooftop Solar PV Mounting Structure Subject to Wind Load**" is solely my research work with no significant contribution from any other person. Small contribution/help wherever taken has been duly acknowledged and that complete thesis has been written by me.

I understand the zero tolerance policy of the HEC and Capital University of Science and Technology towards plagiarism. Therefore, I as an author of the above titled thesis declare that no portion of my thesis has been plagiarized and any material used as reference is properly referred/cited.

I undertake that if I am found guilty of any formal plagiarism in the above titled thesis even after award of MS Degree, the University reserves the right to withdraw/revoke my MS degree and that HEC and the University have the right to publish my name on the HEC/University website on which names of students are placed who submitted plagiarized work.

(Arhaam Mubarak)
Registration No: MME201002

Acknowledgement

All praises to Allah the Almighty, the most beneficial and the most Merciful for blessing me with good health, strength, peace of mind, and well-being and enable me to gain knowledge that is mandatory for the completion of my research work. I am honored to be the follower of our Last Messenger **Hazrat Muhammad (PBUH)** who is the sole reason behind the creation of this entire universe and whose way of living is the everlasting source of guidance, inspiration, and knowledge for the whole of humanity.

First and foremost, with great respect and sincerity, I would like to express my warmest gratitude to my honorable and highly qualified research supervisor **Prof. Dr. Mohammad Javed Hyder**, Professor in the Department of Mechanical Engineering of CUST for his scholarly guidance, generous support, continuous encouragement and his endless cooperation that helped me to carry out my research work. With his support and motivational encouragement, every challenge looked merely a small step that I jumped easily. It was he who extended all his technical expertise and assistance even in his leisure time to complete my work on time. His positive attitude, teaching style, eloquence, and enthusiasm left a strong impression on me, that will remain with me all my life.

I also wish to express my gratitude to **Prof. Dr. Muhammad Mahabat Khan** Head of the Department of Mechanical Engineering, Capital University of Science and Technology for his cooperation and for providing me with all the possible facilities which permitted me to follow my goals and complete my research work. His day-to-day regular inquiry asking about the progress of the thesis kept me juvenile and on track.

It would be an injustice to not pay thanks to the people of the workshop, laboratory, and computer lab who helped me when I needed support. The graduate office also guided me in the garnishing of the thesis in Latex and gratitude is extended to **Mr. Khalid Mahmood** and his team. My company's directors **Mr. Umer Yasin Raja** and **Mr. Ejaz Ahmed** deserve appreciation for sharing my workload and providing me ample time to complete my thesis. I again took this opportunity to pay my regards to my **beloved parents** who have always motivated me and prayed for my success and to my **siblings** for their continuous

support, love, and prayers that helped me to fulfill my dreams.

My hats off salute to **Mr. Ansar Mehmood**, CEO and **Mr. Farrukh**, Director of **ATS Engineering Sales and Services**, who contributed and installed all the setup of solar PV mounting structure, solar panels and the industrial centrifugal fan for proper experimentation in a shed.

I would like to give special thanks to all the faculty members, my colleagues, and my lab fellows for their kind and supportive behavior during my research and for making the lab environment learning and peaceful. To those who indirectly contributed to my research, your kindness means a lot to me.

(Arhaam Mubarak)

Abstract

There was a sudden increase in the usage of solar photovoltaics after the Government of Pakistan introduced the Net-Metering facility in 2015. As the usage of solar PV modules increases, the manufacturing of solar PV mounting structures has started on a large scale in different regions of Pakistan. During extreme weather conditions, it was observed that the solar PV mounting structure was greatly damaged. Therefore, the need arose for a thorough analysis of the solar PV mounting structure. In this work, experimental and computational methods were used to evaluate the effect of different wind velocities on solar PV mounting structures installed on flat roofs. The equivalent stress and total deformation of standard solar PV mounting structures installed on a large scale in Pakistan were studied. Usually, 14 gauge solar PV mounting structures are being installed on a large scale in Pakistan. Some installers often use 16 gauge solar PV mounting structures, so failure analysis of 14 and 16 gauge structures was studied. 14 gauge solar PV mounting structure deforms at 79 km/h wind velocity and fails at 110 km/h wind velocity. Meanwhile, a 16 gauge structure deforms at 75 km/h and fails at 100 km/h wind velocity. The 12 gauge structure deforms at 90 km/h wind velocity but does not fracture at 120 km/h wind velocity. However, the 14 and 16 gauge structures fail at less than 120 km/h wind velocity, which is the minimum required by the building code of Pakistan.

Keywords: Solar PV mounting structure, equivalent stress, total deformation

Contents

List of Figures

List of Tables

Abbreviations

ASCE	American Society of Civil Engineers
CFD	Computational Fluid Dynamics
FSI	Fluid–Structure Interaction
IEC	International Electrotechnical Commission
NDMA	National Disaster Management Authority
NEPRA	National Electric Power Regulatory Authority
MOHW	Ministry of Housing & Works
MS	Mild Steel
PV	Photovoltaic
RANS	Reynolds-Averaged Navier–Stokes

Symbols

kW	kilo Watt
kWh	kilo Watt Hour
k	turbulent kinetic energy
ω	specific rate of dissipation
MPa	Mega Pascal
mm	millimeter
y	y-axis centroid of C-channel in m
A	Area (m^2)
I	Moment of inertia (m^4)
w	Load (N/m)
M_x	Moment at x (Nm)
σ_{max}	Maximum stress (MPa)
y_{max}	Maximum deflection (mm)

Chapter 1

Introduction

Renewable energy sources, which are the most debatable sources of the current century, are derived from nature. The most commonly used natural resources are solar and wind power. Many theorists believe that after the use of solar and wind power, there will be a drastic decline in the depletion of fossil fuels. These sources, like sunlight and wind, are not only abundant but constantly replenishing [1]. The main natural renewable sources that are converted into energy are;

1. Photovoltaic or Solar
2. Wind source
3. Geothermal source
4. Hydropower source
5. Ocean source
6. Bio sources

Since this study is focused on solar energy, the main explanation will surround the solar energy-related discussion. Solar energy is rapidly transforming the energy world. Solar power harnesses the energy from the sun by converting it into usable energy. This energy can come in two forms: electricity and heat, which are captured using solar panels. These panels come in various sizes and designs, from

small residential rooftop panels to large-scale solar farms that take up multiple acres of land.

Humans have been utilising solar energy by using sunlight to ignite fire by directing sun rays onto a reflective material since the 7th century B.C. [2]. The Greeks and Romans in the 3rd century B.C. also used mirrors to direct the sun's rays to light torches for religious rituals. The photovoltaic cell evolution came after the research of a French physicist, Edmond Becquerel, who divulged the photovoltaic effect in 1839 at just 19 years of age. His discovery came after the metal electrode cells experiment to find the energy solution. He found that these cells generated more energy as they were directed towards the sun. This was the first known photovoltaic cell. The birth of PV technology occurred in 1954 after the robust research by Daryl Chapin, Calvin Fuller, and Gerald Pearson when they created the silicon PV cell in Bell Labs. This was the first solar cell able to effectively absorb and convert the sun's energy into power that could be used to operate everyday electrical equipment. Now most satellites, space stations, and spacecraft revolving around the earth are powered by solar energy [2].

1.1 Difference between Solar PV Panels and Solar Thermal Panels

The generation of electricity is from solar PV panels that convert the energy radiations from the sun, and heat comes from solar thermal panels. In both systems, the primary source of energy is the sun, but the technology used in each is distinct from one another. The generation of electricity through solar PV relies on the photovoltaic effect, where photons (the unit of light) collide with a semiconductor surface such as silicon, resulting in the release of an electron. On the other hand, solar thermal is a relatively simpler process that produces heat by contacting sunlight and heating water or other fluids. This is the reason that all thermal panels are placed on a rooftop towards the sun to heat water or fluid in the thermal tubes for domestic and commercial use. One other use of solar thermal is in power stations [3].

1.2 Solar Irradiance in Pakistan

As Pakistan's energy demands continue to increase, the development and efficient utilisation of renewable energy have become a crucial concern. This has prompted various national and multinational companies to devise and implement comprehensive plans for the conservation of energy and the optimal use of renewable energy sources, such as photovoltaic solar modules of varying sizes and wind turbines. Figure 1.1 shows the potential in different colours in different areas of Pakistan [4]. The red area is more susceptible to photovoltaic radiation as compared to the light blue. Solar panels in red-shaded cities will generate more power as compared to the cities in the light blue area shown in figure 1.1. Baluchistan province has the highest potential for photovoltaic power. Sindh also has great potential for photovoltaic power.

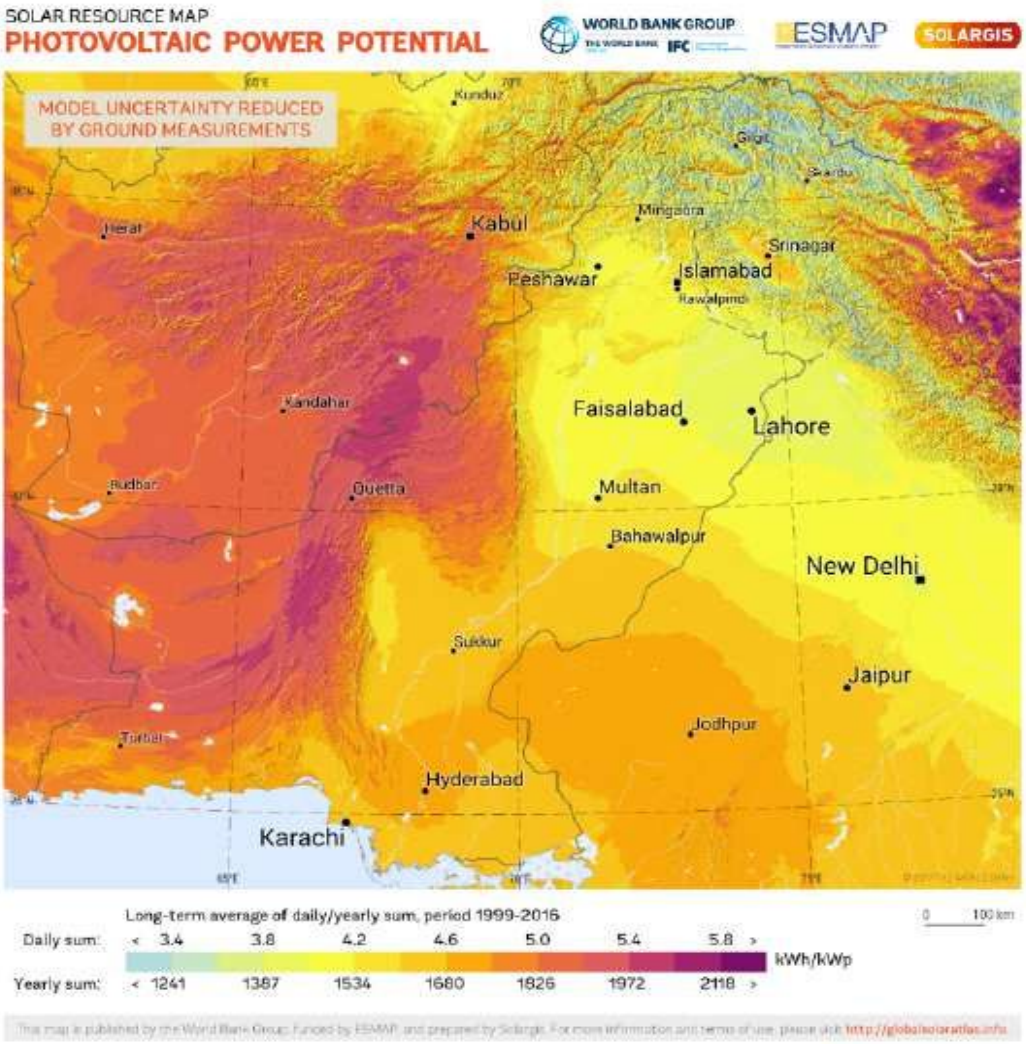

FIGURE 1.1: Photovoltaic Power Potential in Pakistan [5]

Figure 1.2 shows the global horizontal irradiation in Pakistan. The average calculation of the yield of one kW of solar panels depicts different kWh per kWp in different geographical areas of Pakistan. The more photovoltaic-induced area will yield more solar energy.

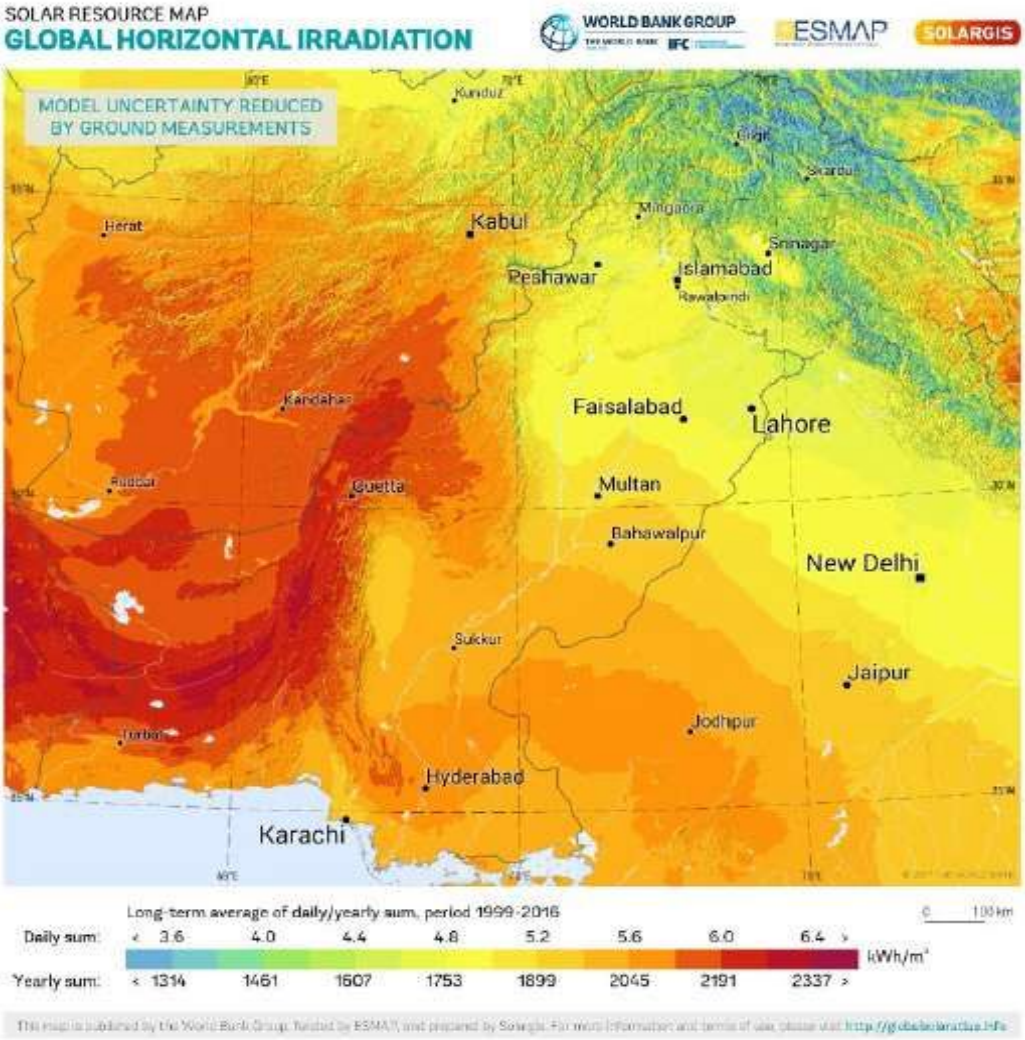

FIGURE 1.2: Global Horizontal Irradiation of Pakistan [6]

Figure 1.3 shows that the direct normal irradiance of the photovoltaic pattern is quite similar to the horizontal influx of photovoltaic irradiance. In a normal photovoltaic pattern, the solar energy yield is the same at high photovoltaic irradiance and is lower at low photovoltaic irradiance.

The study conducted by the US related to solar radiation in Pakistan depicts that a 1 kW solar system yields in one sunny day from 2 kWh to 6 kWh in different geographical areas in different seasons in Pakistan. The dark brown areas are under high photovoltaic irradiance, and the light yellow areas are under low photovoltaic

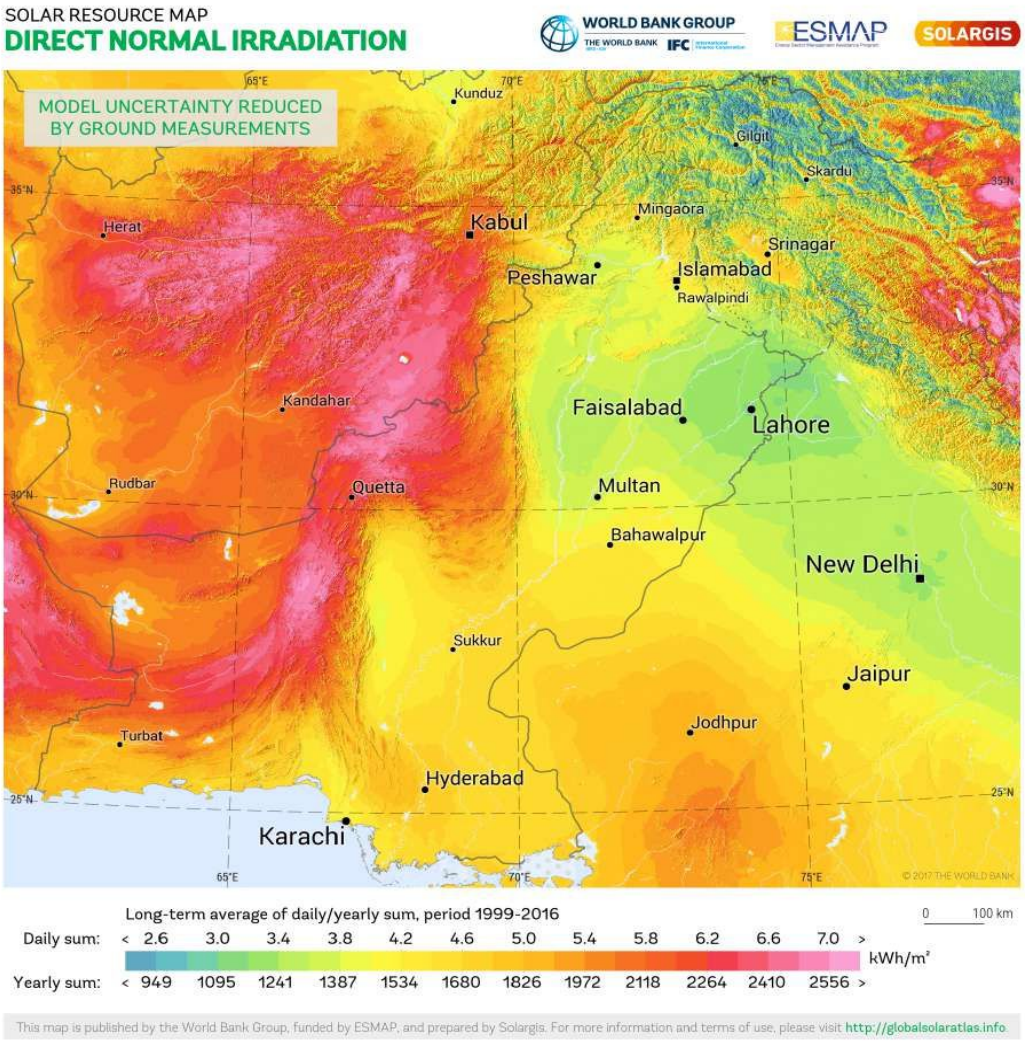

FIGURE 1.3: Direct Normal Irradiation of Pakistan [7]

irradiance. A month-by-month plot of solar radiation is depicted in figure 1.4. The graph in the figure shows that from April to July, the photovoltaic irradiance remains very high. There is also one reason for the duration of the daytime. Along with the increased irradiance, the duration of the day also increases.

1.3 Region-wise charts and plots

1.3.1 Northern Areas and Azad Kashmir

The graph in Figure 1.5 shows a similar pattern of photovoltaic radios as shown in the month-wise radiations in Pakistan. The graph shows that Gilgit has higher

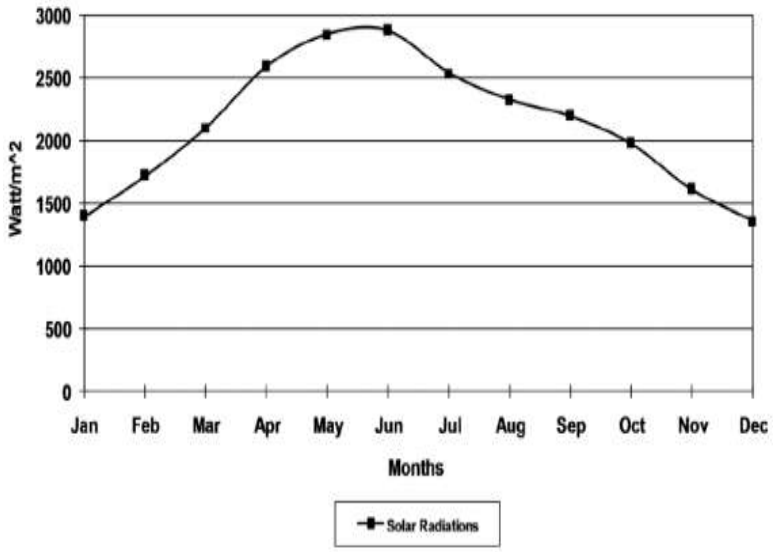

FIGURE 1.4: Average Annual Solar Radiation Intensity in Pakistan [4]

solar irradiation compared to other northern areas. Other areas have less solar radiation intensity, with a maximum of $300W/m^2$.

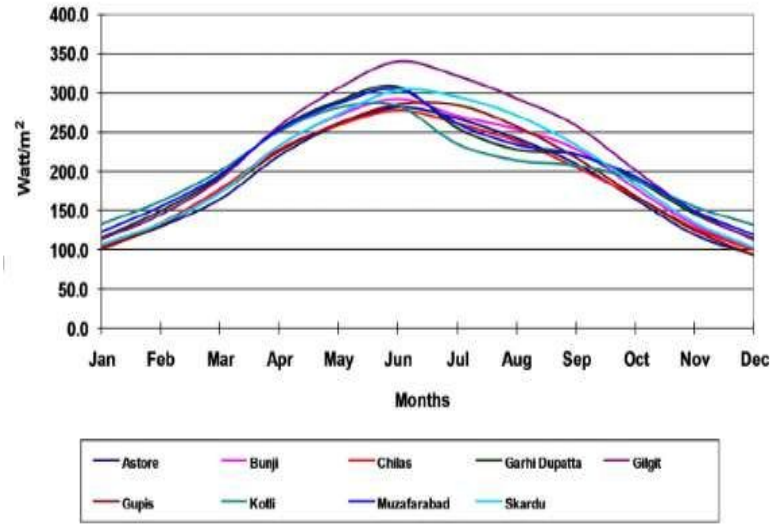

FIGURE 1.5: Solar Radiation Intensity (W/m^2) in Northern Areas and Azad Kashmir [4]

1.3.2 KPK Region

The graph in figure 1.6 shows that in KPK, the highest photovoltaic radiations are from April to July. The solar energy yield will be high from April to July. Cherat has minimal solar irradiation as compared to other cities. So, solar PV modules installed in the Cherat region will produce fewer units than solar PV modules installed in other cities in KPK.

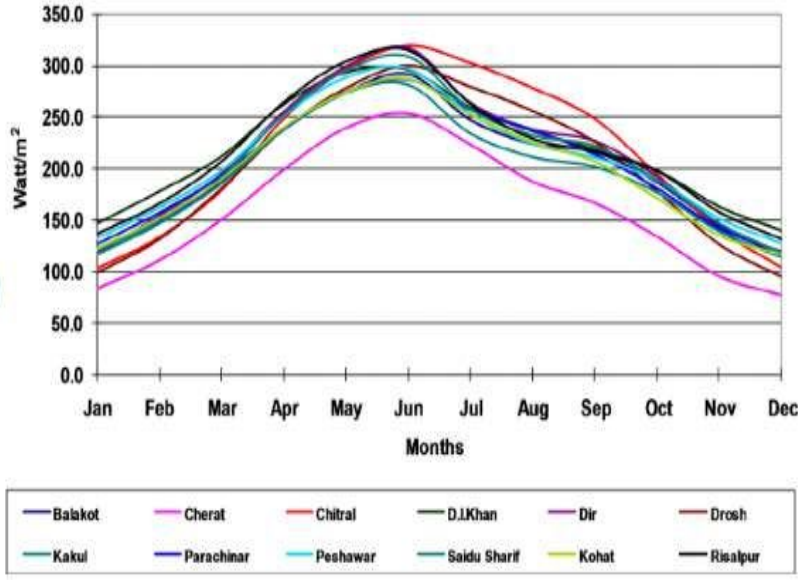

FIGURE 1.6: Solar Radiation Intensity (W/m^2) in KPK [4]

1.3.3 Punjab Region

The graph in Figure 1.7 shows a similar pattern of photovoltaic radios as shown in the month-wise radiations in Pakistan. Punjab is blessed with excess solar radiation. Solar PV modules can be installed in the south to harness solar radiation and convert it into useful energy. The weather in Punjab remains sunny for 300 days throughout the year. The solar radiation intensity is highest in the summer and lowest in the winter.

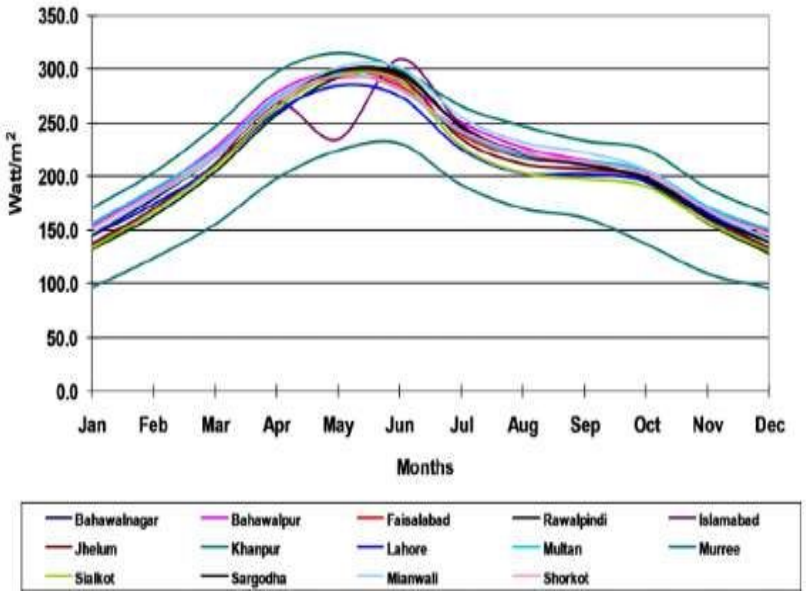

FIGURE 1.7: Solar Radiation Intensity (W/m^2) in Punjab [4]

1.3.4 Baluchistan Region

The graph in Figure 1.8 shows that in Baluchistan the solar yield is better than in KPK and Azad Kashmir. Baluchistan falls under the more intense irradiance of photovoltaic.

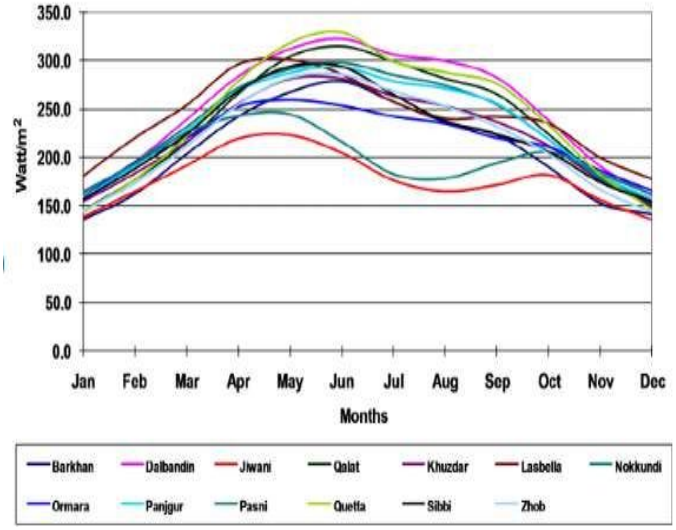

FIGURE 1.8: Solar Radiation Intensity (W/m^2) in Baluchistan [4]

1.3.5 Sindh Region

The graph in Figure 1.9 shows the solar yield in the province of Sind. Contrary to Baluchistan Province, the maximum solar yield is restricted to April and June [4].

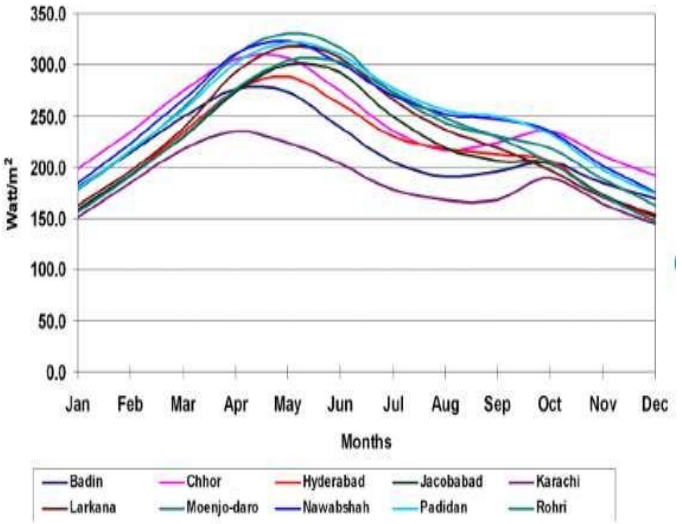

FIGURE 1.9: Solar Radiation Intensity (W/m^2) in Sindh [4]

1.4 Type of Mounting Structures

Mounting structures constitute 5% to 30% of the total cost of the solar system, depending on the type and design of the structure. The life of the 70% system depends upon the solar structure. If the solar structure is not appropriate and does not meet the requirements, the solar system will become gloomy. This study is about the solar structure and its robustness against the wind to ensure the life of the solar system. It is important to know first about the types of solar structures. There are four main types of solar PV mounting structures:

- Roof Mounted Racks
- Ground Mounted Racks
- Top-of-pole Mounted Racks & Side-of-pole Mounted Racks
- Tracking System Mounted Racks

1.4.1 Roof Mounted Racks

For the effective utilisation of solar energy, the distance between the solar array and battery bank or inverter should be kept to a minimum to reduce the wire run distance. However, this method requires the penetration of rowel bolts and drilling in the roof, which can lead to small crack leaks. Therefore, it is essential to ensure that the roof is properly sealed, as depicted in Figure 1.10.

FIGURE 1.10: Roof-Mounted Racks [8]

1.4.2 Pole Mounts

Figure 1.11 displays the pole mounts that are used to secure and install solar panels on the poles. The two types of pole structures—the top of the pole and the side of the pole—are commonly used in solar panel installation. Solar panels are used on top of the pole structure, many feet above the level of the ground. The side-of-pole mount attaches the solar panels to the side of the pole.

FIGURE 1.11: Pole Mount [8]

In top-of-pole fixed rack structures, poles are anchored in the ground and secured with concrete. This type of structure has the advantages of avoiding hooliganism, the filth of leaves, and snow accretion in the bottom. Due to its height, it is difficult to clean. Another option is side-of-pole, which is often used for solar photovoltaic systems with a small number of solar panels.

1.4.3 Tracking System Mount

A typical configuration of the tracking system-mounted type of panels is illustrated in Figure 1.12. Mostly, such structures are ideal for solar water pumping systems and where solar electricity is needed at an optimum level, which is achieved by tracking the sun's direction and adjusting the tracking mounting system accordingly. The tracking system may be embedded with an automatic or manual design and is good for hot regions. Axis and two-axis solar tracking systems are another

two types used to track the sun's radiation. The one-axis tracking structure moves only from east to west to capture the maximum sun radiation. In two-axis trackers, the trajectory of the sun from east to west with low and high tilt features adjusts the trackers for all seasons and gives optimum solar power. Their common use is with PV concentrator systems [8].

FIGURE 1.12: Solar Trackers installed in Dera Ghazi Khan, Punjab

Solar trackers are both manual and automatic and are designed to track the sun's movement throughout the day to generate maximum power from solar panels. This design compensates for the losses that occur in a fixed structure. These structures are expensive and can only be installed on grounds or in low-wind areas. Due to the daily tracking of movement, mechanical issues may arise, and maintenance and breakdown of the structure remain another serious concern.

1.4.4 Roof-Ground Mounts

Roof-ground mounts, also known as hybrid mounts or rooftop mounts, are similar in appearance to standard ground mounts but vary in design to sit on the roof. They have a little bit of an edge on the flush mount structure depending on the design and type of the roof, as shown in Figure 1.13. Solar generation can be optimised with its adjustable feature. In Pakistan, the majority of solar systems are installed with this type of structure.

FIGURE 1.13: Roof-Ground Mounts installed at different locations in Pakistan

It is important to study the structure, which is mostly used in Pakistan. In this study, the total deformation and equivalent stress of 14- and 16-gauge rooftop mounting structures are studied. Many accidents have already taken place due to the miscalculation of wind and structure designs in solar installations that have damaged the premises' financial health and human lives. The type of rooftop mounting structure designs are made from 2 panels to 14 panels and are denoted as L2 to L14 structures. The structures for rooftop mounting are also designed in an elevated or customised form. In customised rooftop structures, MS (Mild Steel) galvanised or powder-coated H-beams or pipes are used. In a customised structure, if the proper care of installation, fixing, and supporting is not taken, it becomes dangerous in the wind and flies or falls on any precious non-living or living entity. Special safety considerations are needed while fixing such a type of structure.

1.5 Types of Roof Mounts

1.5.1 Flush Mounts

A flush mount system is a type of solar panel mounting system that is designed to be installed flush with the roof surface. These systems are generally low-cost

and easy to install with framed solar panels. They typically feature metal clamps that clench the panels in place, resulting in a gap of 2–4 inches between the top and bottom of the panel. This permits an ample flow of air, which helps to keep the panels cool and efficient.

1.5.2 Ballasted Mounts

Ballasted mounts are a type of solar panel mounting system that uses weights to keep the panels in place, similar to flush mounts. This design can be cost-effective and time-saving, but it also presents the challenge of transporting and placing the weights on the roof, which can be another challenge for larger solar system installations. They do not require penetrating or drilling in the roof, making them fast and economical to install. This design gives a 20-degree tilt to the solar panel to face the sun for optimal yield. However, they also add additional weight to the roof, have a lower power density, and are not as well-suited for high-wind areas. Their utility is also limited when the surface of the roof is very high and in a sloped form.

1.5.3 Hybrid Mounts

Hybrid mounts, as the name suggests, are a mixture of flush and ballasted mounts. The hybrid structure is used when the roof does not support one type of structure. They are used with minimum penetration in the roof, attaching and adjusting the weight according to the type of roof design and strength. Although they are easy to install, they take up more roof space and become expensive for large installations.

1.6 Wind Velocity in Pakistan

1.6.1 Federal Capital

The maximum wind speed recorded ever in Pakistan was in the Islamabad-Rawalpindi region, where it was recorded at 104 mph (or 167 kph). On the other hand, the

extreme wind speed recorded in Islamabad is shown in table . The average wind speed in Islamabad is less than 12km/h. This speed is not devastating for the solar structure and solar panels. The wind from May to August occasionally crosses 100 km/h, and that can be devastating [9]. The metrological data from Islamabad and Rawalpindi depict that the wind speed remained at 167.5km/h. This speed is also a lethal speed for the solar structure.

TABLE 1.1: Extreme Wind data of Islamabad and Rawalpindi

Metrological Office Islamabad/Rawalpindi Wind Data Historical Events		
Station	**Highest Wind Speed (km/h)**	**Date**
Islamabad	167.5	13-10-2006
Rawalpindi	167.5	13-10-2006
https://rmcpunjab.pmd.gov.pk/P-historical.html		

1.6.2 Punjab Region

The metrological data of the Lahore office depicts that the wind speed exceeded its lethal limit in Lahore, Multan, and Faisalabad. Wind speeds greater than 120 km/h must be taken into serious consideration while designing the solar structure [10].

TABLE 1.2: Wind Velocities (km/h) in Punjab Region

Metrological Office Lahore Wind Data Historical Events		
Station	**Highest Wind Speed (km/h)**	**Date**
Lahore	146.5	02-6-2009
Multan	195	09-06-2005
Faisalabad	151	02-06-2000
https://rmcpunjab.pmd.gov.pk/P-historical.html		

1.7 Wind-Induced Damage to Rooftop Mounting Structure in Pakistan

Solar structures are more vulnerable to wind loads than any other factor. The wind load is simply the load that is exerted or flows on the premises or solar panels in a particular place. The wind-induced loads' proper pre-evaluation plays

a pivotal role in designing and fixing solar structures. The research shown by different researchers and innovative engineers has depicted the different results of the load on structures but could not conclude the exact structure compatible with the wind load. Serious wind-induced damage has been observed in many cases when the proper care of solar structure type, design, direction, and building codes were not taken into consideration. While evaluating the designs of different types of structures by researchers and engineers, the author of this research found that the poor designs of the structures were based on incorrect calculations and compromised the safety of the structure against wind due to opting for the easy and convenient method.

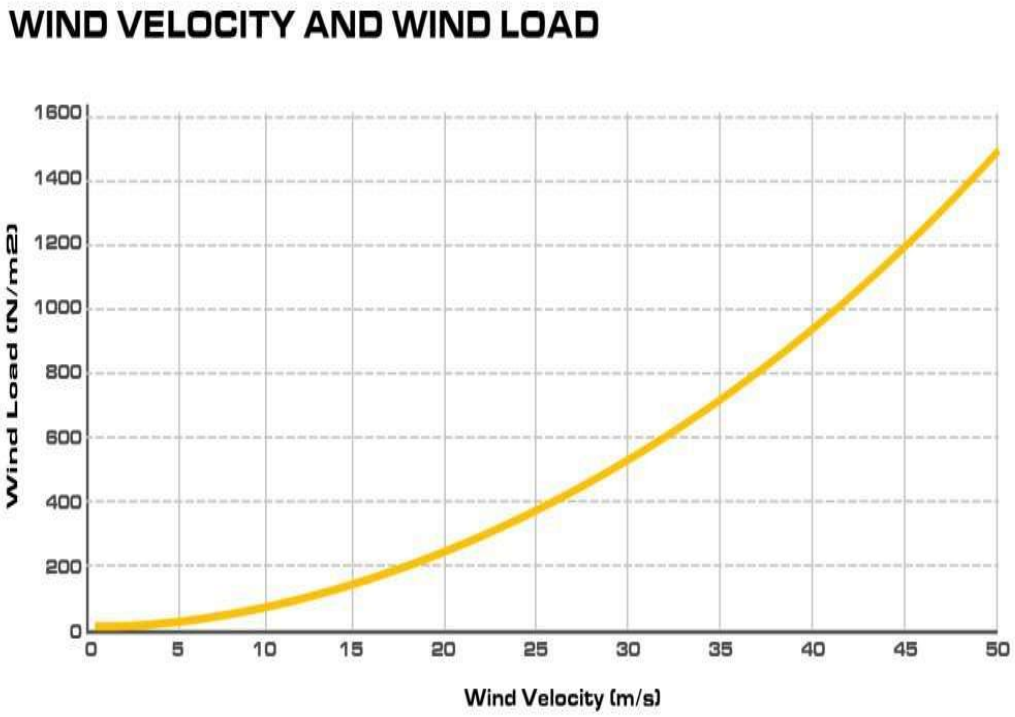

FIGURE 1.14: Relation of Wind Load (N/m^2) to Wind Velocity (m/s) [11]

Solar panels from manufacturers are rigorously tested to ensure the engineering robustness to withstand wind forces that bear pressure on the panel from the front and back and push up from the gap underneath the panel. The wind load rating of the PV panels is of paramount importance to determining the robustness of the panel to withstand the storm. The wind load that presents the wind speed is measured in pascals (N/m^2) and considered the unit of pressure measurement exerted by wind. Figure 1.14 shows the linear relationship between wind velocity and wind load; an increase in wind velocity increases the wind load, and vice versa.

The wind load increases to 1600 $N/m2$ when the velocity reaches 50 m/s [11].It depicts that the velocity of the wind cannot be ignored while designing the solar structure.

1.7.1 Protection of Solar Panels from the Wind

Knowing the wind conditions and direction can guide the installation of the panels to reduce wind exposure. Wind detectors to assess wind conditions will help. Moreover, wind deflectors, when installed properly, can add more wind downforce over the panels, reducing lift, cooling the panels down, and adding efficiency.

1.7.2 Wind-Induced Damage to Solar Mounting Structure in Pakistan

In the past few years, the world climate has changed due to the increased use of fossil fuels and air conditioning systems. The wind velocities of the different regions have increased, and the damage ratio of the structures has also increased. In 2021, at least 34 solar mounting structures were damaged in Islamabad and Rawalpindi. The mounting structures damaged the infrastructure of the building and damaged the objects wherever they fell. The issue was not raised and taken seriously because most of the damage was caused by the solar installation and fabrication companies. The following Figure 1.15, Figure 1.16 and Figure 1.17 show the damages to the solar structure and solar panels due to wind load created by wind velocity.

FIGURE 1.15: Damage caused on June 13, 2021, Bahria Enclave, Islamabad

FIGURE 1.16: Damages caused by Wind at Different Locations

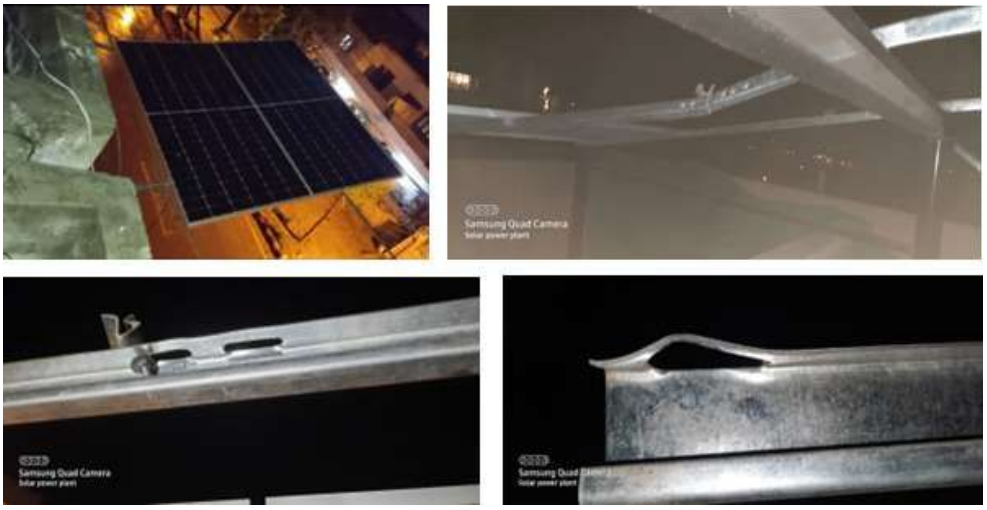

FIGURE 1.17: Wind Damage to an Elevated Solar Structure on June 13, 2021 in DHA Phase 2, Rawalpindi

1.8 Pakistan Solar Energy Scenario

1.8.1 Overview

Pakistan's energy sector, due to poor planning and extreme reliance, is facing many complex challenges, like costly fuel sources, dependence on imported energy commodities, acute shortages of natural gas, a big liability in the power sector, and ageing transmission and dispersion systems. These hindrances have kept the power sector away from growth and opted for modern techniques in energy infrastructure. The country has made some progress in addressing these issues with the help of U.S. and international assistance, but the future of Pakistan's energy

sector can only be saved from uncertainty and gloom with right-directed reforms. The National Electric Power Regulatory Authority (NEPRA) in its 2021 annual report showed the different sources of power generation in Pakistan. Currently, 39,772 MW, or is 63% of the total power generation, comes from fossil fuels [12]. Hydro contributes 25%, nuclear power plants 6.5% and only 5.4% is contributed by renewable energy. The government has a focus on renewable energy and has made some significant amendments to the 2019 Renewable Energy Policy. According to this renewable energy policy for 2019, 60% the country's requirements until 2030 would be fulfilled with renewable and hydropower generation. It clearly shows that this decade belongs to renewable energy and especially solar installations.

1.8.2 Solar Energy of Pakistan

Nearly a 700 MW increase in power demand is needed every year in Pakistan to mitigate the power crisis. Though different efforts are being made to increase power generation and snub the power blackouts in recent years. Additionally, the government has introduced support policies to foster the development of renewable energy, particularly solar power. The report published in the Pakistan Economic Survey 2021 shows the focus of the government on solar systems by installing different types of solar projects with a total of 430 MW of capacity in the last five years for commercial operation. Many industries and commercial organisations in Pakistan have started to set up their captive power plants with rooftop solar installations due to an increase in electricity costs and unstable grid supplies. The government aims to add 3000 MW of solar power to the national grid by net metering through one million facilitated customers [13].

The Government of Pakistan is determined to enhance the renewable energy percentage from 5.4% to 30% in the total energy mix of the country by 2030. One way they are doing this is through the use of solar PV power. Pakistan is geographically located to face the sun, and the average sunny day is nine and a half hours daily, which is ideal for solar installations and solar power generation projects. Due to climate change and the increase in electricity demand, the government supported renewable energy in 2013, and up to 430 MW of capacity in six solar

projects were completed. Additionally, the World Bank is also providing support to the Sindh Solar Energy Project of $100 million for 400 MW of different projects and the solarization of 200,000 households by the private sector [14].

1.9 Scope and Objective of this Study

The current study helps resolve the issue of the solar structure against the wind load. The effect of wind velocity on the solar PV mounting structure was investigated in experimental and numerical setups. The problems in standard solar PV mounting structures installed in Pakistan were addressed with results from numerical simulation.

1.10 Thesis Overview

Chapter 2 narrates the different types of structures studied in different research. The relevant work related to the study has been discussed in this chapter. A detailed and in-depth literature review has been carried out about the different types of structures and the pressure of the wind load on solar panels.

Chapter 3 is about the experimental setup for the wind velocity on the solar structure and solar panels. This chapter explains the complete methodology of the study and the numerical method used to evaluate equivalent stresses and total deformation of solar PV mounting structures. All different setups of the equipment have been explained and discussed in this chapter.

Chapter 4 is about the results of the study. This chapter explains all the results of the study obtained in different ways. The result of the study has been shown in different graphs, tables, and narrations. All equivalent stresses and total deformation of the structure have been shown with empirical values too.

Chapter 5 explains the conclusion of this research study. It also provides future guidelines and recommendations.

Chapter 2

Literature Review

The solar PV mounting structure plays a pivotal role in PV installation and its smooth performance over a long life. The mounting structure holds the solar panels at an optimum angle, which allows them to generate the most electricity. In PV installations, the solar structure has always been a neglected aspect. There is a dire need for a study to explore the effect of wind and its angles on solar electricity yield and durability. The solar structure must withstand extreme weather conditions, i.e., thunderstorms, monsoon rains, and heavy snowfall. Two flat roofs are mounting PV types made with mild steel structures in attached and ballasted designs used for the fixing of solar modules. The type 1 attached mounting designs are fixed in the roof by penetration to support the array, and ballasted designs, contrary to bearing weight on their feet, are additional supports to withstand the wind and are not penetrated [15]. Attached PV mounting structures, in comparison to ballasted structures, are more costly but stronger against the wind load [16]. In high-wind areas, the attached mounting structure is preferable to the ballasted structure. Ballasted mounting structures are cheaper and reduce the installation cost, but ballasted mounting structures are unreliable to withstand the high wind until a dead load is increased on the roof [17]. To withstand wind, the load of the ballasted structure on the specific location of the roof must be carefully considered in PV system design.Road maps used in the solar panel design and their connections depend on the mounting system type used to bind the panels to the roof [18]. The structural analysis study becomes more useful when it classifies the

solar panel support systems based on the load transferred between the panels and the roof. Furthermore, the approach in the installation of solar panels on flat as well as pitched roofs is either parallel or not parallel depending upon the space and direction [19]. While considering the mounting methods, practically three types of roof mounting systems are used, e.g., roof bearing, fully framed, and building-integrated systems [19]. The beauty of building integrated systems is that they have no effect on the roof profile. Hence, there is a marginal effect on the structure due to the resulting load of solar panels. Generally, PV system based on mounting configuration is divided into two broad categories, ground-mounted, and roof-mounted structure systems. Different studies by Stathopoulos et al. [20], [21], [22] and Kopp et al. [23], [24], [25], showed a clear difference in the wind pressure effect on both ground-mounted and roof-mounted systems attributed to the building effect on the wind pressure over the solar panels. Unlike aerodynamic bodies, Holmes [26] showed that when a sheer body is subjected to wind, the flow of the wind separates at the leading edge corners and surface pressure on the solar panels and generates a vortex as shown in the following Figure 2.1.

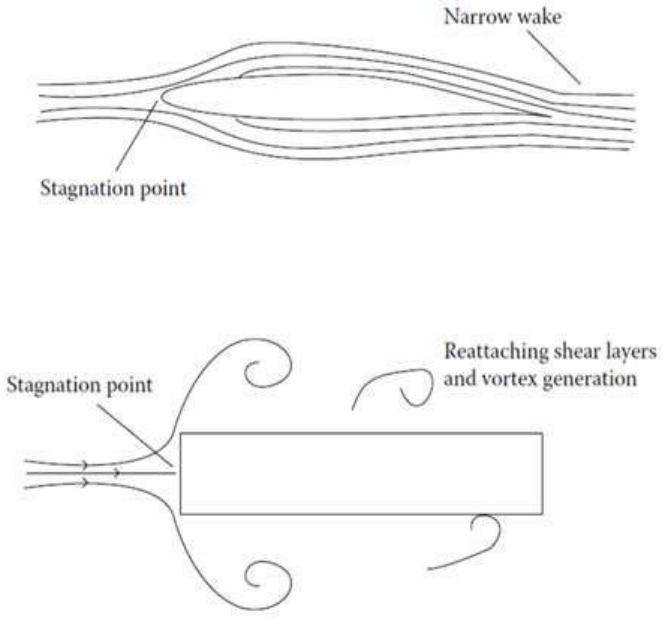

FIGURE 2.1: Vortex Generation on Solar Panels [26]

The wind effect is not as dangerous as the effect of the vortex. The vortex pressure on the solar panels is from all sides and helps to uproot the structure from the ground or detach the solar panels from frames [27]. Mostly, solar structures are designed to bear the wind pressure, but the vortex effect is always ignored.

Sometimes, the wind pressure is very high, but the direction of its flow does not make a vortex. Similarly, sometimes the wind pressure is low but directed on the leading edges of the structure and generates a powerful vortex to dismantle the mounting structure system. While designing the mounting structure, the direction of the building and the wind flow play a pivotal role in the installation of the solar mounting structure system.

A report published by Pakistan's National Electric Power Regulatory Authority (NEPRA), for the financial year 2021–22 shows that 44.74 MW and 243.43 MW of power were purchased by the national grid through solar power purchase agreements and 7032 licences of solar net metering systems [28]. The other licences issued for power generation were for natural gas, hydropower, and coal. The large solar project licence remained at 20 MW, and the hydropower project had a capacity of 152.12 MW and was the largest project. The NEPRA report also shows the annual growth of the power sector, reaching 40.000 MW of current installed capacity from all energy sources. The hike in solar and wind power generation was seen after the embargo on the requirement of a solar net metering licence from NEPRA was lifted up to 25 kW and the authority was decentralised to the distribution companies. The total solar power generation capacity approved by NEPRA was 288 MW in 2021–22. The excess solar power produced and exported to the national grid by the net-metered households is adjusted at Rs. 9/kWh instead of based on the rate at which electricity is sold to the households. Pakistan is the least carbon-emitting country in the world and continuously shows determination in carbon reduction, as highlighted in its intended nationally determined contribution in carbon reduction policy submitted in November 2016 [28]. Pakistan's government has set a target of achieving 20% of its total energy mix from solar power by 2030 and will spend $40 billion to reduce its 20% carbon emissions. The initial plan depicts that 10% of emissions would be reduced with $5.5 billion and a $15.5 billion investment will achieve the 15% reduction in carbon emissions due to solar installations. To achieve these emission targets, Pakistan needs international support, otherwise, it is not possible. Global warming, the skyrocketing price of fossil fuels, incentives by the government, and increasing public awareness of sustainable energy supplies at cost-effectiveness have triggered and instigated

solar installations in all cities of the country [28]. In the majority of the sites, the southerly-facing rooftops remain in focus due to their economical installation and higher yield of solar electricity. The mounting structure, when installed on the rooftop, adds load to the building lintel or building structure. A careful load calculation is needed for the load of the solar panels and mounting structure on the existing building [29]. The best mounting structure and solar panel installation are when they do not harm the existing building infrastructure with proper load and angle calculations. The structural engineer must design the structure to comply with the solar installation methods, building codes, and safety standards to combat wind flow, snow weight, and seismic shocks [30]. However, the mounting structure economy varies depending on whether the building structure is made of wood, wood beams, steel, or pre-cast roofs. In the economy of the structure, the height, material, and design of the structure also play an important role. A structural engineer is the best judge to design an economical and robust structure for the existing building rooftop. After the common man learned about the solar system, a variety of structures evolved to complement the appearance of the building. The versatility and ease of the installation of the mounting system depend upon the design, material, and weight [31]. To safeguard the mounting system from wind flow and vortex, the material plays an important role in making the total solar system last for at least 25 years. The contour and the prevailing environment of the installation area determine the type and strength of the material. Generally, a rust-free, corrosion-resistant, and robust material is used for the solar mounting systems on rooftops and ground-mounted. Galvanised and powder-coated steel is the most viable, conveniently available, and affordable material used in different designs, weights, and lengths. Hard-dip galvanised steel is the best option for a long life and is resistant to all types of weather.

For the optimisation of the solar system, along with solar structure, other factors like the solar module, type of cables, direction, dust factor, and temperature should also be kept in mind [32], [33], [34]. From a safety point of view, along with a robust structure, there is a need to do proper grounding, earthing of the structure, inverter, solar panels, all material appliances, surge protectors, and the installation of a lightning arrester to safeguard the building and human lives must

be incorporated [35]. The mounting structure, simply, is installed after segregating the zone into a wind, seismic, or snow zone. It will help to determine the height, weight, length, and type of material needed. We can simply say that the environment and topography of the site play an important role in the selection of the type of mounting structure [36].

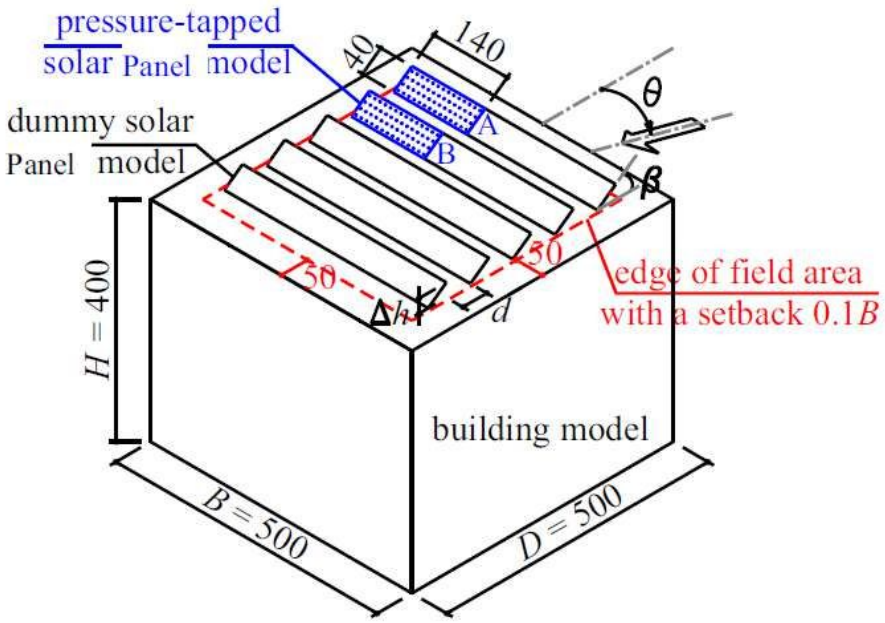

FIGURE 2.2: Experimental Setup of Cao et al. Investigation [37]

Different wind tunnel experiments have been performed on standard PV modules on flat roofs to calculate the average wind and module pressure on the module surface area [38]. While considering design parameters, the angle of the tilt, the distance of the module arrays, building depth, and the effect of parapet height are also considered. The study shows the more unfavourable negative coefficient of a single array than in multi-array cases. The tilt angle with array distance also increases the negative module force, but the building depth and parapet height effect remain unclear. In solar photovoltaic systems, the module support structures of solar panels remain of paramount importance. Since the solar system would bear the environmental and wind loads all its life, it is imperative to know the effect and distraction of the module support due to these loads. To evaluate wind loads on solar panels, Cao et al. [37] performed experiments on a series of wind tunnels installed on flat roofs, which can be seen in Figure 2.2. Previous research focused on calculating the average net pressure of the wind load on the solar modules, similarly to non-standard size. The investigation of module force

characteristics was based on the study of different design parameters, including tilt angle, array inter-distance, building depth, and parapet height (building parameters). In comparison with multi-array cases, single-array cases resulted in much larger negative module force coefficients, which were unfavourable, whereas tilt angle and inter-array distance also increased negative module forces, and building depth and parapet height had no significant effect on negative module forces.

Similarly, the effect of array spacing on tilt angle, building parapet height, and the wind force coefficient on solar module size was investigated in the study of Li et al. [39]. Their investigation focused on the different characteristics of wind load on photovoltaic panel arrays fixed to a flat rooftop mounting structure. Surprisingly, they found in flat rooftop structures that the wind load pressure was higher in the first two rows and the last two rows. The wind pressure on the edge panel was unfavourable when an oblique wind direction occurred, but on the middle solar panel unit, the unfavourable pressure remained when the wind direction was 0° or 180°. It was also noticed that the negative extreme wind pressure was reduced when the space in the middle of the arrays was increased. Furthermore, the most unfavourable negative extreme wind pressure of the panel decreased with an increase in array spacing for panels located in the middle of the array, which was analogous to the pass over parallel hills (or dunes). The wind load remained high in the middle of the arrays, especially on M3, and showed turbulence, leading to an unwanted minimum pressure coefficient. Finally, the negative relationship between extreme wind pressure and array spacing was discovered. The solar module tilt angle plays an important role in pressure equalisation from different angles of the wind. It was found that the lift force increased with an increase in the panel inclination angle, resulting in greater overpressure. The results indicated that for a tilt angle of 10°, the suction and overpressure of the panel array were significantly lower than for tilt angles between 20° and 40°. This was attributed to the flow separation observed at higher tilt angles. The parapet height was also noted to affect the lift and overpressure forces of the panel unit. A parapet height of 2h was found to be the critical height for the minimum and maximum force coefficients. Increasing the parapet height can reduce the extreme lift and overpressure forces. The design force coefficients recommended for different area sizes

at different locations were given, along with a uniform force coefficient proposed for the design of rackets.

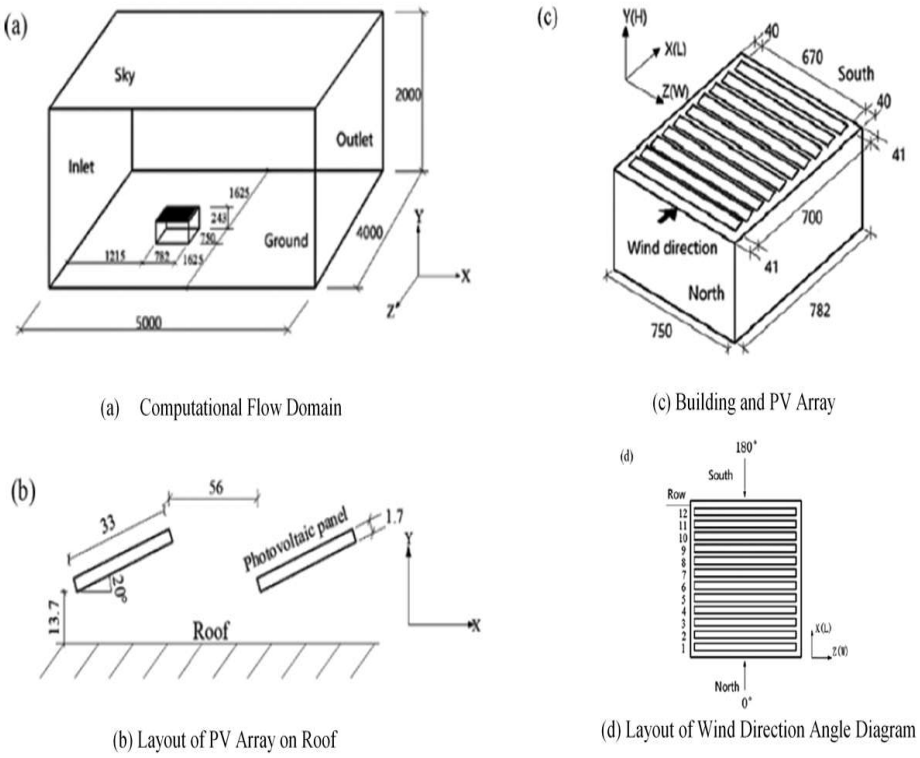

FIGURE 2.3: Diagram of the Flow Domain and PV Array Layout on the Roof (mm) [19]

The study of Alrawashdeh et al., [40] provided a comprehensive review of the results of the experimental criteria set out to study wind-induced pressure in flat roof-mounted solar structures with geometric scale. Their study revealed a significant finding about the wind load on rooftop mounting structures and obstacles in the evaluation of the wind load. They also suggested that wind tunnel models are of paramount importance in obtaining the result of wind load on solar modules. They overcome the limitation effect by performing the proper codification process and thorough examination. Their research was based on geometric ratios, and they designed three models (1:50, 1:100, and 1:200) and tested them in a Concordia University atmospheric boundary layer wind tunnel. The result of the study showed the importance of the geometric test in simulating solar panel models with atmospheric boundary layer wind tunnels for wind loads on solar modules. Their insight provided an in-depth analysis of the data collected from the experiments and presented the conclusions from this research. Wind pressure distribution on

photovoltaic (PV) arrays is an important factor in wind resistance design. Turbulence caused by building edges can significantly affect the flow field associated with the pressure and thus must be taken into consideration in such investigations.

Most CFD studies of wind pressure distributions on PV arrays focus on ground-mounted PV arrays and neglect the effect of the building. Hence the study of Li et al., [19] expanded the CFD application to the PV arrays of roof-mounted structures. They found the result with the help of fluent software in the calculation of wind pressure distributions with the Reynolds-averaged Navier–Stokes (RANS) approach. Different RANS models were tested, but the results that were coherent with the wind flow in comparison to the wind tunnel experimental model were considered accurate. The SST k-ω model was found to be the most effective in guiding the highest net mean wind uplift located upstream. In parameter analysis, this model remains quite helpful for a roof-mounted PV array installation. In 20-minute intervals, wind flows at angles between 0° and 180° were observed, and a numerical simulation helped calculate the net pressure distributions at different tilted angles. In the investigation, it was seen that the tilted angle of the PV array also influenced the wind pressure distributions in the flow field. Furthermore, their research work also examined the influence of the gap between the photovoltaic array and the roof with tilted PV arrays on the flow fields and pressure distributions.

Sauca et al., [41] executed an analysis of the effect of wind on solar arrays at Kalaburagi, Karnataka, India. They analysed the wind effect on solar panels by using the numerical analysis tool ANSYS Fluent. In their study, they used a setup of twelve solar modules measuring 1.2m in length and 0.6m in width. These solar panels were designed in four columns and three rows and inclined southwest at 18 degrees. The wind pressure of varying velocities ranging from 5 to 25 m/s was applied by changing the tilt angle of solar modules from 0, 30, 45, 60, 135, and 180 degrees. The high wind pressure suction load was observed at angles of 0, 30, and 180 degrees at velocities from 5 to 25 m/s on solar modules. A difference of 30% in the wind attack effect was seen from 0 to 30 tilt angles of the solar modules. Their result helped to design and manufacture the solar structure with the proper tilt angle to safeguard the solar structure and modules

from the wind pressure from different angles. Georgeta et al. [42] also performed experimental research on wind load on photovoltaic modules at different angles. They designed a setup of solar modules consisting of 12 panels with an angle tilted at 30 degrees based on the location of Romania. They used ANSYS CFX code to analyse the effects of changes in the angle of the lethal effect of the wind on solar modules, tilting them from 0 to 180-degree angles. The analysis yielded pressure and velocity contours for each panel, as well as the pressure distribution of each panel. Stathopoulos et al. [43] also contributed by studying the wind effect on standalone solar panels on different bases, like the ground, a flat rooftop, and a gable building roof. They observed the devastating wind effect on the solar module at the different inclinations of the arrays, ranging from 105 degrees to 180 degrees. The highest effect of the wind on the solar module remained at 135 degrees of the solar mounting. The crux of the research was amazing, and there was no harmful effect of wind observed on a standalone solar module due to the building height and placement of solar panels at different locations; the only effect of wind was seen with the tilt of angles varying from 135 to 180 degree angles.

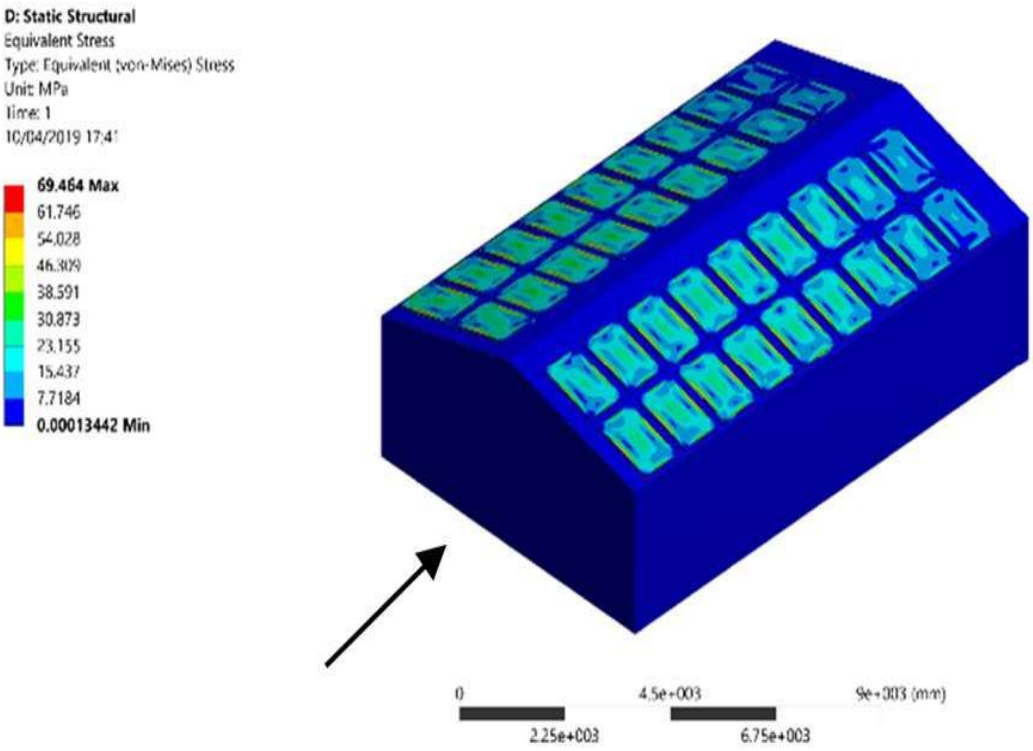

FIGURE 2.4: Equivalent stress at U = 61 m/s and 0° wind direction [44]

Ogedengbe et al. [45] conducted a study to assess the pressure dispersion on a scale model of a ground-mounted solar panel with two different inclinations—25 degrees

and 40 degrees—and measured the wind profiles at four different angles of attack: 0, 30, 150, and 180 degrees. The results showed that the 25-degree inclination produced greater loading compared to the 40-degree case. Additionally, it was observed that the gap between the upper and lower panels has a significant effect on the pressure distribution and should be taken into account while designing the panel structurally. Warsido et al. [46] performed wind tunnel testing to check the wind load effect on solar mounting row spacing on flat roofs and ground-mounted solar structures. They studied a 1:30 geometric scale model with a 25-degree tilt angle, and to find results, they used the varying wind pressure angles ranging from 0 to 180 degrees with 10-degree intervals for each wind attack on the mounting structure. During the experiment, it was observed that wind attack was higher on isolated solar panels than on those mounted in arrays. Detailed numerical modelling and research were conducted by Sharif et al. [47] and analysed the numerical values obtained through ANSYS software of wind pressure on different solar arrays. There had been a significant amount of damage to solar arrays due to wind attacks with strong wind speeds. An investigation was carried out in the study to check the displacement of the mounting structures around the solar panels. The different wind pressure was applied to the solar panels fixed at the same location with the same arrays facing the same direction. In the following model, a wind velocity ranging from 10 m/s to 25 m/s to 50 m/s was applied to calculate the displacement of the mounting structure from its base with varying wind stresses. Their model performed two different studies. In the first study, to calculate and control the turbulence around the panels, a turbulent flow, which is a k-ϵ physical interface, was applied. In the second study, they used the solid structure as a physical interface to protect the displacements due to periodic wind stresses. To determine and link the boundary load of a fluid flow of a solid region to a fluid region, different tools were applied: fluid-structure interaction and fixed geometry multiple physical coupling. This analysis was based on unidirectional fluid-structure interaction.

Abdollahi et al., [48] implemented computational fluid dynamics (CFD) to evaluate the contortion and robustness of PV panels under a static wind load following the IEC 61215 Standard. To ensure the safety and qualification of the photovoltaic

module, the IEC 61215 specified load tests with wind loads considered uniform static pressure loading at a magnitude of 2400 Pa and 5400 Pa. In their research work, the impact of wind on solar panels was examined for three wind speeds: 32 m/s, which corresponded to Beaufort level 11; 42 m/s; and 50 m/s, which corresponded to Beaufort level 15. At wind speeds of 32 m/s, the panel surface's average stress was 1415.6 psi. When the wind was blowing, 42 m/s was 4379 Pa and 50 m/s was 15142 Pa. As a result, winds faster than 32 m/s cannot be used to install thin-film solar panels. Additionally, with wind speeds greater than 42 m/s, photovoltaic panels made with crystalline technology cannot be deployed. A wind speed of 50 m/s produced a very large displacement that was almost 2.5 times greater than that of winds of 32 m/s and 42 m/s.

Significant changes are being made to the global energy system, including a switch in energy-generating technologies to more renewable energy sources. However, because they are more susceptible to frequent and harsh weather occurrences, renewable energy sources' reliance on regional environmental conditions may also result in more service interruptions. Jackson et al. [49] introduced a novel way to identify and analyse performance consequences resulting from extreme weather occurrences across several geographical locations by integrating three different datasets (operations and maintenance tickets, meteorological data, and production data). Snow, hurricanes, and storms were shown to be the most common extreme weather occurrences affecting photovoltaic facilities in the United States by text analysis of maintenance requests. The scope and variety of these effects on site performance were subsequently determined using statistical approaches and machine learning. Impacts varied depending on whether there was an event or not, with snow occurrences having the biggest impact (54.5%), followed by hurricanes (12.6%) and storms (1.1%). Low irradiance, geographic location, meteorological characteristics, and site size were just a few examples of the major factors that machine learning analysis uncovered in evaluating whether a day is classified as low performing. Yemenici et al., [50] identified the wind directions and tilt angles at which the entire ground-mounted panel suffered the maximum wind loading, and then conducted numerical and experimental tests. The wind patterns and panel tilt angles had a big impact on the flow structures. In contrast to the straight

wind directions, which had symmetrical distributions and lower velocities, the oblique wind directions exposed the panel to higher wind speeds and asymmetric distributions. Stronger vortex shedding variations, higher velocity zones, and higher shedding frequencies were influenced by the increased panel tilt angle. The greatest positive and negative pressure values for the 0° and 180° wind directions, respectively, were measured near the leading edge of the panel for both panel tilt angles. The trailing edge then showed gradual declines. Additionally, there was more pressure as a result of the higher panel tilt angle. The panel's maximum drag coefficient was measured at a tilt angle of 45° for a wind direction of 0°, while its lowest value was discovered at a tilt angle of 25° for a wind direction of 120°. The panel's positive and negative lifts were largest at a 45° tilt angle for the 180° and 0° wind directions, respectively, while they were lowest at a 25° tilt angle for the 120° and 60° wind directions. When tilted at 45 degrees, the panel's BLUE-peak values were 24.1% and 23.5% higher than the mean values for the 30-degree and 150-degree wind directions, respectively, while tilted at 25 degrees, they were 29.4% and 25.7% higher.

An array of tilted solar photovoltaic panels is vulnerable to extremely high winds during hurricanes and typhoons. It's crucial to ascertain the system's aerodynamic properties to ensure appropriate operation. In recent years, offshore photovoltaic (PV) systems have been created. Wind, wave conditions, and tidal regimes all affect wind loads. On average, 20 typhoons make their way to the Philippines each year. Communities damaged by the storm are left without electricity as a result of the hurricane's devastation to the infrastructure. During blackouts, the affected population may receive power through solar panels. However, these facilities are also structurally weak against severe weather, including winds equivalent to typhoons. A low-rise gable building with solar panels positioned on the roof uses a Fluid-Structure Interaction (FSI). Using computational fluid dynamics (CFD) analysis, typhoon-force winds were applied to these types of buildings by Pantua et al. [44]. Figure 2.4 depicts the FSI result. The FSI results highlighted the panels' failure points at the installation site. However, BES (building energy simulation) studies revealed that a building with a roof pitch of 14° and a 90° building orientation had the maximum potential for power generation. To support occupancy

loads, it was advised to put the panel system configuration on a roof with a 26° pitch.

Sheikh et al., [51] also engaged computational fluid dynamics to simulate steady-state Reynolds-averaged Navier-Strokes (RANS) for a fixed tilt ground-mounted photovoltaic (PV) module system (CFD). Initial experimental results from the literature were used to validate the 2D and 3D numerical models. The study of drag and lift coefficients on solar systems erected over incline terrain was the main focus of their work (hills). Over the subsequent seven rows of the solar panel array, three distinct hill profiles with heights of 100 metres and ratios of 0.5, 0.75, and 1 were taken into consideration. It had been noted that when a hill's stiffness increases, the forces of lift and drag increase correspondingly. Therefore, installing solar panels on steep hills was not advised. Additionally, the parametric investigation was done on the effects of panel length, the spacing between subsequent panels, clearance height from the ground, wind speed, and tilt angle. From their numerical study, it can be seen that as the H/L ratio was raised from 0.5 to 1, the wind loads for the corresponding situations also rose, which resulted in stronger drag and lift forces for steep hills. Furthermore, it was also noted that the drag and lift forces were greatest on the first row of solar panels and fell dramatically over the second row due to the wake effect (creation of vortices). It then gradually increased after the third row before being practically constant after the fifth row.

Waqas et al. [52] developed the Finite Element Method (FEM) to examine the effects of different wind loads on the structural strength and dependability of solar panel-supporting structures. The analysis of the mounting structures supporting solar panels employed wind speeds of 20, 25, 30, 35, and 40 m/s. Additionally, wind loads were computed using a mathematical method. The findings demonstrated that the wind load on the solar structure is reciprocal to the wind loads exerted on the photovoltaic modules. Their findings from the FEM analysis showed that increasing the wind loads resulted in greater overall deformation and maximum equivalent stresses. The solar panel supporting the structure's joint sections had the highest equivalent stress values, while the structure's centre and base had the highest total deformation. At 40 m/s and 20 m/s, respectively, the comparable

stress values of 62.866 MPa and 15.75 MPa may be determined. Similar to this, for 40 m/s and 20 m/s, respectively, the greatest and minimum values of total deformation were found to be 0.3631 mm and 0.0911 mm. While designing the solar structure to support the solar modules, the structure must be designed for stability and hydro photovoltaic panels, and in-depth knowledge of wind stress distribution and displacement with deformation of the mounting structure is very essential.

This thesis focuses on analysing the effect of wind loads on rooftop solar PV mounting structures in Pakistan. Many researchers around the world studied wind loads on solar PV mounting structures, but limited research work was found on FSI analysis of solar PV mounting structures. Westin [16] and Alrawashdeh [18] investigated the experimental analysis of scaled down model wind effects on solar PV mounting structure in the Netherlands. Zhang and Stathopoulos [22] studied wind loads on solar panels mounted on flat rooftops in Korea. Roecker [15], Alrawashdeh and Stathopoulos [18], and Ferreira et al. [29] discuss the design and analysis of mounting structures for solar panels, but they do not address the effect of wind loads on the structural integrity of these structures. Alrawashdeh and Stathopoulos [18], Li et al. [19], Zhang and Stathopoulos [22], and Pratt and Kopp [24] investigate the effect of wind loads on solar PV arrays on rooftops, but they do not consider the mounting structure for analysis. In Pakistan, some researchers put effort into a study related to wind loads on rooftop solar PV mounting structures installed in Pakistan, but insufficient research work was found on structural integrity and FSI analysis. Waqas et al. [53] studied stress distribution and equivalent stress on elevated rooftop mounting structures using Ansys static structural modules, but didn't justify the stress distribution and considered a fixed base for analysis. Gul et al. [54] studied the impact of static wind load on the mechanical integrity of different commercially available monocrystalline photovoltaic modules. Gul et al. [55] then studied the effect of wind load on the performance of PV modules available in Pakistan. Hence, the need arose to study the impact of wind loads on the structural integrity of solar PV mounting structures in Pakistan due to wind induced damage reported to solar PV mounting structures in the past few years.

Chapter 3

Problem Formulation

Creo Parametric 7.0 was used to model the solar PV mounting structure with two solar panels mounted with bolts. The standard mounting structure, which is widely used in Pakistan, consists of eight parts in pairs of two, such as the main support, the back support, the upper foot, and the lower foot. The 3D model is based on the most common solar PV mounting structure for two solar panels, which is widely used for mounting solar panels with powers ranging from 250W to 650W. Figure 3.2 demonstrates the solar PV mounting structures that are currently being installed on a large scale in Pakistan. Figure 3.1 and 3.3 shows main support and back support dimensions respectively. Real-life dimensions were considered while 3D modelling. The tilt angle of solar PV mounting structure is fixed throughout the study. Pakistan is located in a region with high solar irradiance, and a relatively shallow inclination angle is sufficient to capture a high amount of solar energy.

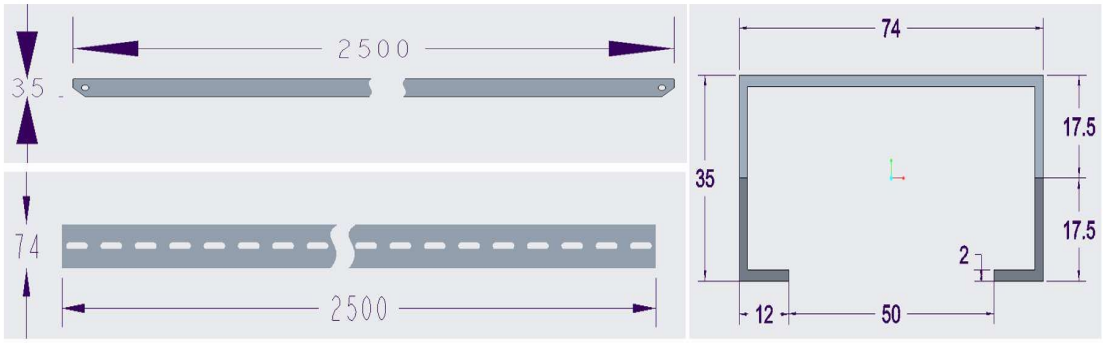

FIGURE 3.1: Main Support of Solar PV Mounting Structure (dimensions in mm)

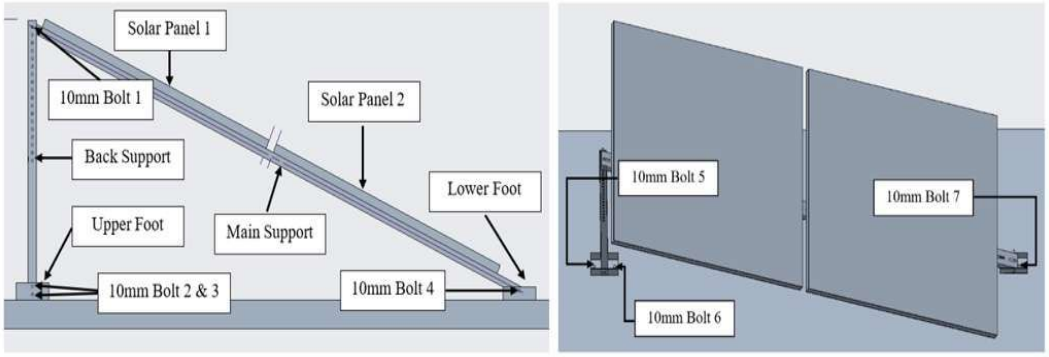

(a) Isometric side view of solar PV mounting Structure (b) Isometric side view Showing bolts location

(c) Real-life Standard Solar PV Mounting Structure installed on rooftop of residential building

FIGURE 3.2: Standard Solar PV Mounting Structure

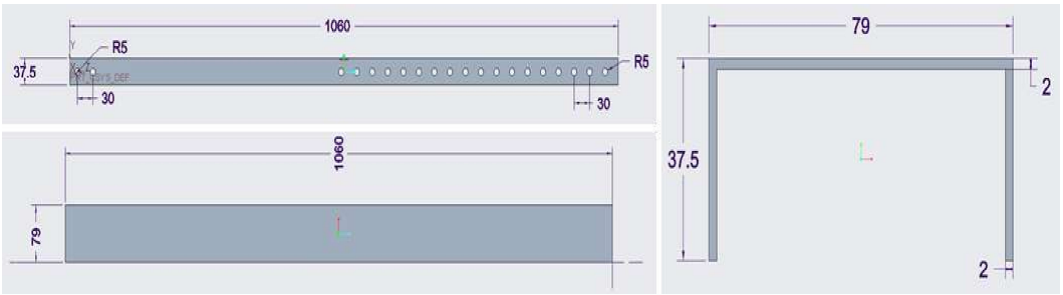

FIGURE 3.3: Back Support of Solar PV Mounting Structure (dimensions in mm)

According to Shabbir et al. [56], the optimal tilt angle for solar panels in Pakistan ranges from 23 to 32 degrees at 180 degrees south in the Punjab region. Uzair et al. [57] studied optimised performance of PV panels and site selection for a solar park in Pakistan. Uzair et al. [57] Karachi for solar panel installation with an annual fixed tilt of 26°. Hence, the solar PV mounting structure subject to wind

load at different wind speeds with a fixed average tilt angle 24° in different regions of Pakistan was studied. The height of 2 solar PV mounting structure at 24° angle varies from 700 mm to 1500 mm.

The symmetric Standard solar PV mounting structure is shown in figure 3.2 (a & b). Two solar PV modules are mounted on the structure. Each part of the solar PV mounting structure is defined, and these names were referred to throughout the research. Standard solar PV mounting structure installed on the rooftop of a residential building in Lahore, Punjab.

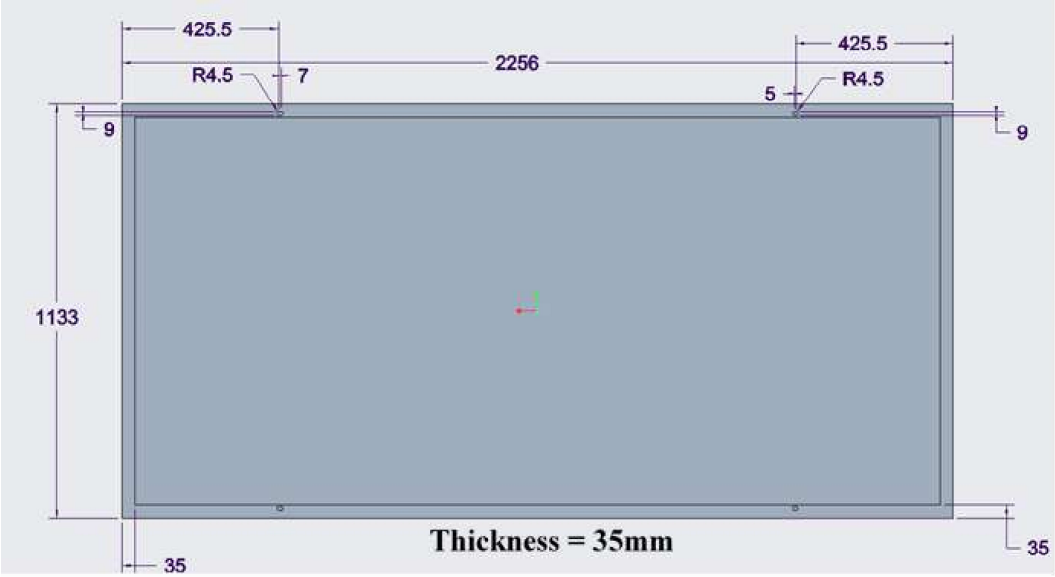

FIGURE 3.4: Back view of Longi 545W Solar Panel [58]

There are various dimensions of solar panel sizes and different types of rooftop solar PV mounting structures being used around the world. The most popular brands of solar PV modules include Longi Solar, Jinko Solar, JA Solar, Trina Solar, and Canadian Solar. The power ranges from 150 W to 660 W around the world. The size of the solar PV modules increases according to their power. But in Pakistan, most of the solar panels installed range from 250 W to 650 W in power, with average dimensions of 2256mm in length and 1133mm in width when used with 14 and 16 gauge mounting structures. Generally, the highest storms recorded in the past decade have had less than 80 km/h wind speeds in Pakistan. Therefore, the need arose to in-depth analyse real-life solar PV mounting structures structural integrity and stresses at different wind speeds. It was also necessary because during the last few years, severe damage to the rooftop mounting structure had been observed.

3.1 Experimental Setup

(a) Side view of SWSI Centrifugal Fan

(b) The diffuser outlet of Centrifugal fan facing the inlet of the Solar PV Mounting Structure

(c) Front view of Solar PV Mounting Structure

(d) Air Velocity measurement by digital anemometer

FIGURE 3.5: Configuration of Centrifugal Fan Setup

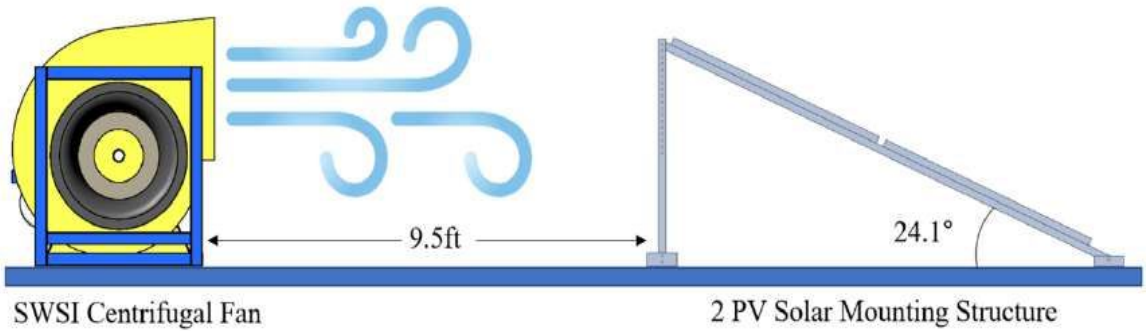

FIGURE 3.6: Centrifugal Fan setup with Solar PV Mounting Structure

For this study, a 20-inch Single Width Single Inlet (SWSI) high-pressure centrifugal fan setup was used for validation, as illustrated in Figure 3.5 and 3.6. The SWSI centrifugal fan consists of a 20-inch-diameter impeller with 12 backward-inclined blades, which is coupled with a belt-driven shaft to a 3-hp, three-phase motor. The fan outlet measures 335mm in width and 616mm in height. The velocity at the fan outlet is 31.67 km/h (1732fpm) measured from a digital air velocity metre with an articulated tube. High-pressure centrifugal fans and industrial blowers help move air and gases for industrial and commercial purposes.

The centrifugal high-pressure fan and testing facility were sponsored by a private company for the experimental purposes of this study. For validation of the experimental to numerical setup, a high-pressure centrifugal fan was placed behind the 2 PV Solar Mounting Structure. The experiment was performed in a shed. The distance between the fan and mounting structure was 2896mm (9.5ft). The distance between the fan diffuser and mounting structure was enough to distribute an approximately equal flow of air at the inlet of the mounting structure. Three virtual planes with 25 points for air velocity measurement were considered, as depicted in Figure 3.7. Plane 1 was the reference plane, which was at the start of the mounting structure. Plane 2 was taken at the centre of the mounting structure, which is at the gap between the solar panels. Plane 3 was at the last edge of the solar mounting structure. Three virtual planes were at equal distances, as shown in the air velocity measurement. The height and width of the planes are 872mm (2.86ft) and 2256mm (7.39 ft), respectively, as shown in Figure 3.7.

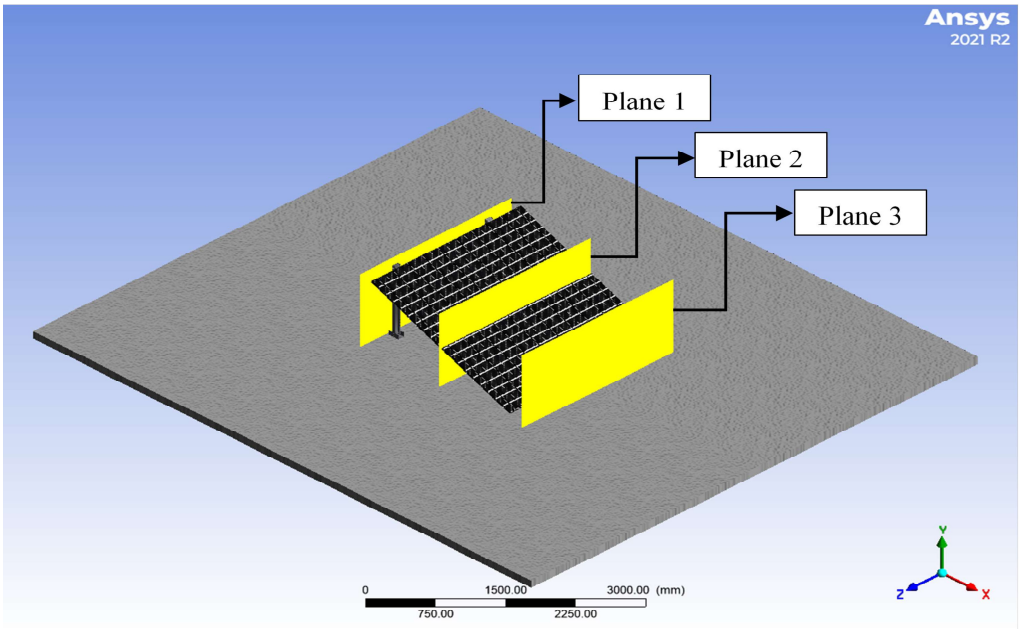

FIGURE 3.7: Planar Description of Virtual Planes Locations

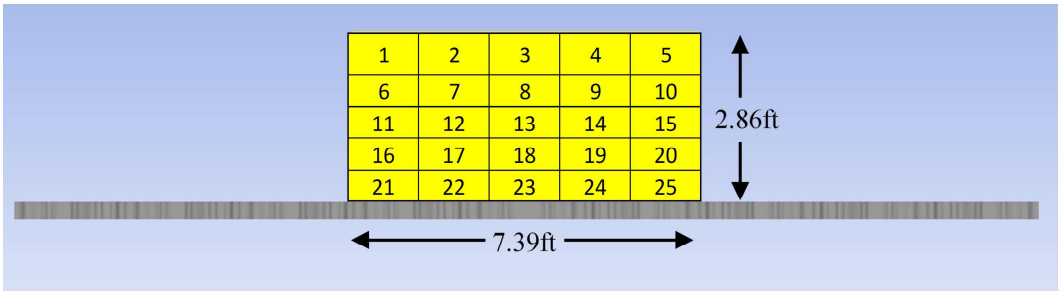

FIGURE 3.8: Description of Virtual Points on Virtual Planes from Inlet view

The 25 virtual points on virtual planes are shown below in Figure 3.7. The air velocity was recorded at these points on each plane. The experiment was carried out three times to get the mean value.

3.2 Computational Analysis

For this study, the Fluid Flow (Fluent) package of ANSYS Workbench 2021 R2 was used to study the wind induced damage to rooftop solar mounting structure at different wind velocities. Assumptions taken for this study were in the incompressible and steady-state flow domains. The angle of the solar PV mounting structure is 24° which is fixed throughout the study. Atmospheric pressure of air was considered to carry to the experimental and computational methods. Non-slip wall conditions were initialised. Conditions for FSI (Fluid-Structure Interaction) were setup accordingly.

3.2.1 Setting of Flow Field

Natural, strong winds are the main load source for solar PV mounting structures, and the supporting structure is subjected to a small wind load. The 3D geometry was imported into the ANSYS Workbench fluid-flow (Fluent) model after the appropriate fluid domain was created. The wind flow through the solar PV mounting structure is subjected to turbulence as it is mounted on a rooftop or on the ground in an open environment. So, $k-\omega$ SST turbulence model was used to carry out computational simulation. Compared to most RANS models, the $k-\omega$ SST model offers superior flow separation prediction and performs well in adverse pressure gradients. It has the capacity to consider the transportation of the main shear stress in boundary layers subjected to adverse pressure gradients [59]. The $k-\omega$ SST turbulence model is a widely used and well-validated model in the field of computational fluid dynamics (CFD). The following are some benefits of using the $k-\omega$ SST model for FSI simulation:

1. **Improved Accuracy Near Walls:** The $k-\omega$ SST model accounts for the wall effects and resolves the boundary layers more accurately than other models, making it ideal for FSI simulations where fluid flow interacts with solid boundaries Chong2017.

2. **Reduced Sensitivity to Free-Stream Conditions:** The $k-\omega$ SST model is less sensitive to the initial and boundary conditions in the free stream, improving the reliability of FSI simulations compared to other turbulence models [60].

3. **Compatibility with FSI Solver:** The $k-\omega$ SST model can be easily integrated with FSI solvers, allowing for seamless coupling between fluid flow and structural response [61].

4. **Applicability to a Wide Range of Flow Regimes:** The $k-\omega$ SST model can be applied to various flow regimes, including laminar, transitional, and turbulent flows, making it suitable for a wide range of FSI applications [60–62].

The incompressible air fluid was initialised with a constant density of $1.225kg/m^3$. Coupled scheme with a steady-state solver was carried out for the solution method. Maximum pressure, maximum velocity, and wind load were reported for plots. The residuals were set to $10e^{-5}$ which was converged after some attempts and setting up fluent.

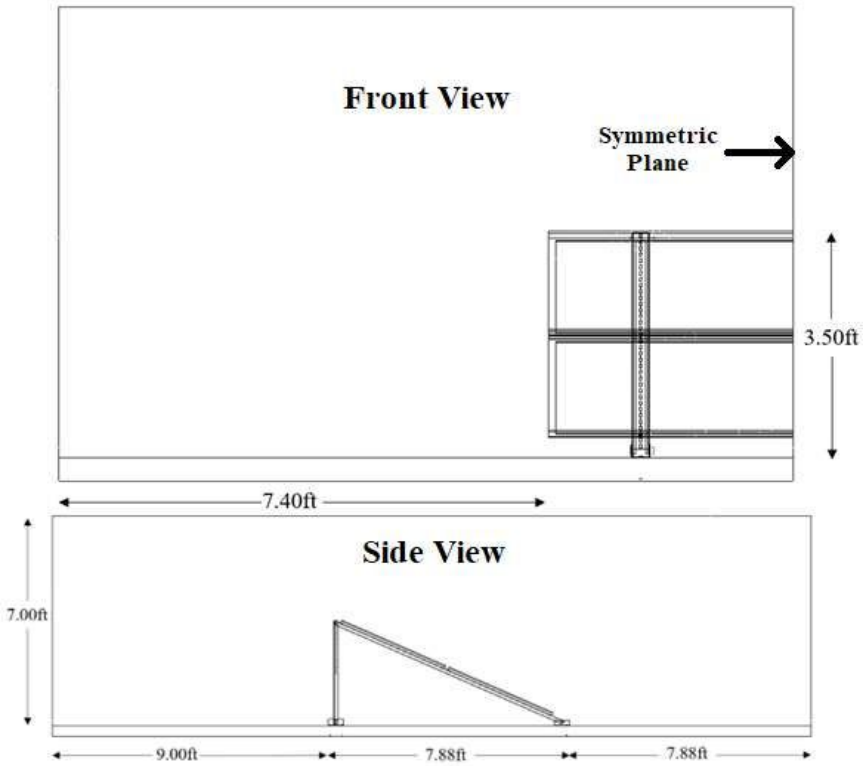

FIGURE 3.9: Geometry Under Study

3.2.2 Fluid Flow (Fluent)

3.2.2.1 Geometry

The assembled parts of a solar PV mounting structure with two solar panels were exported in a STEP (.stp) file to import as assembled in ANSYS. For further improvement and creating fluid domain, the imported geometry was opened in design modeller. A fluid domain was created on a concrete floor. The height of the fluid domain is twice the height of the solar PV mounting structure. The default body of any extruded geometry is solid, so it was changed to fluid under the properties tab of the fluid domain part geometry. The mounting structure for solar panels was subtracted from the fluid domain with a boolean tool. All parts were selected under the "parts and bodies" tab, and the "form new part" option was used to resolve connection issues between parts in the model tab.

3.2.2.2 Model

The geometry file was updated and transferred to the model in ANSYS Workbench. Automatic contact regions were formed under the connection tab. The automatic contact regions were only for fluent analysis. The manual contact regions with proper face selection for each part were further selected appropriately for static structural analysis. In the mesh tab, the sizing and quality of the body were initialised. For reliable and accurate results, the independence of the mesh was checked to achieve accurate and reliable results. Three meshes with different numbers of nodes and elements were modelled with a tetrahedral mesh, and different computational analyses were performed to achieve reliable results. Figure 3.10 shows the number of nodes and elements for models with tetrahedral meshes. The number of elements in body sizing was varied for mesh convergence.

The equivalent stress calculated with three meshes is shown in figure 3.11. The difference in result between a mesh with 671,322 nodes and one with 907,785 nodes is negligible compared to a mesh with 356,288 nodes. The mesh with 907,785 nodes and 487,074 elements was considered sufficient to proceed with the computational analysis of a rooftop solar PV mounting structure subject to wind load.

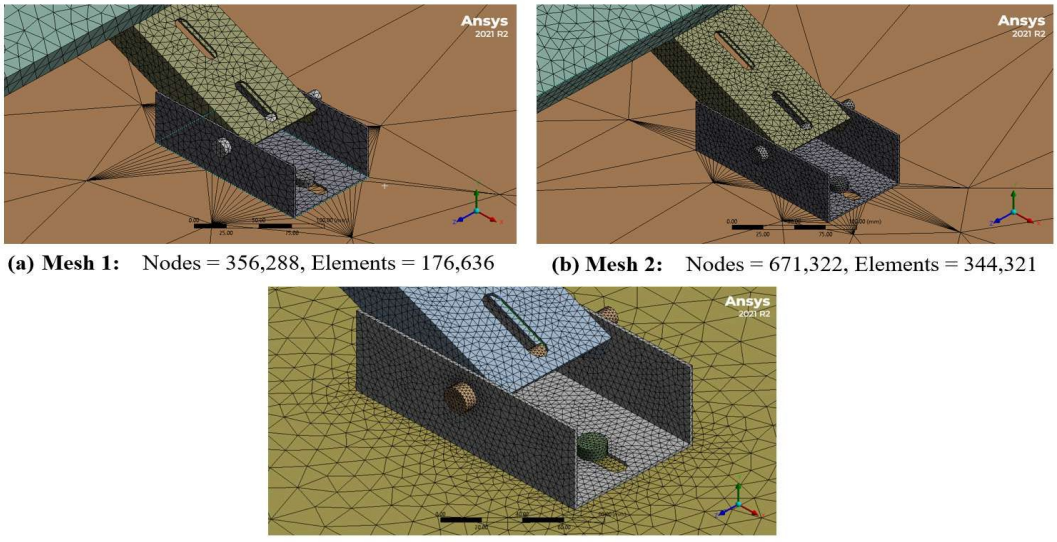

(a) Mesh 1: Nodes = 356,288, Elements = 176,636 **(b) Mesh 2:** Nodes = 671,322, Elements = 344,321

(c) Mesh 3: Nodes = 907,785, Elements = 487,074

FIGURE 3.10: Nodes and elements of 3 tetrahedral meshes

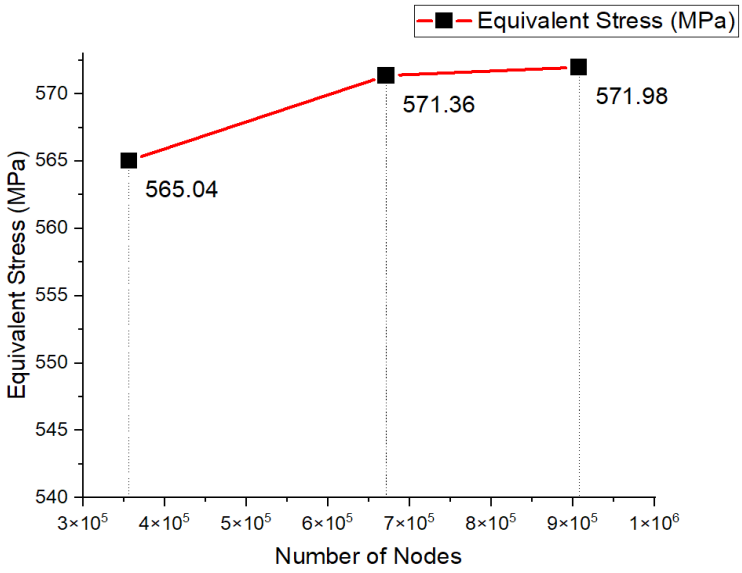

FIGURE 3.11: Nodes and elements of 3 tetrahedral meshes

For meshing, element size 50mm was selected for overall meshing. The mesh feature size was set to 0.25 mm. Mesh inflation was set to"smooth". ANSYS Fluent and Static Structural software provides the option of using a "smooth" or "sharp" inflation for the mesh inflation layer in FSI simulations. The "smooth" inflation option generates a gradual increase in mesh density from the outer boundary towards the inner boundary of the mesh inflation layer, while the "sharp" inflation option generates a steep increase in mesh density at the interface of the fluid and solid domains [63]. All other mesh settings were set to default. For the mesh method, the automatic method was selected for all 19 bodies. Now body sizing was selected to create more nodes and elements for the desired part. In the insert

option under the 'mesh' tab, 'sizing' was selected. 10 mm and 6 mm bolt bodies were selected based on geometry. The element size was set to 2 mm, defeature size was set to 0.005 mm and the behaviour was set to hard. Now body sizing was selected for the mounting structure. The main support, the back support, the upper foot, and the lower foot were selected. The element size was set to 5 mm, defeature size was set to 0.005 mm and the behaviour was set to hard. Now body sizing was selected for the mounting structure. Now body sizing was selected for solar panels. Both solar panels were selected. The element size was set to 10 mm, defeature size was set to 0.005 mm and the behaviour was set to hard. Now body sizing was selected for the concrete floor. The element size was set to 100 mm, defeature size was set to 0.005 mm and the behaviour was set to hard. A total of four body sizes were initialised. Then a mesh was generated with 919,113 nodes and 5,375,524 elements in a fluid domain, as shown in figure 3.13. While the mesh for static structural analysis was generated with 907,785 nodes and 487,074 elements. The mesh conditions and body sizing were the same in the fluent and static structural analyses (FSI).

The fluid domain was automatically set under mesh conditions. The element size of fluid domain was set to 50 mm. The mesh of all bodies is shown in Figure 3.12. The inlet, outlet, wall, and symmetry were initialised under 'named selection' tab. The inlet and outlet planes were at the start of the upper foot and the end of the lower foot, respectively.

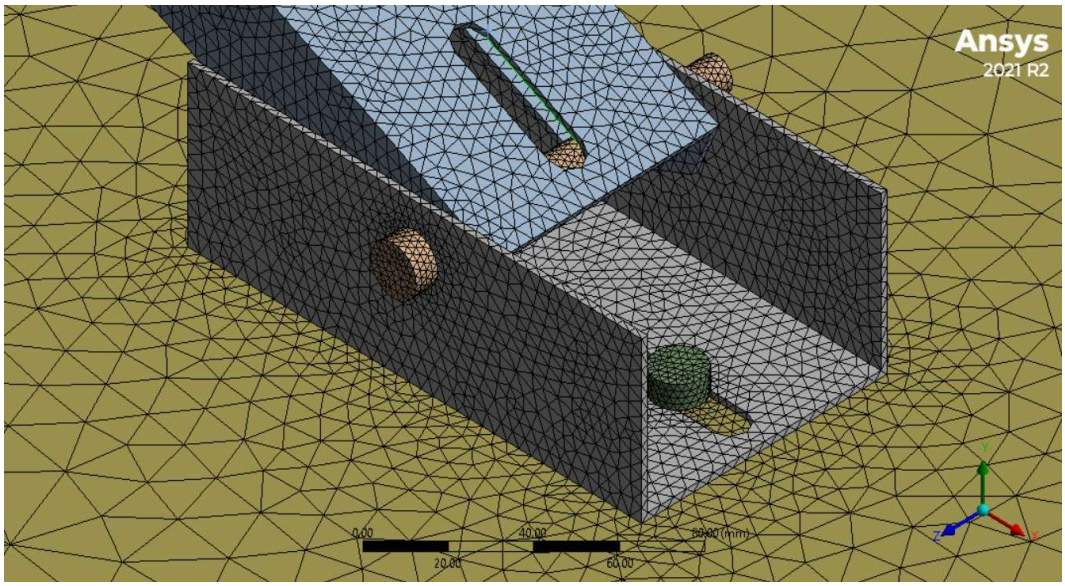

FIGURE 3.12: Modeling and Meshing close view

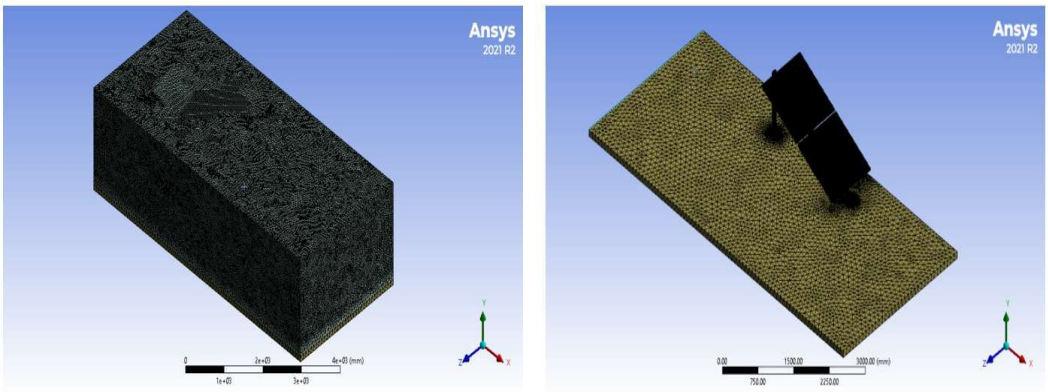

(a) 3D model mesh (b) 3D model mesh inside fluid domain

FIGURE 3.13: 3D solar PV mounting structure mesh

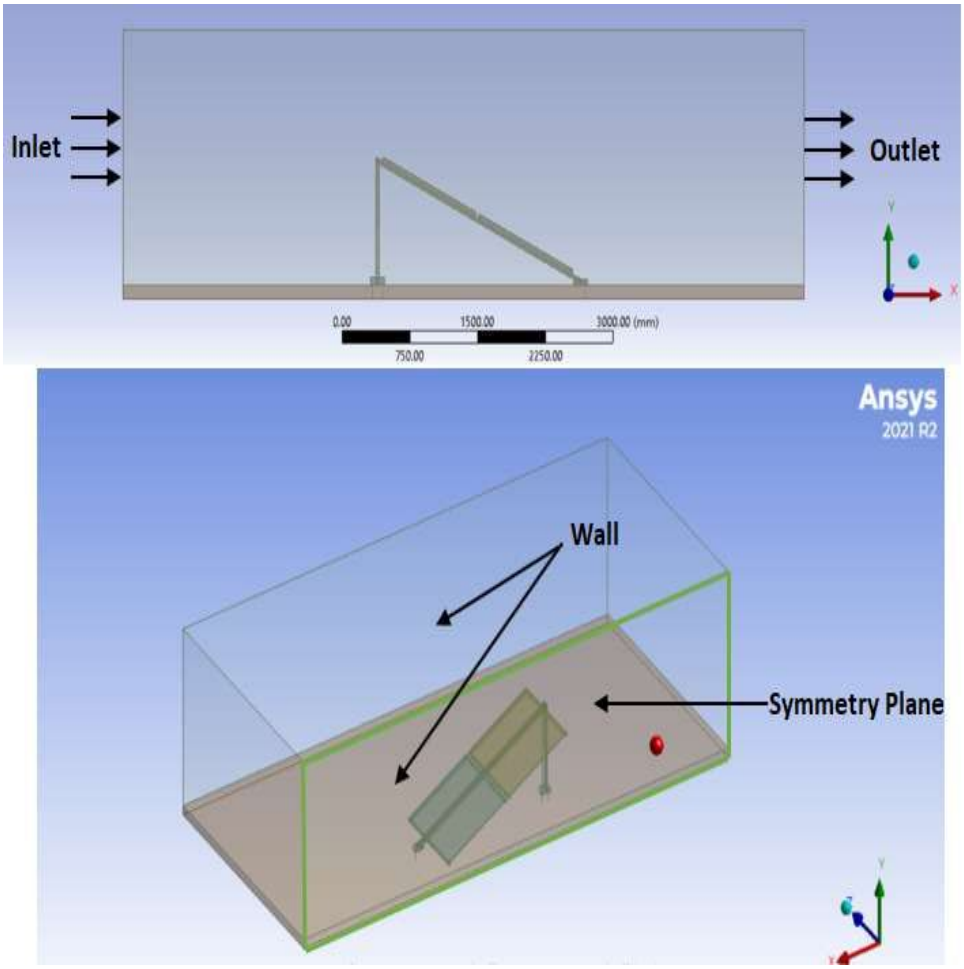

FIGURE 3.14: Named Selections

3.2.2.3 Setup

After setting up the model, the 'model' parameters were updated so they will be imported by the 'Setup' tab. The double precision checkbox was checked. Under 'General' tab, pressure-based solver was checked with Steady time. Viscous

$k-\omega$ model was used for simulation because it predicts better flow separation than most Reynolds-averaged Navier-Stokes (RANS) models and accounts for its good behaviour in adverse pressure gradients. This model has been used by many researchers for the flow field around PV panels and has been proven to have superior prediction [64], [65], [66]. Additionally, Shademan et al., [67] validated different turbulence models using inclined 2D flat plate calculations, and the mean pressure coefficient was compared with the experimental measures on the plate published by Fage et al., [68]. Default $k-\omega$ SST values were used for simulation. Under 'Materials' tab, air was used for the fluid domain with a fluid database. For solid materials, steel was selected for 10 mm bolts, 6 mm bolts, and the mounting structure. Aluminium is the material used for solar panels. Concrete (Portland cement) is used for concrete floors. The materials were appropriately selected according to a real-life rooftop solar PV mounting structure.

3.2.2.4 Boundary Conditions

Boundary conditions are most essential in ANSYS for mathematical modelling. At the inlet of the fluid domain, a uniform wind velocity of 10.3 km/h, 25 km/h, 50 km/h, 75 km/h, 100 km/h, and 120 km/h were applied with turbulence intensity of 5% and air density of $1.225 kg/m^3$. The air viscosity and turbulent viscosity ratio were set to default. At the outlet, atmospheric pressure of 298.15K was set to streamline the flow characteristics. The non-slip boundary conditions were considered for the walls. The side and top of the wall of the computational fluid domain were far enough from the Solar PV Mounting Structure for smooth flow. The roughness was set to smooth for the wall conditions. No-slip wall conditions were used for both walls.

3.2.3 Fluid Structure Interaction (FSI)

The geometry from Fluid Flow (fluent) was imported into the static structural geometry after the successful simulation results. Material properties were defined first after linking fluid flow (Fluent) with static structural properties. Structural steel, aluminium, and concrete were copied in engineering data. The setup of

Static Structural was further modified to set it up for structural analysis. The fluid domain was suppressed because imported pressure from fluid solid bodies was considered for study. The symmetric model was applied, and the symmetric region was defined as having three faces on a symmetric plane normal to the Z-axis. 48 contact regions were carefully created to bind the parts as they are installed in real-life. The mesh and body sizing were defined the same way as for Fluent Analysis. Now for static structural analysis, careful supports and imported loads needed to be defined. Fixed support was applied to the concrete floor only for real-life like simulation. For imported loads, the pressure was imported for all solid bodies.

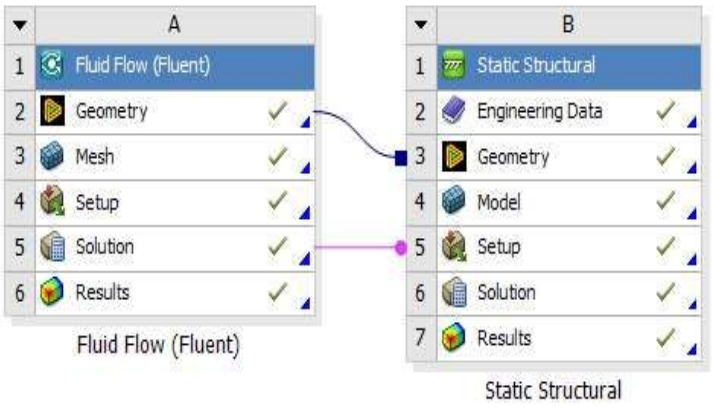

FIGURE 3.15: Fluid-Structure Interaction (FSI) coupling

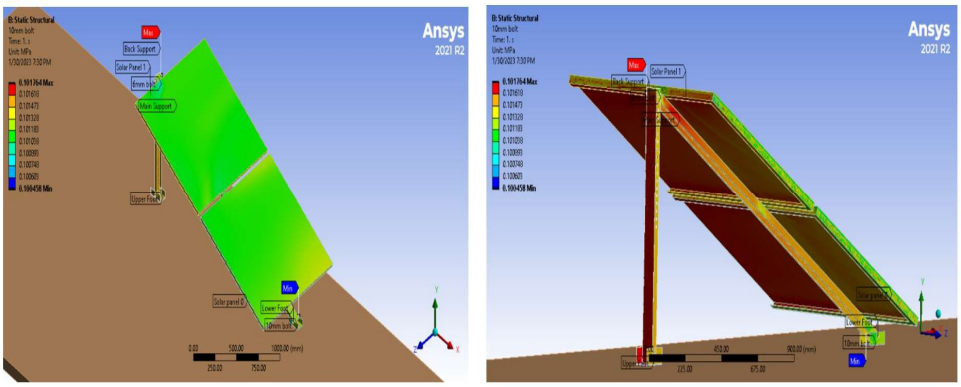

FIGURE 3.16: Imported Pressure Geometries

Figure 3.16 shows the imported pressure from fluent at 75 km/h wind velocity. The pressure on top of the solar panels is very low and near atmospheric pressure. The variation in contours is due to vortices of turbulent flow. The pressure at the back of the solar panel is highest because drag and lift forces both act on it. The pressure was imported successfully after carefully setting up the FSI.

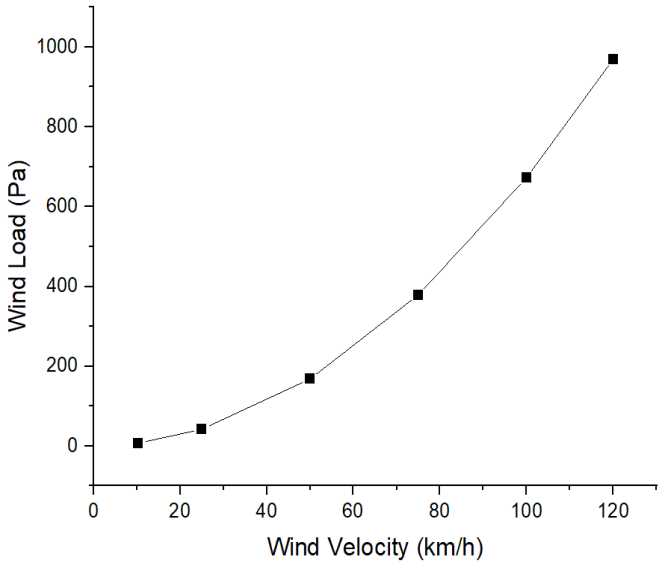

FIGURE 3.17: Wind Load at different wind velocities

The wind load was calculated at different wind velocities by a computational method. All manufacturers of solar panels perform experimental and computational tests to calculate the wind load at desired wind velocities, as shown in figure 1.14. Similar computational calculations were performed to obtain wind loads at different wind velocities. The graph shown in figure 3.17 was obtained by a computational method and follows the same trend as shown in figure 1.14.

Chapter 4

Results and Discussion

In this study, the wind effect on 14 and 16 gauge standard solar PV mounting structures was studied. Experimental and computational studies were conducted. For experimental validation, a SWSI centrifugal high-pressure fan was arranged, and a cardboard diffuser was crafted to distribute the air. The two PV solar mounting structures were placed in front of the centrifugal high-pressure fan, and the air speed was distributed accordingly to average 10.3 km/h across the inlet plane. The velocities at plane 1, plane 2 and plane 3 were measured and compared with the computational result for validation. The experimental method was validated.

Computational simulation was carried out after experimental validation. Wind velocities at different regions on the Beaufort wind scale [69] were considered for computational FSI analysis. Wind velocities from 10.3 km/h to 120 km/h were initialised for analysis. According to the building code of Pakistan by Ministry of Housing & Works (MOHW) and the Government of Pakistan (GOP) [70], the structures in a city should bear at least 120 km/h wind velocity. The wind speed in Pakistan exceeded 150 km/h in different cities of Punjab in 2000's as reported by the Regional Meteorological Centre, Punjab [10] but recent storms were occurred at 80 km/h wind speed. The study for solar PV mounting structure integrity was evaluated computationally and validated analytically. Equivalent stress and total deformation on different parts of the solar PV mounting structure were studied using computational analysis.

TABLE 4.1: Average recorded air velocity values in km/h on different planes

Plane 1				
9.9	10.3	10.3	10.3	9.9
10.3	10.3	10.3	10.3	10.3
10.3	10.3	9.9	9.9	10.3
10.3	10.3	10.3	10.3	10.3
9.9	10.3	10.3	9.9	9.9

Plane 2				
7.7	4.5	4.5	4.5	7.7
2.1	2.1	1.4	2.1	1.4
8.1	8.1	8.1	8.1	8.1
8.1	8.1	7.3	8.1	8.1
8.1	8.1	8.1	8.1	8.1

Plane 3				
1.4	3.1	1.4	3.1	1.4
2.4	2.4	1.4	2.2	3.1
3.1	1.4	1.4	2.2	2.4
2.4	1.4	1.4	1.4	2.4
10.3	9.9	9.9	9.9	10.3

4.1 Experimental Validation

For benchmarking a study, either experimental or existing numerical validation is required to carry out the research process. Experimental validation was considered as the resources were available to carry out the experiment. The experiment was carried out on October 7, 2022, a sunny day. A centrifugal fan was placed 9 ft behind the 2 PV mounting structure. At 9 feet away, the air velocity at different points was varying from 9.9 km/h to 11.2 km/h at the inlet plane. Most of the points had 10.3 km/h air velocity, so 10.3 km/h air velocity was considered the average velocity. A digital anemometer was used to measure the wind velocity during the experiment. The threshold velocity of a digital anemometer is 1.3 km/h for operation. The digital anemometer was held steady for five seconds at each point to note down the air velocity value. A similar method was carried out for each plane, with 25 points on each plane. The experiment was carried out three times to take the mean of the air velocity at 25 points on each plane.

4.1.1 Experimental and Computational Air Velocity Comparison on Plane 1

The first plane is the reference virtual plane, which is beside the back support of the solar panel. The difference between experimental and computational values varies from 0 to 12.79 percent. This difference is due to human error, digital anemometer tolerance, and weather conditions. Overall, the error between experimental and computational values is less than 10%.

The table 4.2 shows the percentage error in experimental and computational values at each virtual point. The error was calculated using the following formula:

TABLE 4.2: Percentage error in Experimental and Computational Values at Plane 1

Plane 1			
Virtual Points	**Experimental Velocity (km/h)**	**Computational Velocity (km/h)**	**Percentage error (%)**
1	9.9	10.314	-4.182
2	10.3	9.668	6.136
3	10.3	9.492	7.845
4	9.9	9.668	2.343
5	9.9	10.314	-4.182
6	10.3	9.650	6.311
7	10.3	8.983	12.786
8	10.3	10.300	0.000
9	10.3	8.983	12.786
10	10.3	9.650	6.311
11	10.3	9.925	3.641
12	10.3	9.032	12.311
13	10.3	9.157	11.097
14	9.9	8.856	10.545
15	10.3	9.925	3.641
16	10.3	10.041	2.515
17	10.3	9.056	12.078
18	10.3	9.124	11.417
19	10.3	9.056	12.078
20	10.3	10.041	2.515
21	9.9	10.046	-1.475
22	10.3	9.323	9.485
23	10.3	9.346	9.262
24	10.3	9.323	9.485
25	9.9	10.046	-1.475

$$PercentageError = \frac{Velocity_{experimental} - Velocity_{computational}}{Velocity_{experimental}} \times 100$$

4.1.2 Experimental and Computational Air velocity comparison on Plane 2

The second virtual plane was considered in the gap between two solar panels. Maximum 12.19% error was recorded at point 9. The pressure below the solar panels is higher than above the solar panels. The percentage error at five points was greater than 10% as shown in table 4.3. All the other experimental values were nearly equal to the computational values which shows that the experimental validation approach was valid.

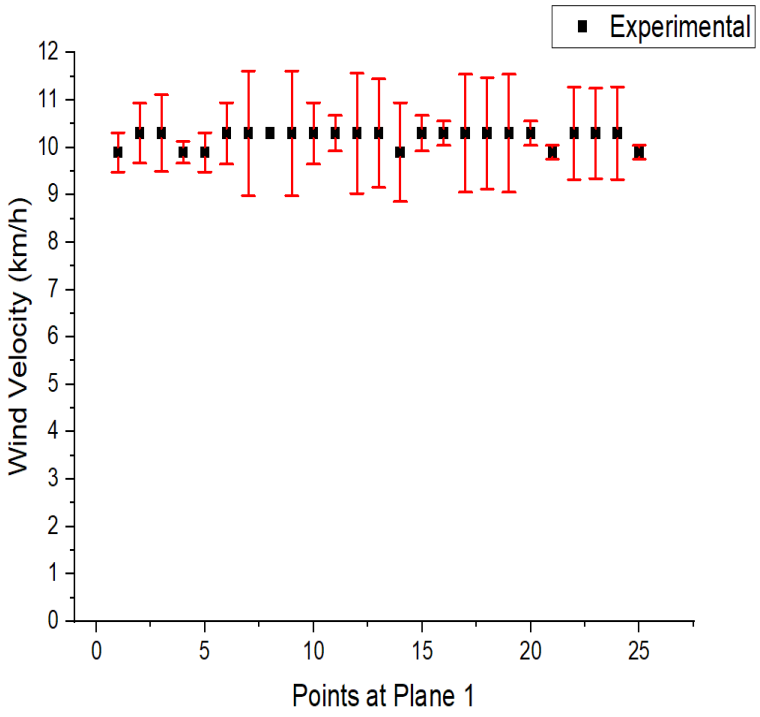

FIGURE 4.1: Experimental Wind Velocity on Plane 1 (bars represent deviation from Computational values)

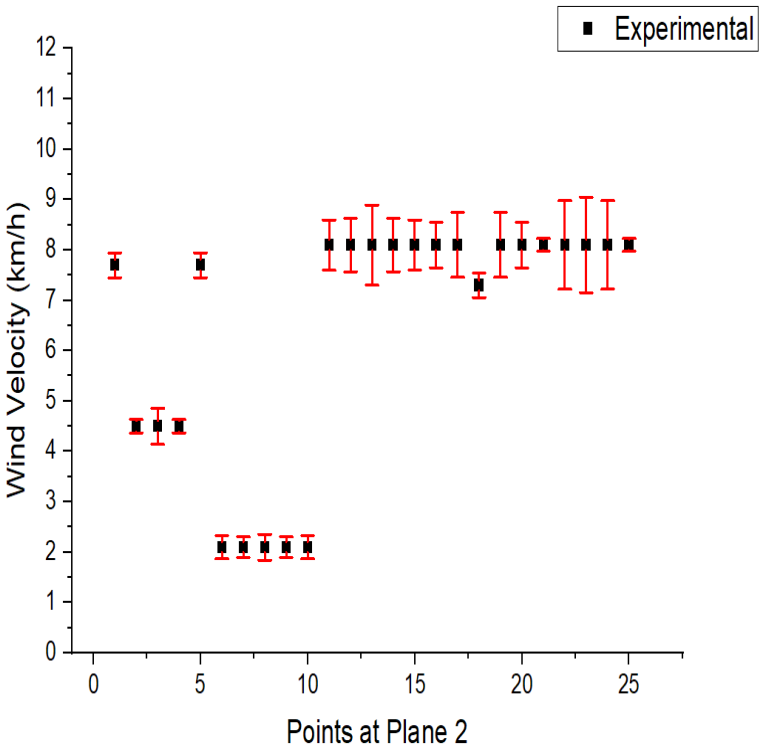

FIGURE 4.2: Experimental Wind Velocity on Plane 2 (bars represent deviation from Computational values)

The table 4.3 shows the percentage error in experimental and computational values at each virtual point. These values were shown graphically in figure 4.2.

TABLE 4.3: Percentage error in Experimental and Computational Values at Plane 2

Plane 2			
Virtual Points	**Experimental Velocity (km/h)**	**Computational Velocity (km/h)**	**Percentage error (%)**
1	7.7	7.454	3.195
2	4.5	4.369	2.911
3	4.5	4.141	7.978
4	4.5	4.369	2.911
5	7.7	7.454	3.195
6	2.1	1.870	10.952
7	2.1	2.305	-9.762
8	2.1	1.844	12.190
9	2.1	2.305	-9.762
10	2.1	1.870	10.952
11	8.1	8.599	-6.160
12	8.1	7.569	6.556
13	8.1	7.304	9.827
14	8.1	7.569	6.556
15	8.1	8.599	-6.160
16	8.1	8.554	-5.605
17	8.1	8.745	-7.963
18	7.3	7.057	3.329
19	8.1	8.745	-7.963
20	8.1	8.554	-5.605
21	8.1	8.223	-1.519
22	8.1	8.977	-10.822
23	8.1	7.151	11.716
24	8.1	8.977	-10.822
25	8.1	8.223	-1.519

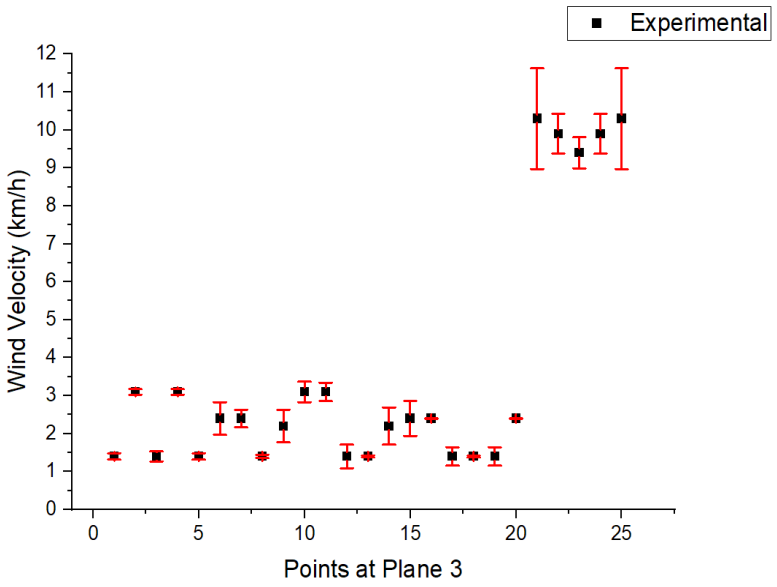

FIGURE 4.3: Experimental Wind Velocity on Plane 3 (bars represent deviation from Computational values)

4.1.3 Experimental and Computational Air velocity comparison on Plane 3

The third virtual plane was considered after the lower foot. At the third plane, the vortex generates and the pressure is maximum at the bottom. Maximum 22.29% error was recorded at point 12. There were seven points where the error percentage was greater than 10%. This error is due to vortex generation in turbulent flow.

TABLE 4.4: Percentage error in Experimental and Computational Values at Plane 3

Plane 3			
Virtual Points	**Experimental Velocity (km/h)**	**Computational Velocity (km/h)**	**Percentage Error (%)**
1	1.4	1.486	-6.143
2	3.4	3.024	2.452
3	1.4	1.272	9.143
4	3.1	3.024	2.452
5	1.4	1.486	-6.143
6	2.4	2.829	-17.875
7	2.4	2.630	-9.583
8	1.4	1.357	3.071
9	2.2	2.630	-19.545
10	3.1	2.829	8.742
11	3.1	2.859	7.774
12	1.4	1.712	-22.286
13	1.4	1.425	-1.786
14	2.2	1.712	22.182
15	2.4	2.859	22.182
16	2.4	2.396	0.167
17	1.4	1.160	17.143
18	1.4	1.423	-1.643
19	1.4	1.160	17.143
20	2.4	2.396	0.167
21	10.3	11.628	-12.893
22	9.9	9.376	5.293
23	9.4	9.809	-4.351
24	9.9	9.376	5.293
25	10.3	11.628	-12.893

The table 4.4 shows the percentage error in experimental and computational values at each virtual point. These values were shown graphically in figure 4.3.

4.2 Computational Analysis

The experimental analysis was successfully validated. The computational setup was initialised to study the damage induced by wind at different wind velocities. For FSI analysis, the Fluid Flow (Fluent) model of ANSYS Workbench 2021 R2 was carefully setup to study the damage induced by wind at different wind velocities. The boundary conditions were carefully initialised to carry out the research. For FSI analysis, the Fluid Flow (Fluid) model of ANSYS Workbench 2021 R2 was carefully setup. After many attempts, the residuals converged. The CFD-Post was used to visualise pressure and velocity streamlines and contours. The figure 4.4 shows the streamlines at 120 km/h wind velocity. High turbulence is created between the gaps and sides of the solar PV mounting structure.

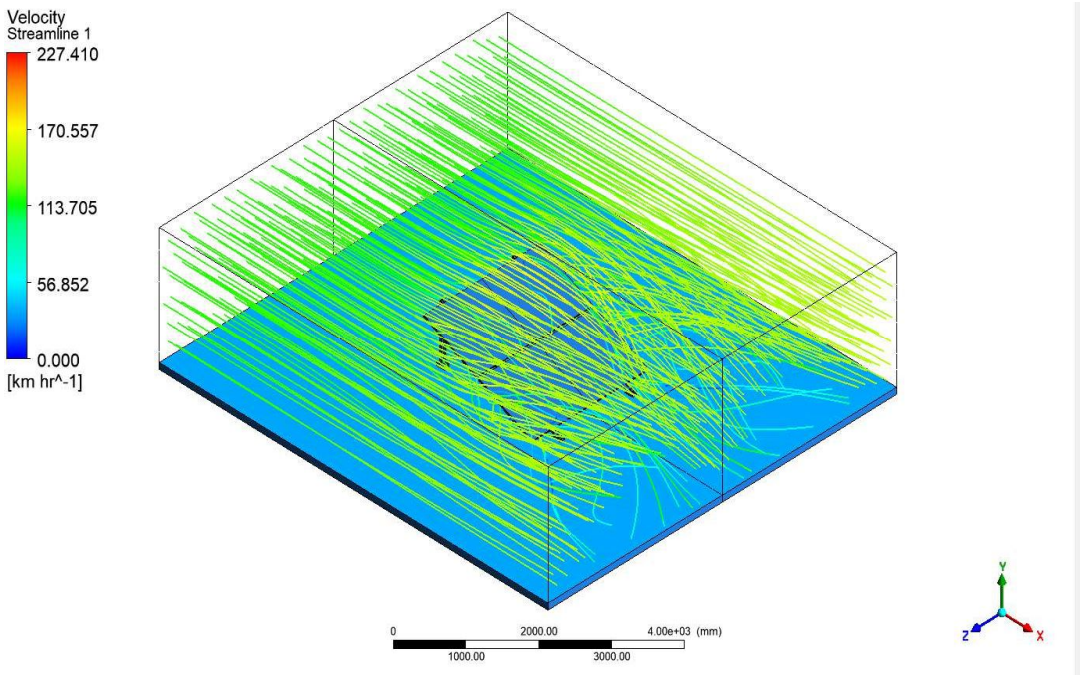

FIGURE 4.4: 120 km/h wind velocity streamlines an isometric view of the solar PV mounting Structure

The figure 4.4 shows the turbulent wind velocity streamlined at 120 km/h from the front view of the solar PV mounting structure.

The figure 4.5 shows the turbulent wind velocity streamlined at 120 km/h from the side view of the solar PV mounting structure. The velocity increases from 120 km/h to 227 km/h which is very high. The velocity exceeded 120 km/h because pressure decreases in above of the solar PV modules and vortex formed.

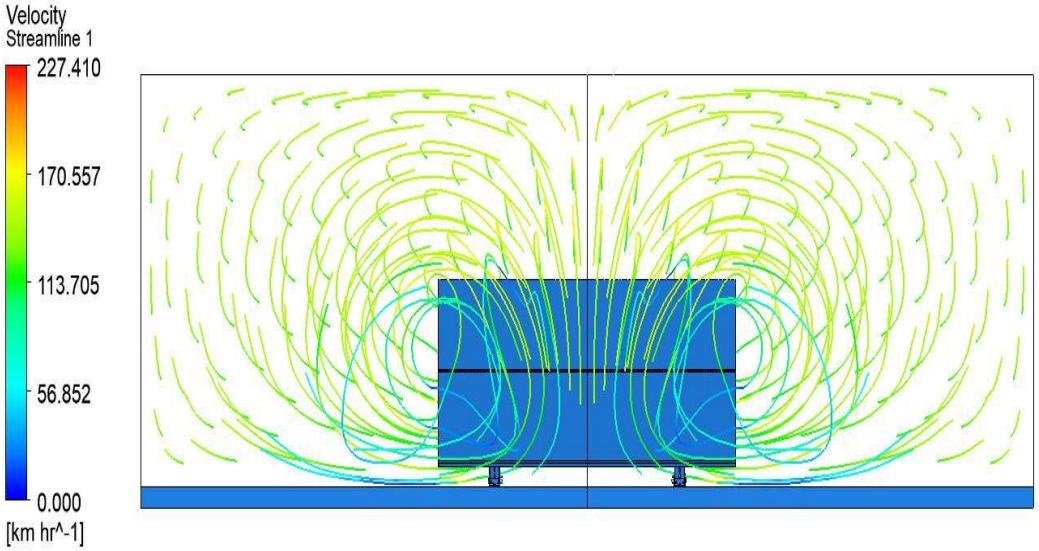

FIGURE 4.5: 120 km/h wind velocity streamlines front view of solar PV mounting Structure

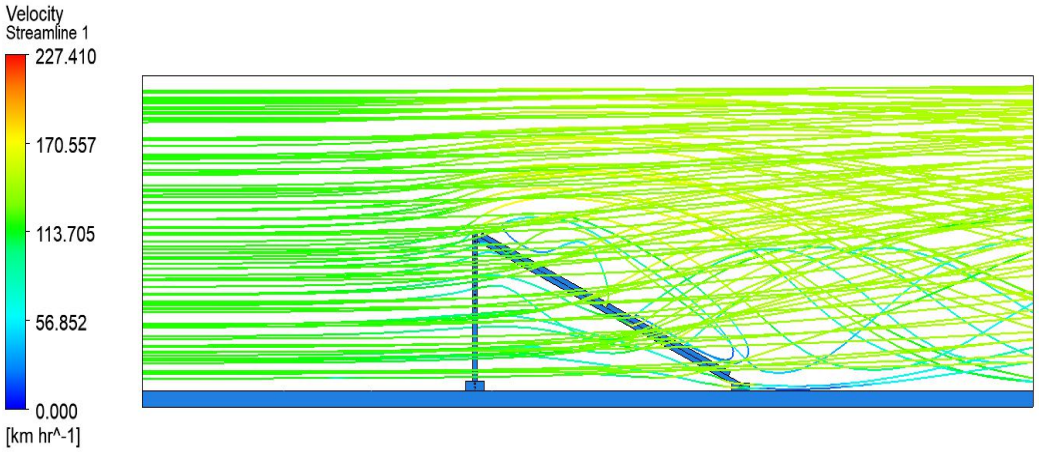

FIGURE 4.6: 120 km/h wind velocity streamlines front view of solar PV mounting Structure

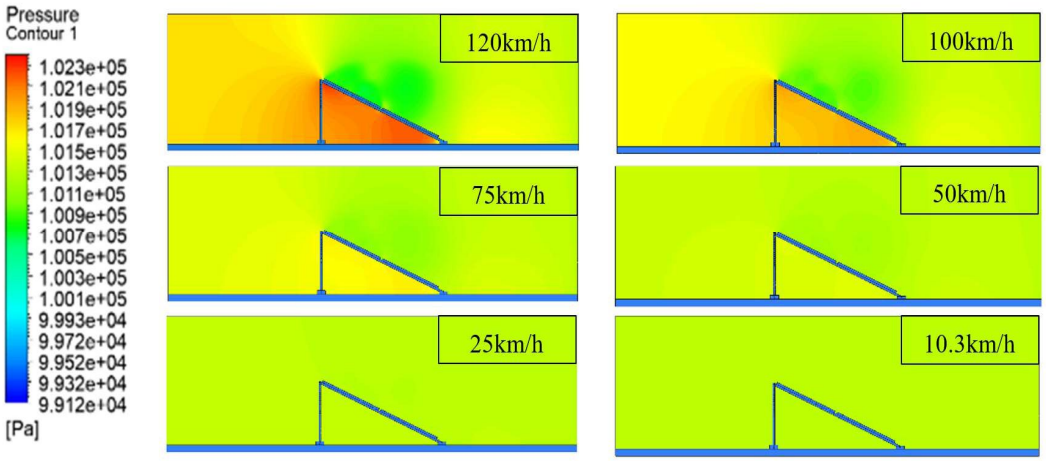

FIGURE 4.7: Pressure Contours on symmetric plane of Solar PV Mounting Structure

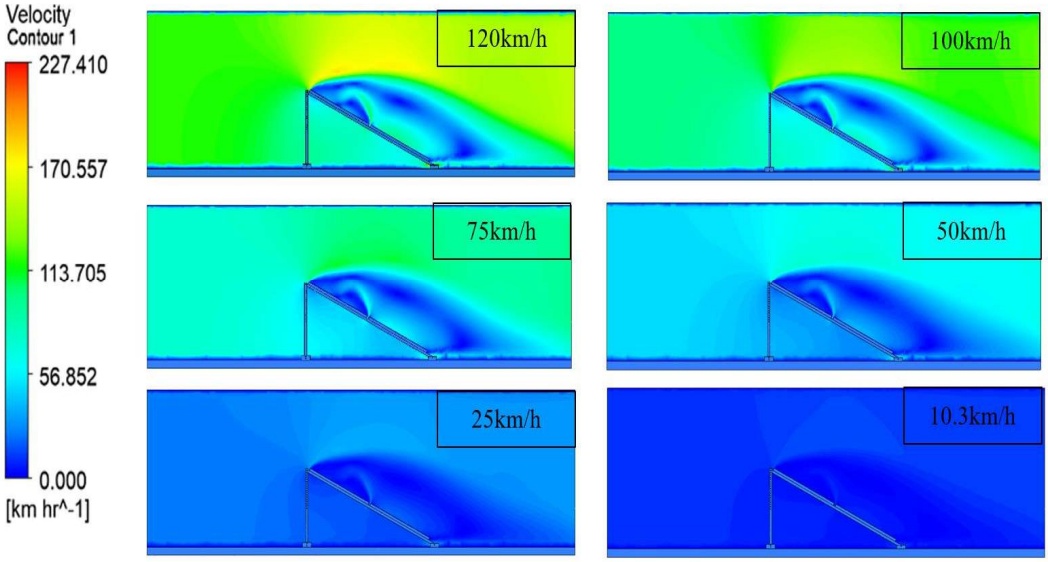

FIGURE 4.8: Velocity contours on symmetric plane of Solar PV Mounting Structure

The figure 4.6 shows the pressure contour from 10.3 km/h to 120 km/h wind velocity. Wind speeds ranging from 10.3 km/h to 50 km/h put little strain on the solar PV mounting structure. The pressure increases as it enters the gale region. At 75 km/h wind velocity, the pressure at the back of the solar panel increases rapidly, and the mounting structure deforms at 100 km/h wind velocity.

The plane in the symmetric region of the 3D model was considered to visualise the contours of velocity. Figure 4.7 shows the velocity contours of the solar PV mounting structure.

4.2.1 Graphical Representation of 14 Gauge Solar PV Mounting Structure

The solution of fluent data was integrated with static structural data in the ANSYS workbench to perform FSI analysis. The equivalent stresses and total deformations of the solar PV mounting structure at different wind velocities were calculated. Equivalent stresses on each part of the mounting structure were calculated in solution. The results show that the solar PV mounting structure for 2 solar panels bears wind pressure in a gale region and does not exceed yield strength. The

structure deforms at 79 km/h wind velocity and exceeds ultimate tensile strength at 110 km/h. The results indicated that the mounting structures for solar panels installed in Pakistan are not safe.

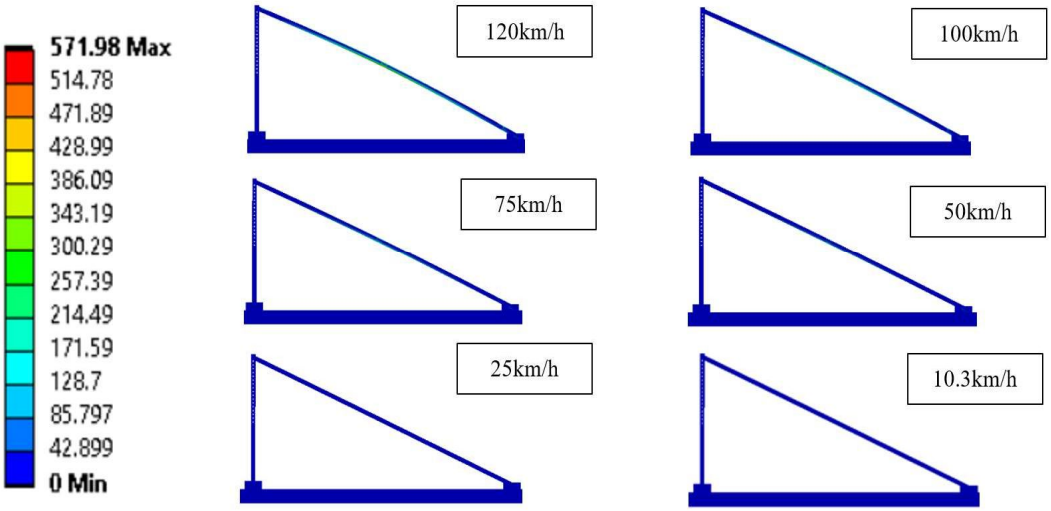

FIGURE 4.9: Equivalent Stress (MPa) of 14 Gauge Solar PV Mounting Structure

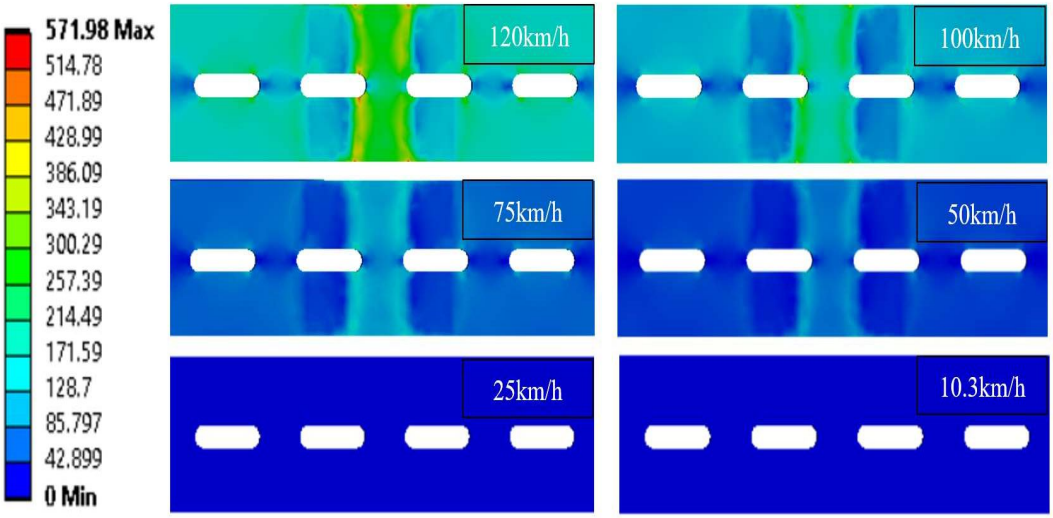

FIGURE 4.10: Equivalent Stress (MPa) on centre-top of Main Support of 14 Gauge Solar PV Mounting Structure

The top view of equivalent stresses on the main support at different wind velocities is shown in figure 4.10. The legends were set according to the equivalent stress at 120 km/h wind velocity. The equivalent stress contours show the effect of wind velocity on the main support of the solar PV mounting structure. It resulted in the main support having its maximum load at the centre, where the solar panels are bolted. The main support damages at 79 km/h wind velocity with 260 MPa equivalent stress and breaks at 110km/h wind velocity.

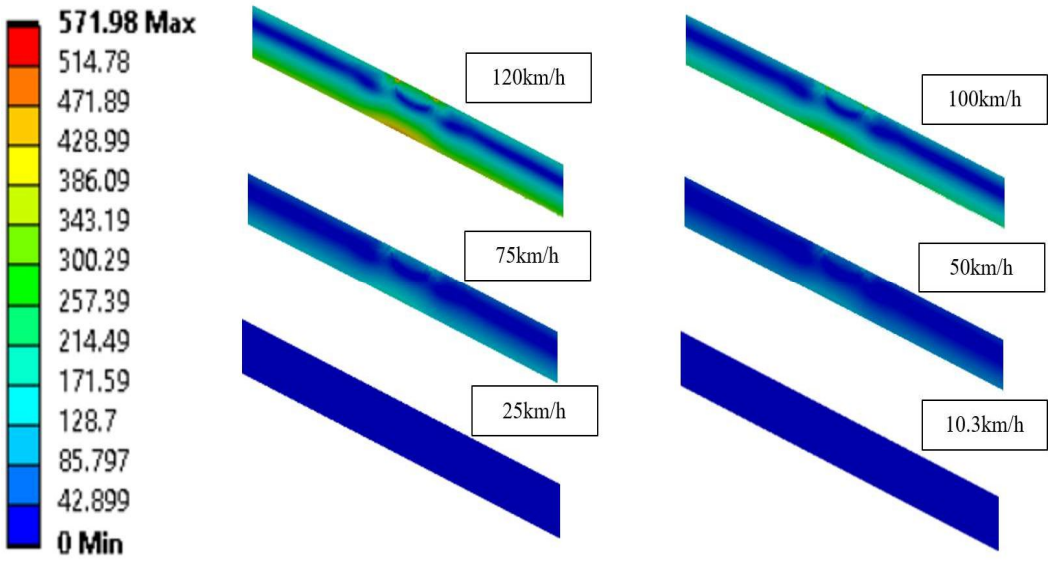

FIGURE 4.11: Side view Equivalent Stress (MPa) 14 Gauge Structure

The side view of equivalent stresses on the main support at different wind velocities is shown in figure 4.11. The results show that the main support has maximum load at the centre where the solar panels are bolted, as shown in figure 4.11. The contours show the structural changes according to wind velocity.

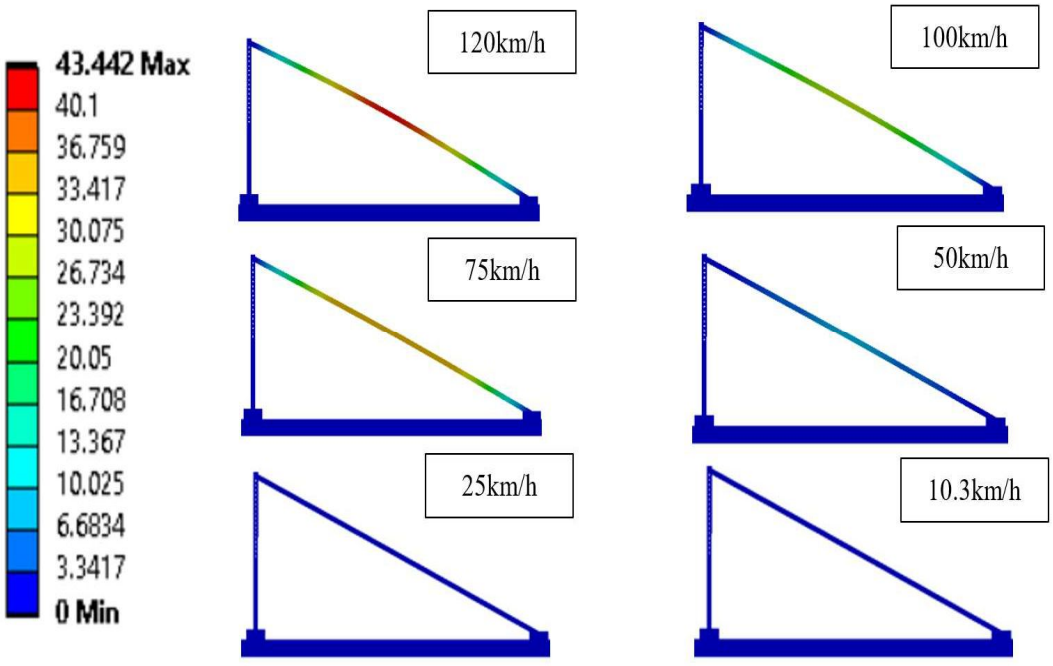

FIGURE 4.12: Total Deformation (mm) of 14 Gauge structure

The wind velocity induces stress in the solar PV mounting structure, and the structure deforms according to wind velocities. The total deformation in solar PV mounting structure is shown in figure 4.12 according to wind velocities under study.

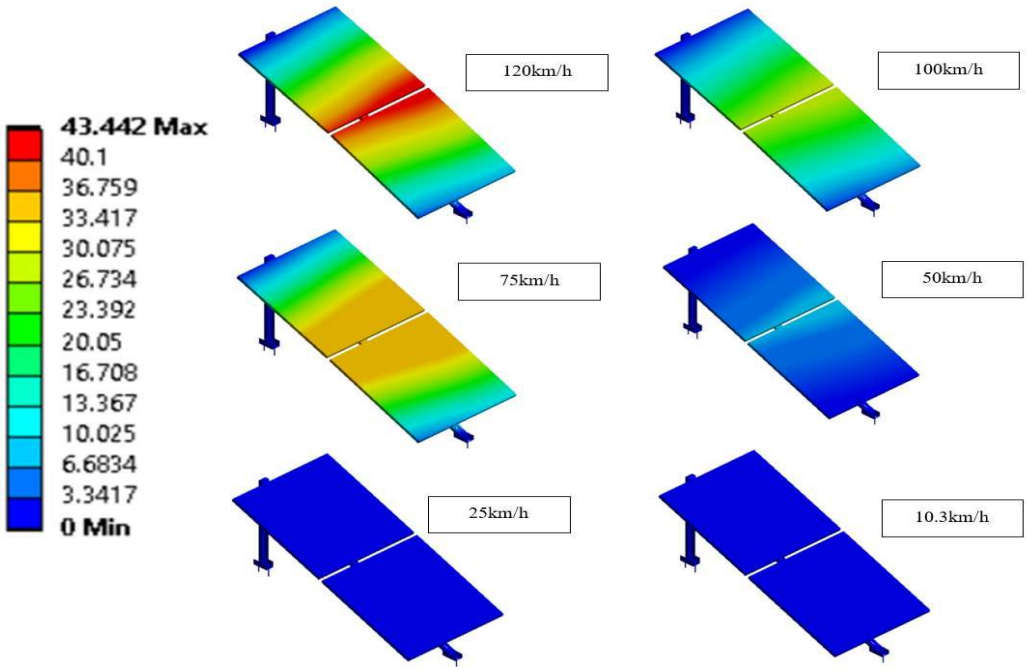

FIGURE 4.13: Total Deformation (mm) of symmetric 14 Gauge structure in isometric view

The figure 4.13 shows total deformation in half of the PV mounting structure with solar panels. The deformation occurred in the main support of the mounting structure and resulted in deformation of the solar panel.

4.2.2 Equivalent Stresses of 14 Gauge Solar Mounting Structure

4.2.2.1 All Parts

The equivalent stress of all parts was measured using an ANSYS static structural solution. The contact regions were carefully defined to extract the FSI results. This study focuses on rooftop solar PV mounting structures only. The deformation and stresses on solar panels will not be considered because solar panels are designed to bear high wind pressure, depending on the region class of solar panels. The manufacturer of solar panels defines the solar panels according to country or region and mentions the class on the specification sheet. In this graph, all the equivalent stresses on 18 parts of a 14 gauge solar mounting structure at each air velocity were compared and plotted in figure 4.14.

The equivalent stress of main support is maximum at each velocity. This graph shows that the equivalent stress is increasing rapidly as wind velocity increases. The 14 gauge solar mounting structure is stable when wind velocity is in the start of the strong gale region on the Beaufort wind force scale, which is from 75 km/h to 88 km/h. At the strong gale region, which starts at 75 km/h wind velocity, the equivalent stress on the main support of the structure is 221.62 MPa which is less than the yield strength of steel, which is 250 MPa. Ultimately, it fails below 100 km/h wind velocity, which is less than the structural stability at 120 km/h minimum assigned by the NDMA in the Pakistan Building Code. The minimum safety factor assigned in Pakistan's building code is 1.25. So, the solar PV mounting structure should withstand at least 150 km/h wind velocity.

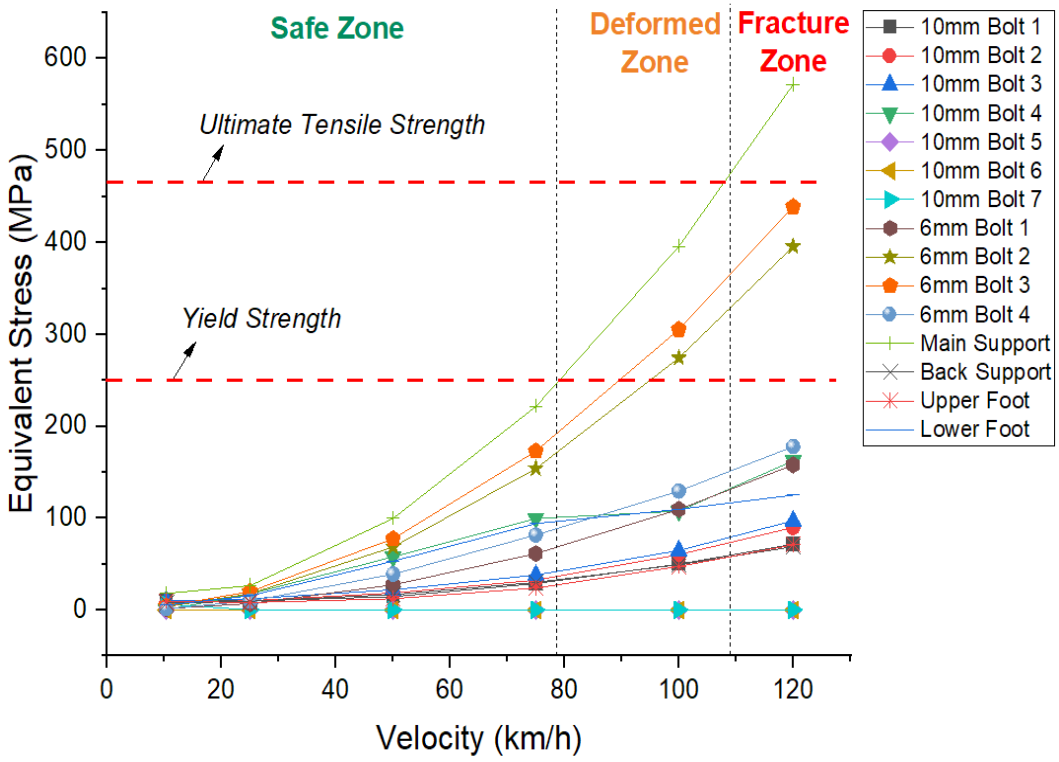

FIGURE 4.14: Equivalent Stresses of different parts at different velocities of 14 gauge solar PV mounting structure

4.2.2.2 10mm Bolts used to Fix the Mounting Structure

The 10mm bolts that are holding the mounting structure are not failing in high wind velocity. There are a total of 14 bolts of 10 mm in structure. In symmetric analysis, seven of the bolts were considered for study. The 10 mm bolts used to fix

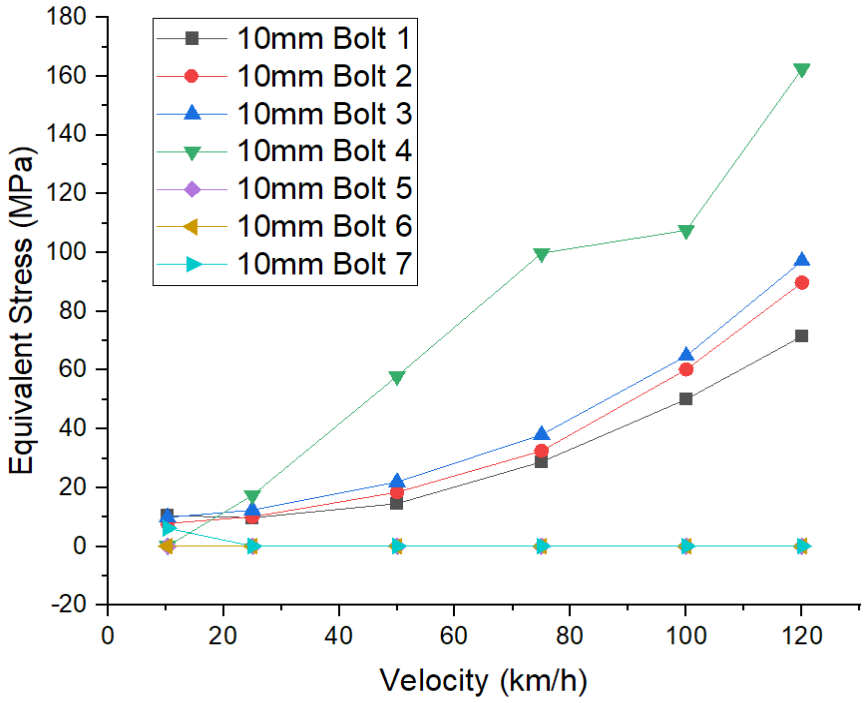

FIGURE 4.15: Equivalent Stresses of 10 mm bolts in 14 gauge solar PV mounting structure

the solar PV mounting structure, whereas the 6mm bolts were used to fix the solar PV modules with the main support of the solar PV mounting structure. The 4^{th} bolt that is holding the lower foot and mounting structure is bearing maximum stress. While the 5^{th}, 6^{th}, and 7^{th} 10mm bolts have the least amount of stress because they keep the upper and lower foot in contact with the concrete body, the stress is transferred from the main and back supports to the bolts, and then from the bolts to the feet, so the stress is minimal in 5^{th}, 6^{th} and 7^{th} 10mm bolts.

4.2.2.3 6mm Bolts used to Fix the Solar PV Modules

6mm bolts are mounted with the main support and solar panels. Each solar panel is mounted with four bolts. The 2^{nd} and 3^{rd} bolts are in the centre of the main support, so their equivalent stress is higher compared to the 1^{st} and 4^{th} bolt. The 2^{nd} and 3^{rd} bolts of 6mm diameter deform at 90 km/h and 100 km/h respectively as shown in figure 4.16. The main support is failing to withstand strong gale so 6mm bolts will also fail in strong gales as they are dependent on the main support of the structure.

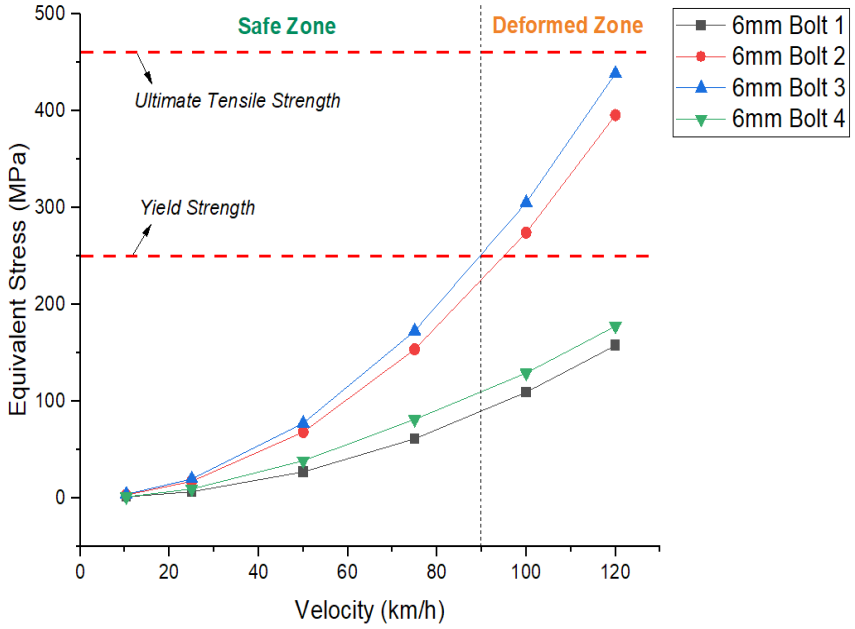

FIGURE 4.16: Equivalent Stresses of 6 mm bolts in 14 gauge solar PV mounting structure

4.2.2.4 Main Support of 14 Gauge Solar PV Mounting Structure

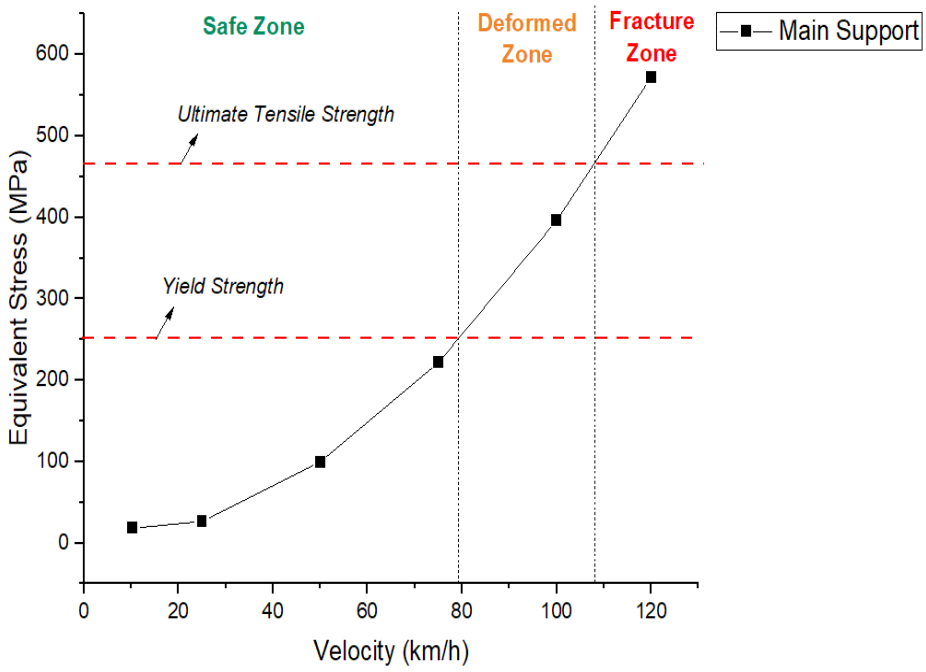

FIGURE 4.17: Equivalent Stress of Main Support in 14 gauge solar PV mounting structure

The main support is the most important part of the mounting structure. Because the main support is preloaded with the weight of the solar panels, wind loads affect other parts of the mounting structure directly. The main support fails in strong gales, so solar panels unbolt and cause damage as they enter the strong

gale scale. The main support deforms at 79 km/h wind velocity and fractures at 110 km/h wind velocity, which is less than the structure design standard approved in Pakistan.

4.2.2.5 Back Support of 14 Gauge Solar PV Mounting Structure

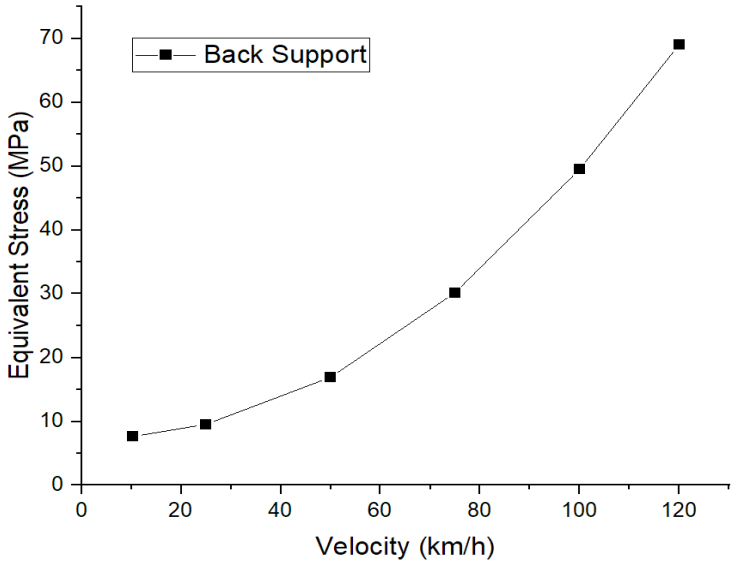

FIGURE 4.18: Equivalent Stress of Back Support in 14 gauge solar PV mounting structure

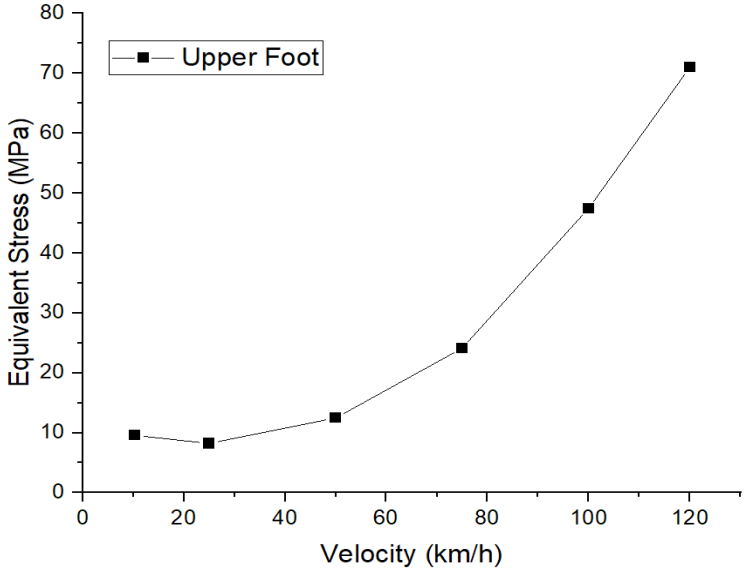

FIGURE 4.19: Equivalent Stress of Upper Foot in 14 gauge solar PV mounting structure

The back support of the solar mounting structure holds the main support and the upper foot of the body. The back support is in contact with three 10mm bolts, so the back support has lower stress than the main support. 4^{th} 10mm bolt is

holding main support with the lower foot, so equivalent stress is lower in the lower foot than 4^{th} 10 mm bolt as shown in figure 4.18.

4.2.2.6 Upper Foot of 14 Gauge Solar PV Mounting Structure

The upper foot holds back support and is connected to the concrete floor via four 10mm bolts. The upper foot is within safe limits when subjected to strong wind velocity because it is constrained with 5^{th} and 6^{th} 10 mm bolts as shown in figure 4.19.

4.2.2.7 Lower Foot of 14 Gauge Solar PV mounting structure

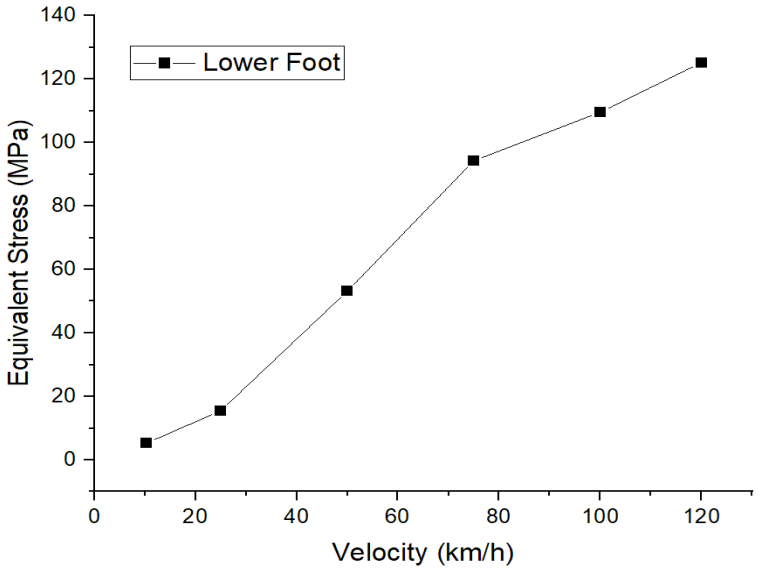

FIGURE 4.20: Equivalent Stress of Lower Foot in 14 gauge solar PV mounting structure

The lower foot is stressed more than the upper support because the main support is directly contacted by the main support via 4^{th} 10 mm bolt as shown in figure 4.20. The equivalent stress transfers from the main support to the lower foot. The lower foot is grounded with a 10 mm bolt on a concrete floor.

4.2.2.8 Equivalent Stress Behaviour at Different Points of Main Support

The Figure 4.21 shows the location of points in main stress.

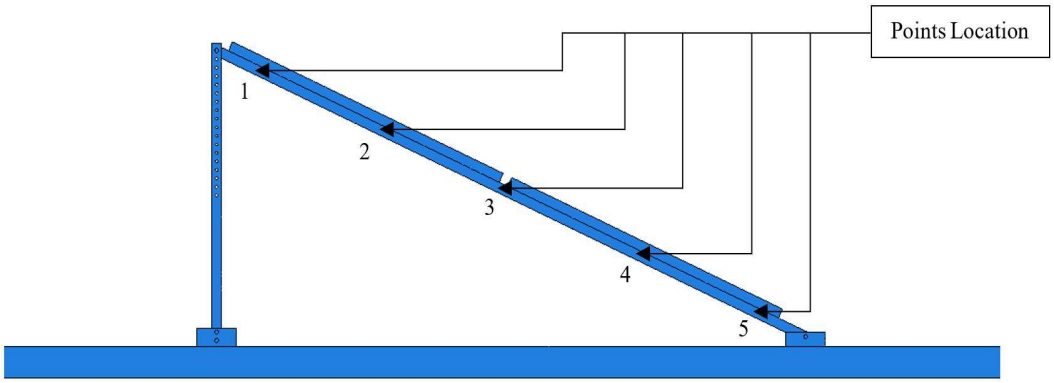

FIGURE 4.21: Points location on main support of mounting structure

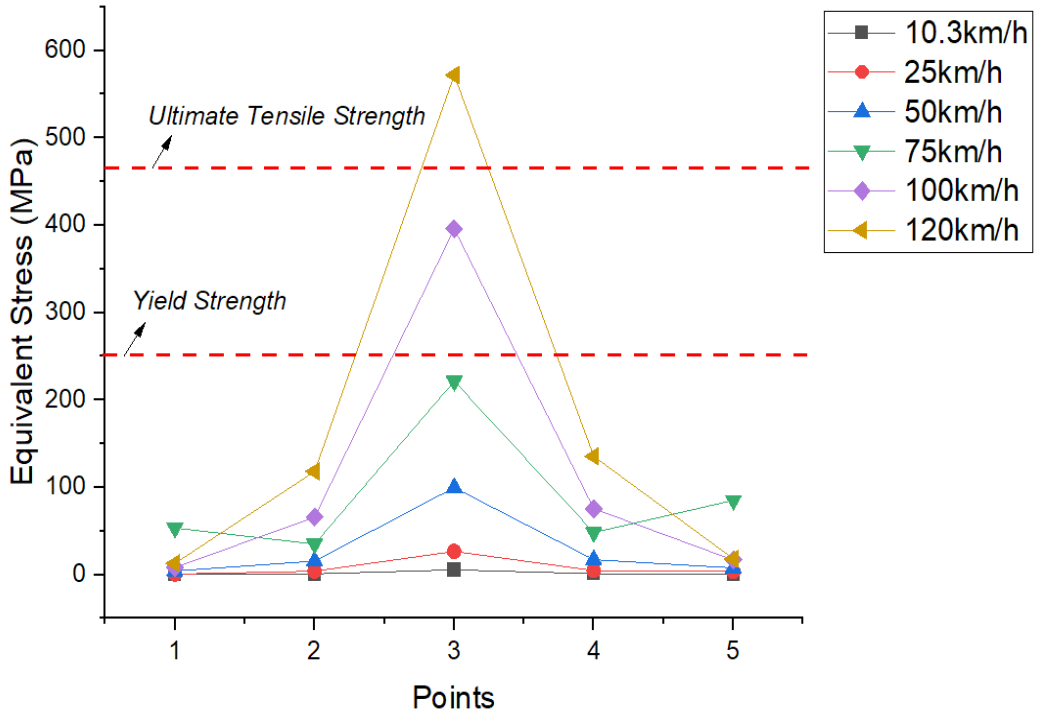

FIGURE 4.22: Equivalent Stress at different points on Main Support of 14 Gauge Structure

In figure 4.22, the graph shows that the main support is failing at point 3, which is located between 6 mm bolt 2 and bolt 3. The wind load is highest at point 3 on each wind velocity. The structure rapidly deforms in less than 100 km/h wind velocity and suddenly fractures at 120 km/h.

4.2.3 Total Deformation at Different Points of 14 gauge Solar PV Mounting Structure

The total deformation of different bodies is directly dependent on the quality of the

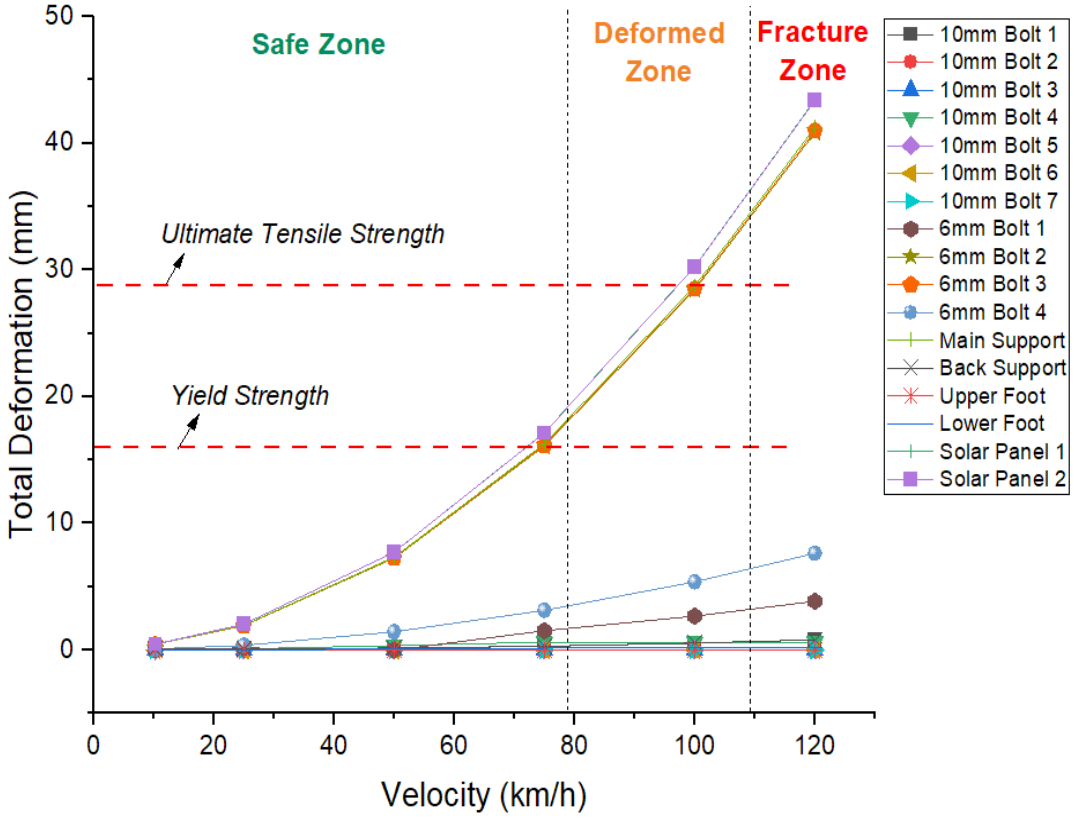

FIGURE 4.23: Total Deformation of Different Parts at Different Velocities of 14 Gauge Solar PV Mounting Structure

solar PV mounting structure. In this case, the main support plays an important role because the whole structure is in contact with the main support due to the preload on the solar panels. The deflection in the main support is 16.232 mm at 75 km/h wind velocity. After 75 km/h wind velocity, the main support fails, so considering other deformation values, we are not concerned.

4.3 Graphical Representation of 16 Gauge Solar PV Mounting Structure

4.3.1 Equivalent Stresses of 16 Gauge Solar Mounting Structure

The figure shows the equivalent stress in the centre of the main support of the 16 gauge solar PV mounting structure. The equivalent stress contours show the effect

of wind velocity on the main support of the solar PV mounting structure. There is a rapid change in equivalent stress when wind velocity increases from 50 km/h to 75 km/h. The contours show the equivalent stress change for different wind velocities. It resulted in the main support having its maximum load at the centre, where the solar panels are bolted. The main support damages at 79 km/h wind velocity with 260 MPa equivalent stress and fractures at 100 km/h wind velocity.

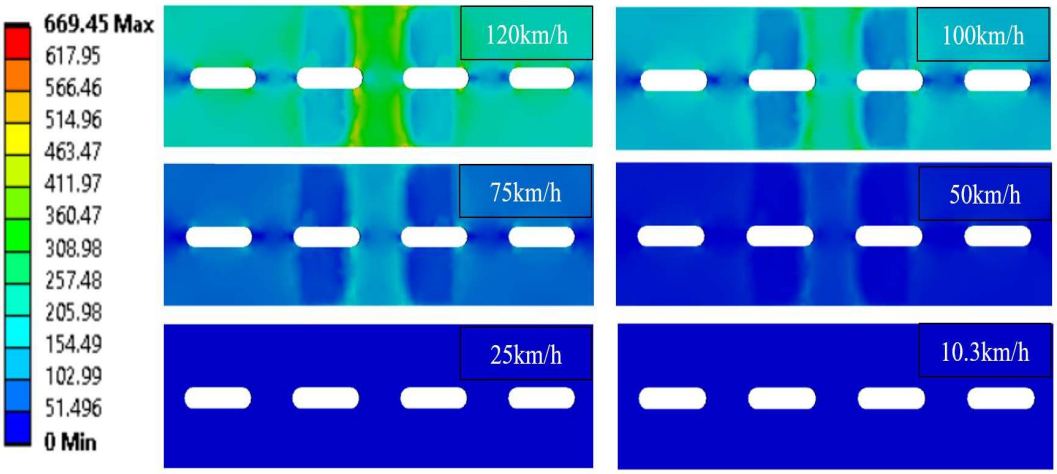

FIGURE 4.24: Equivalent Stress (MPa) on centre-top of Main Support of 16 Gauge Solar PV Mounting Structure

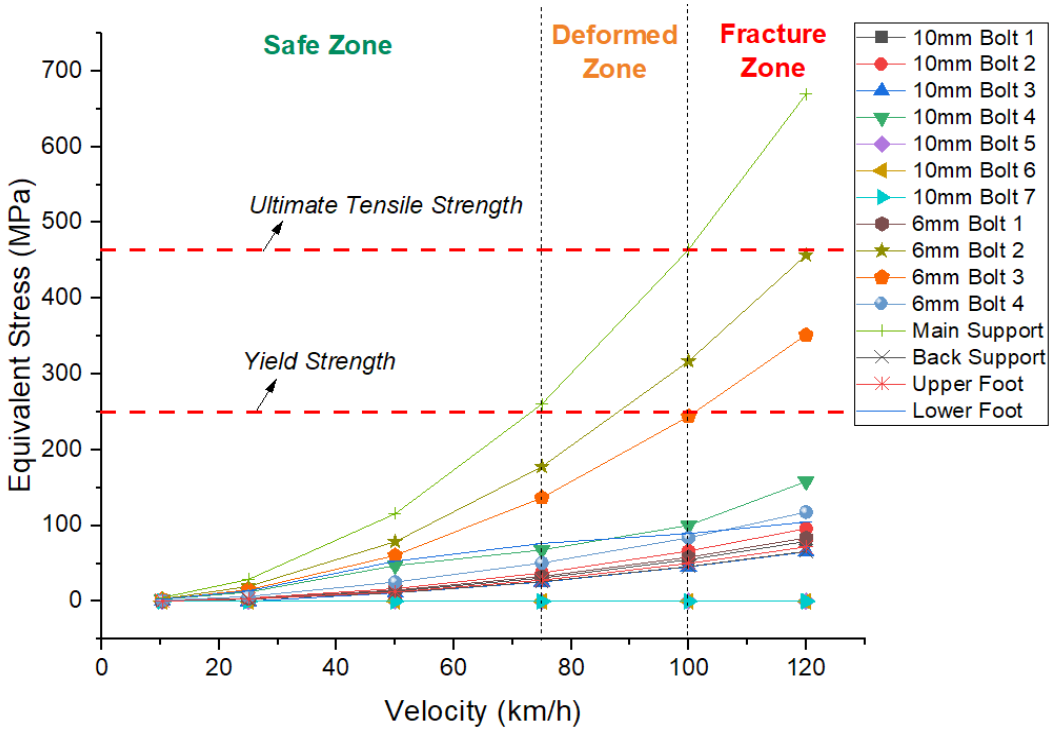

FIGURE 4.25: Equivalent Stresses of different parts at different velocities of 16 Gauge Solar PV Mounting Structure

4.3.1.1 All Parts

The equivalent stress of the main support is also maximum in the 16 gauge solar PV mounting structure for each velocity. The 16 gauge solar mounting structure is stable when wind velocity is in the gale region on the Beaufort wind force scale. At the strong gale region, which starts from 75 km/h wind velocity, the equivalent stress on the main support of the structure is 260.36 MPa which exceeds the yield strength of steel which is 250 MPa. The structure must withstand at least 120 km/h wind velocity, according to Pakistan's building code.

4.3.1.2 10mm Bolts used to Fix the Mounting Structure

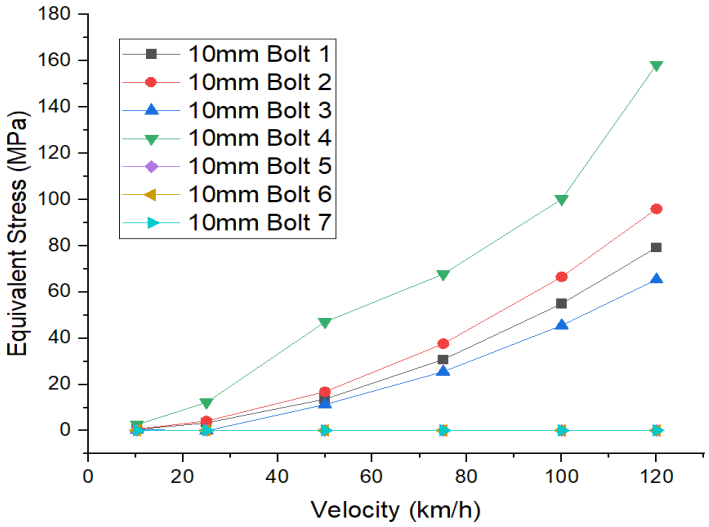

FIGURE 4.26: Equivalent Stresses of 10 mm bolts in 16 Gauge Solar PV Mounting Structure

There are a total of 7 bolts that hold the solar PV mounting structure in a symmetrical body. The 4^{th} bolt has maximum stress because it is linked directly to the main support. The 10mm bolts are within safe limits and below the yield strength of steel.

4.3.1.3 6mm Bolts used to Fix the Mounting Structure

6 mm bolts are contacted with the solar panels and main support. The main support fails in strong winds. The result shows that the 6mm bolts are in the elastic region up to 75 km/h wind velocity.

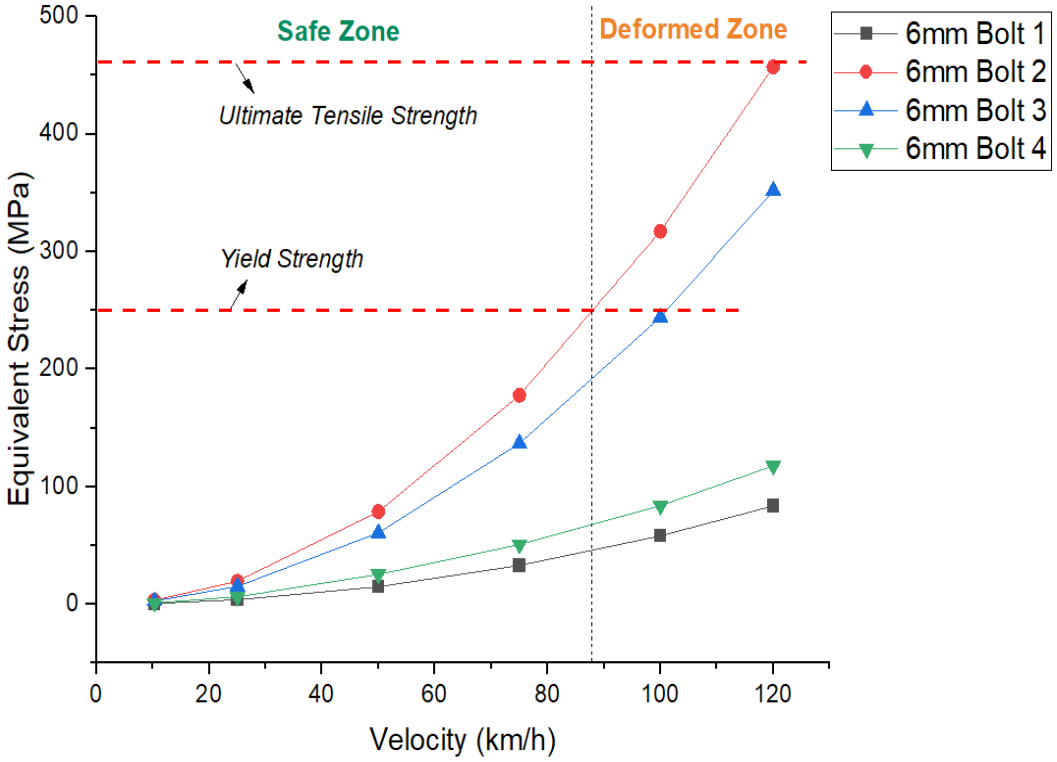

FIGURE 4.27: Equivalent Stresses of 6 mm bolts in 16 Gauge Solar PV Mounting Structure

4.3.1.4 Main Support of 16 Gauge Solar PV Mounting Structure

The whole mounting structure is dependent on the main support. The main support fails to bear wind loads in gale-force regions. The solar structures that were damaged due to high wind velocities were subjected to gales. On June 13, 2021, a maximum wind velocity of 65 km/h was reached when at least 34 solar PV mounting structures were knocked off the ground and damaged in Islamabad and Rawalpindi.

4.3.1.5 Back Support of 16 Gauge Solar PV Mounting Structure

Back support helps to keep the solar PV mounting structure at a specific angle. In our case, both 14 and 16 gauge mounting structures are angled at 24°. The standard solar mounting structure in Pakistan is angled from 23° to 32°. 24° angle is widely used for 52 0W to 550 W solar panels, so 24° angle was considered for this study. The back support is contacted at the upper and lower foot with three

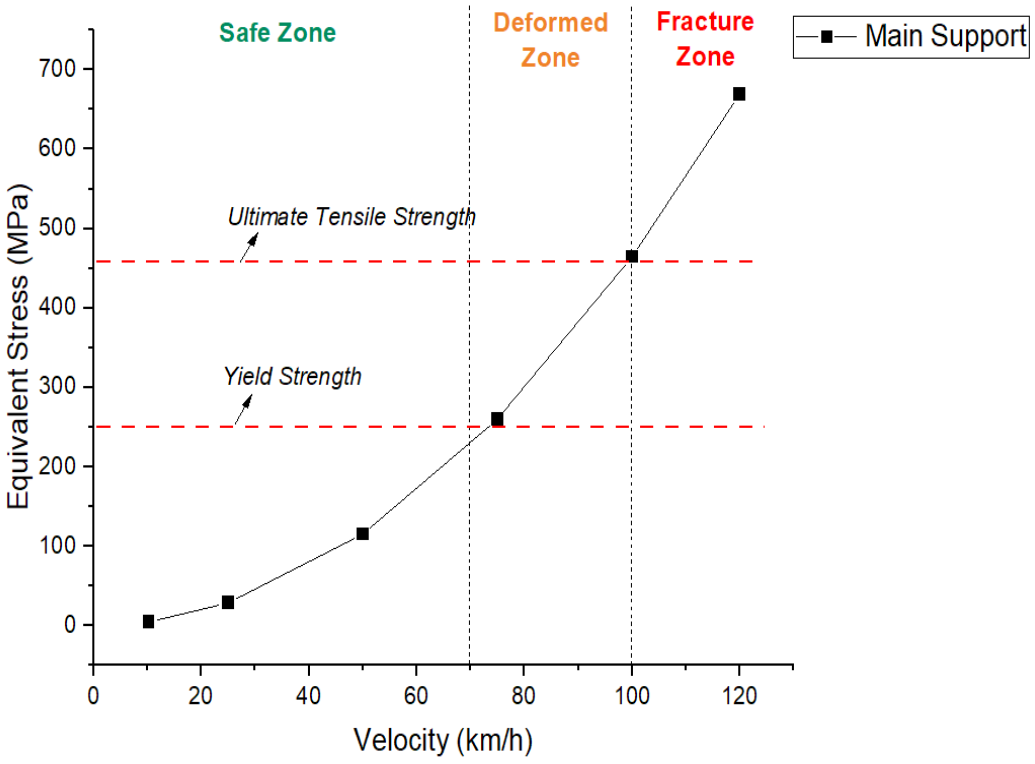

FIGURE 4.28: Equivalent Stress of main support in 16 Gauge Solar PV Mounting Structure

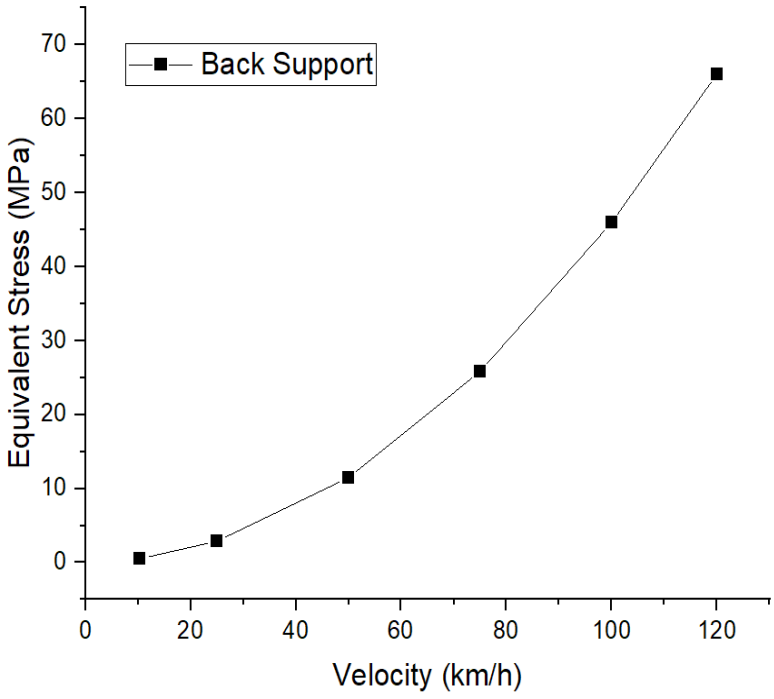

FIGURE 4.29: Equivalent Stress back support in 16 Gauge Solar PV Mounting Structure

10 mm bolts. The back support is at its elastic limit, with a maximum 66 MPa at 120 kmh wind velocity.

4.3.1.6 Upper Foot of 16 Gauge Solar PV Mounting Structure

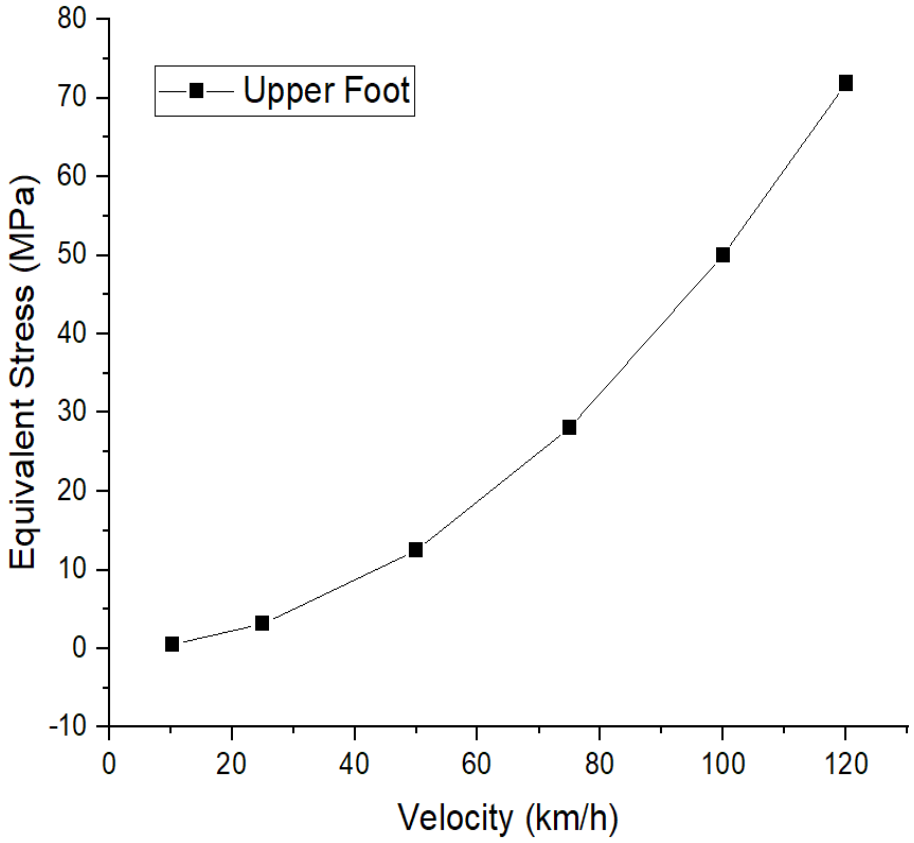

FIGURE 4.30: Equivalent Stress of upper foot in 16 Gauge Solar PV Mounting Structure

The upper foot is the least loaded foot, as it is grounded by two 10mm bolts in the concrete floor. When the solar PV mounting structure is subjected to wind velocity, it transfers the wind load to the main support first. The main support transfers the equivalent stress according to the assembly of the parts. So, it transfers the load to the back support and then to the upper foot. Upper foot has maximum 71.88 MPa equivalent stress at 120 km/h.

4.3.1.7 Lower Foot of 16 Gauge Solar PV Mounting Structure

The lower foot has two punches at the bottom to bolt it. In Pakistan, at most of the sites, the installers drill one hole for each lower foot for their ease, which is modelled while considering real-life scenarios. The lower foot remains in a safe stress range under its elastic limit, which is 104.59 MPa at 120 km/h wind velocity.

4.3.2 Total Deformation at Different Points of 16 Gauge Solar PV Mounting Structure

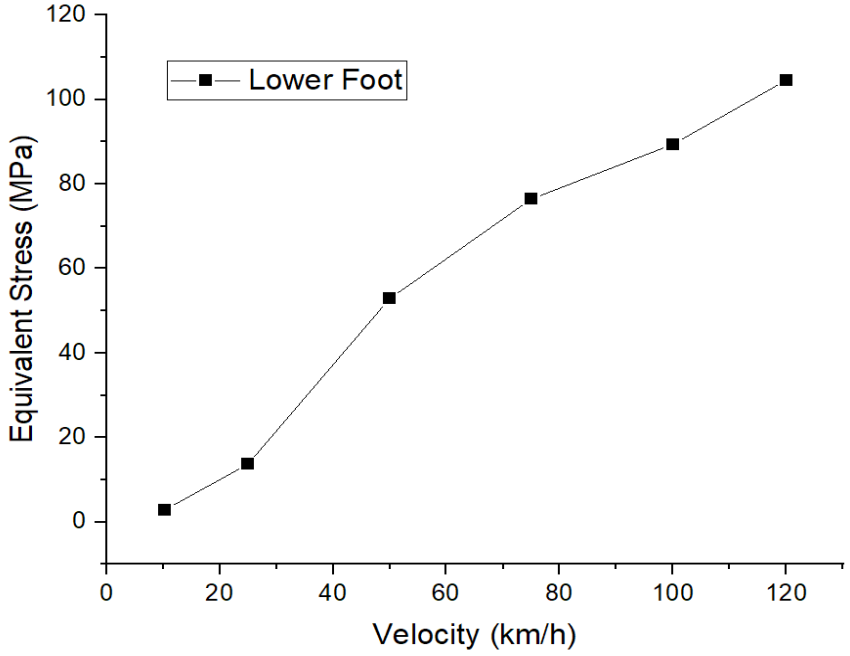

FIGURE 4.31: Equivalent Stress of lower foot in 16 Gauge Solar PV Mounting Structure

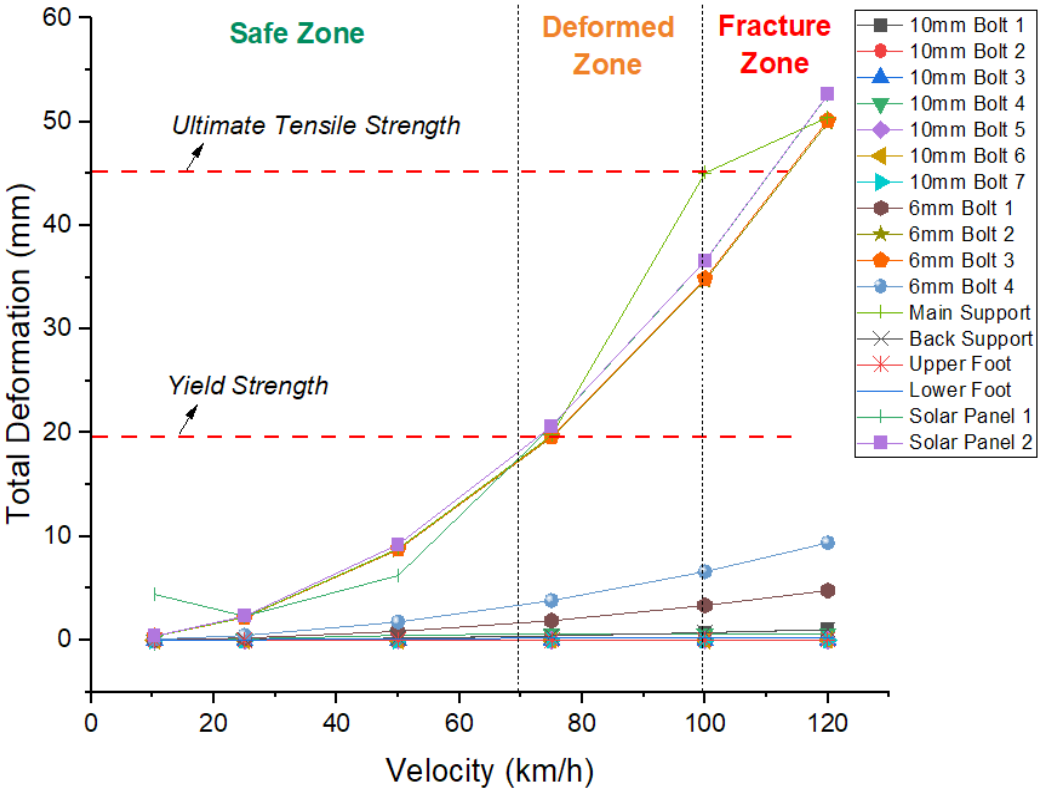

FIGURE 4.32: Total deformation of different parts in 16 Gauge Solar PV Mounting Structure

The total deformation of solar panels is at its maximum because it is dependent on the structure's strength. Main support exceeded yield strength at a strong gale, so solar panels connected to the main support with 6 mm bolts, so they are directly related. The deformation in the main support is defined by the deformation in the mounting structure.

4.4 Equivalent Stress Comparison of 12, 14 Gauge and 16 Gauge Main Support

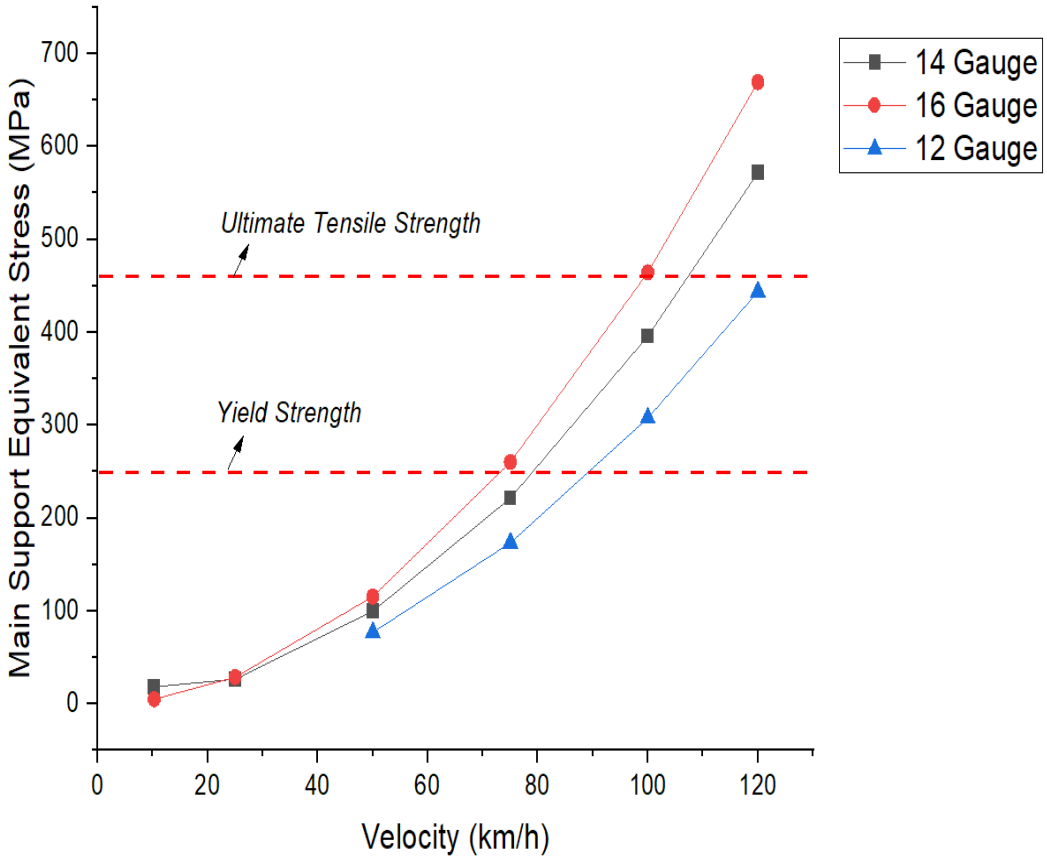

FIGURE 4.33: Equivalent Stress on main support of 12, 14 and 16 gauge solar PV mounting structure

The computational FSI simulation was carried out for a 12 gauge solar PV mounting structure. The 12 gauge structure has a 2.573 mm thickness. All other dimensions of the structure were the same. Although the 12 gauge mounting structure is not used in Pakistan for solar PV module mounting, it was necessary to study the structural behaviour of the superior 12 gauge structure. The 12 gauge structure deforms at 90 km/h but does not exceed the ultimate tensile strength, as shown in

figure 4.33. The 14 gauge steel mounting structure has a thickness of 2 mm, while 16 gauge has a thickness of 1.613 mm. So, the load bearing capacity of 14 gauge structure is higher than a 16 gauge structure but less than 12 gauge structure. The 14 gauge structure is at its elastic limit at a wind velocity of 75 km/h in the strong gale region of the Beaufort wind scale, while the 16 gauge structure exceeds the yield strength and deforms at 75km/h. Both 14 gauge and 16 gauge solar PV mounting structures used in Pakistan fracture below 120 km/h.

4.5 Validation of Computational Analysis with Analytical Method

The equivalent stress and total deformation were calculated numerically to justify the results. 14 gauge structure subject to wind loads at 120 km/h was considered justifiable with computational results. The reactions on the main support were considered for the numerical solution as the stress and deformation are at their maximum in the main support. Figure 4.34 shows the wind load on the main support of the solar PV mounting structure. Main support was fixed at 10mm bolt location 1, and pin joint at 10mm bolt location 4 were considered. The equivalent stress of back support shown in figure 4.18 is very low at 120 km/h wind velocity, so the main support was considered fixed at point A. The equivalent stress of the lower foot shown in figure 4.20 is pinned with a 10mm bolt, so a pinned joint was considered for numerical analysis.

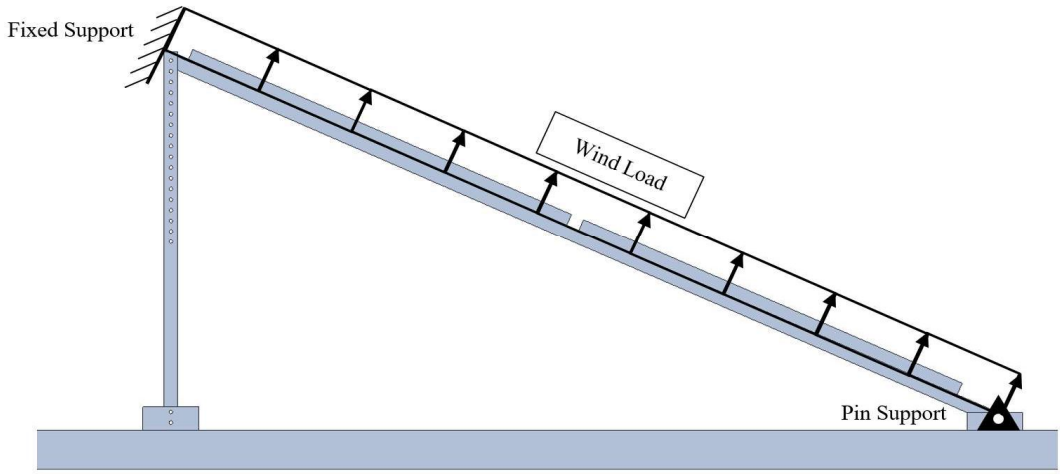

FIGURE 4.34: Wind load on main support of solar PV mounting structure

The main support is 2.5 m long length of C-channel (C-beam) so C-channel cross section formulas were used for calculations. Figure 4.35 shows the section properties of C-channel. The properties of structural steel C-channel was taken from book, Mechanics of Materials in SI units (2017, Pearson), page 317 [71]. A C-channel with cross-sectional dimensions $B \times H$, shelf thicknesses t and wall thickness s shown in figure 4.35.

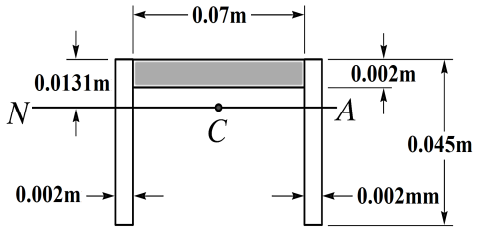

FIGURE 4.35: Section properties of C-channel

For centroid,

$$\begin{aligned}\bar{y} &= \frac{\sum \tilde{y}A}{\sum A} \\ &= \frac{2(0.0225m)(0.045m)(0.002m) + (0.001m)(0.002m)(0.07m)}{2(0.045m)(0.002m) + (0.002m)(0.07m)} \\ \bar{y} &= 0.0131m\end{aligned}$$

Now for moment of inertia,

$$\begin{aligned}I &= \sum \left(\bar{I} + Ad^2\right) \\ &= \left[\frac{1}{12}(0.07m)(0.002m)^3 + (0.07m)(0.002m)(0.0131m - 0.001m)^2\right] \\ &\quad + 2\left[\frac{1}{12}(0.002m)(0.045m)^3 + (0.002m)(0.045m)(0.0225m - 0.0131m)^2\right] \\ I &= 6.682e - 8mm^4\end{aligned}$$

Considering the static response of a one end fixed and other end pinned beam under a varyingly distributed load of trapezoidal shape shown in figure 4.36. The wind load of $969.7Pa$ at point A and the maximum wind load of $1565.2Pa$ at point B were reported from Ansys Fluent. The C-Channel of $2.5m$ length has a mass

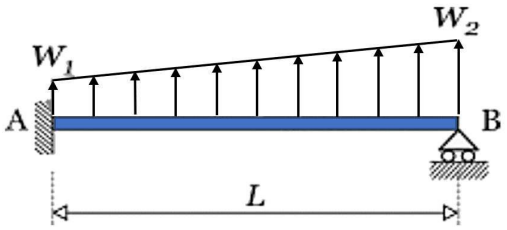

FIGURE 4.36: Fixed - pinned beam with linearly varying distributed load (VDL)

of $5kg$ and the solar panel's mass is $27.2kg$. The solar panels mounting on the structure share half their weight along each length, so, $13.6kg$ mass of each solar panel is loaded on the main support of the solar PV mounting structure. Figure 4.37 shows the distributed load of wind and the forces acting on the beam.

For load w_1,

$$\begin{aligned} w_1 &= (Wind\ Load \times Length\ of\ Beam) + \left(\frac{Mass\ of\ Solar\ Panel \times Gravity}{Length\ of\ beam}\right) \\ &\quad + \left(\frac{Mass\ of\ beam \times Gravity}{Length\ of\ beam}\right) \\ &= \left(969.7\frac{N}{m^2} \times 2.5m\right) + \left(\frac{27.2kg \times 9.81\frac{m}{s^2}}{2.5m}\right) + \left(\frac{5kg \times 9.81\frac{m}{s^2}}{2.5m}\right) \\ w_1 &= 2551\frac{N}{m} \end{aligned}$$

For load w_2,

$$\begin{aligned} w_2 &= (Wind\ Load \times Length\ of\ Beam) + \left(\frac{Mass\ of\ Solar\ Panel \times Gravity}{Length\ of\ beam}\right) \\ &\quad + \left(\frac{Mass\ of\ beam \times Gravity}{Length\ of\ beam}\right) \\ &= \left(1565.2\frac{N}{m^2} \times 2.5m\right) + \left(\frac{27.2kg \times 9.81\frac{m}{s^2}}{2.5m}\right) + \left(\frac{5kg \times 9.81\frac{m}{s^2}}{2.5m}\right) \\ w_2 &= 4039\frac{N}{m} \end{aligned}$$

Now calculating reaction force at point A,

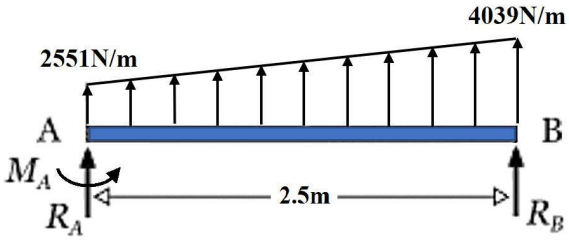

FIGURE 4.37: Applied trapezoidal load in fixed-pinned beam

$$\begin{aligned} R_A &= w_1 \times L \\ &= 2551\frac{N}{m} \times 2.5m \\ R_A &= 6377.5N \end{aligned}$$

For reaction force at point B,

$$\begin{aligned} R_B &= \frac{1}{2}(w_2 - w_1)(L) + (w_1)(L) \\ &= \frac{1}{2}(4039\frac{N}{m} - 2551\frac{N}{m})(2.5m) + (2551\frac{N}{m})(2.5m) \\ R_B &= 8237.5N \end{aligned}$$

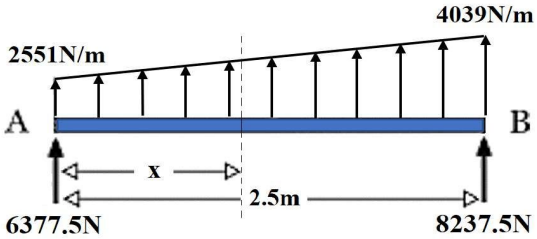

FIGURE 4.38: Loadings at beam with reaction forces and x distance

Calculating moment at x,

$$\begin{aligned} \sum M_x &= -R_A x + (w_1 x)\left(\frac{x}{2}\right) + (w_2 - w_1)\left(\frac{3}{4}x^2\right) \\ &= \frac{w_1 x^2}{2} + (w_2 - w_1)\frac{3}{4}x^2 - R_A x \end{aligned} \tag{4.1}$$

At maximum value of x,

$$\begin{aligned}
\frac{\mathrm{d}}{\mathrm{d}x}|_{x_{max}} &= w_1 x + \frac{3}{2} x\left(w_2 - w_1\right) - R_A = 0 \\
x &= \frac{R_A}{w_1 + \frac{3}{2}\left(w_2 - w_1\right)} \\
&= \frac{6377.5\frac{N}{m}}{2551\frac{N}{m} + \frac{3}{2}\left(4039\frac{N}{m} - 2551\frac{N}{m}\right)} \\
x &= 1.33m
\end{aligned}$$

Substituting $x = 1.33m$ in equation (4.1),

$$M_x = \left(2551\frac{N}{m}\right)\left(\frac{1.33m^2}{2}\right) + \left(4039\frac{N}{m} - 2551\frac{N}{m}\right)\frac{3}{2}\left(1.33m^2\right) - \left(6377.5N\right)\left(1.33m^2\right)$$

$$M_x = -2277.66Nm$$

The negative sign indicates that the moment is acting in a clockwise direction.

For maximum stress,

$$\begin{aligned}
\sigma_{max} &= \frac{M_x \bar{y}}{I} \\
&= \frac{-2277.66Nm \times 0.0131m}{6.682E-8m^4} \\
\sigma_{max} &= -446.5MPa
\end{aligned}$$

The negative sign indicates that stress is increasing. The maximum equivalent stress computed from FSI computational analysis was 435.35 MPa as shown in figure 4.39. Whereas, the maximum stress calculated by the numerical method was 446 MPa. Hence, it is concluded that the computational analysis is valid as the error at the maximum stress point is less than 2.5%.

Hence, it is concluded that the computational analysis is valid as the error at the maximum stress point is less than 2.5%.

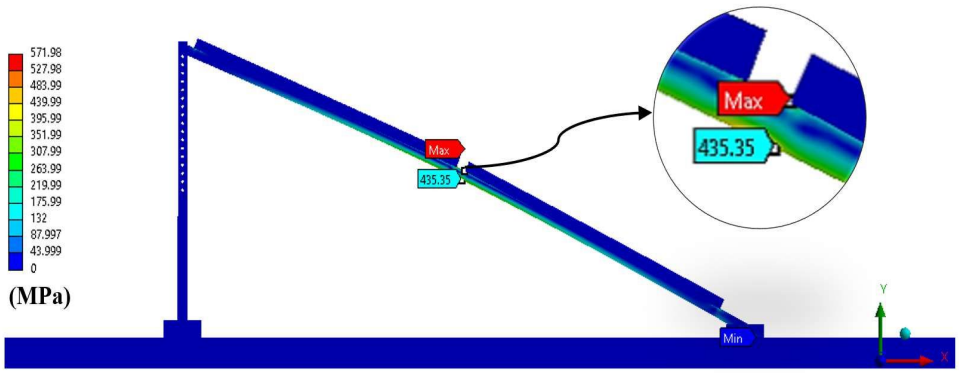

FIGURE 4.39: Maximum Stress from computational analysis at 120km/h wind velocity

For maximum deflection,

$$
\begin{aligned}
y_{max} &= \frac{\left(\frac{w_2+w_1}{2}x^2\right)}{48EI}(L-x)(2x-3L) \\
&= \frac{\left(\frac{4039\frac{N}{m}+2551\frac{N}{m}}{2}\times 1.17^2\right)}{48\times 200E9\times 6.682E-8m^4}(2.5m-1.17m)(2(1.17m)-3(2.5m)) \\
y_{max} &= 0.048m
\end{aligned}
$$

The maximum deformation computed from FSI computational analysis was 0.041 m as shown in figure 4.40. Whereas, the maximum deflection calculated by the numerical method was 0.048 m. The percentage error in computational and numerical analysis is 14.6% only.

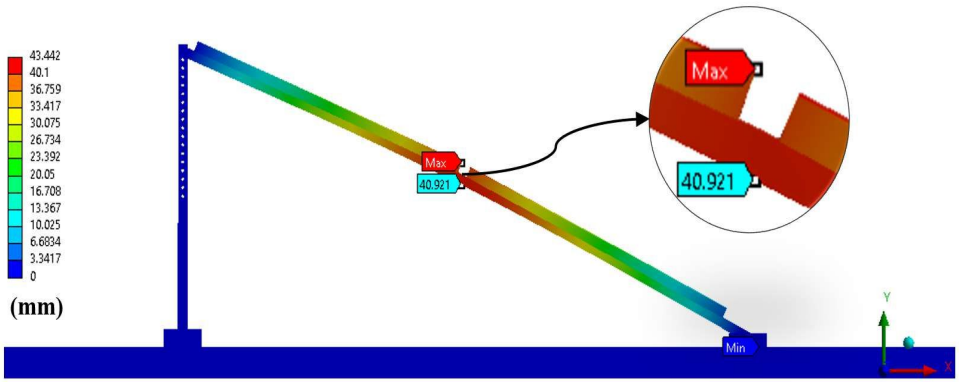

FIGURE 4.40: Maximum deformation from computational analysis at 120km/h wind velocity

Hence again, the deflection result obtained from the analytical method validates the computational analysis.

Chapter 5

Conclusion and Future Works

In this study, it is concluded that the solar PV mounting structures installed in Pakistan do not meet the requirements of the Pakistani building code. The 14 gauge structure is being installed on a large scale in Pakistan, and by computational analysis, it was concluded that the structure is not safe at all and exceeds the yield strength at 79 km/h wind velocity. The 16 gauge structure deforms at 75 km/h wind velocity. The main support bears the whole load of the solar PV mounting structure because solar panels are bolted to the main support. The 2^{nd} and 3^{rd} 6mm bolts of 14 and 16 gauge solar PV mounting structure that holds the solar panels also deform when subjected to high wind velocity. This study addresses the problem with standard rooftop solar PV mounting structures, which are not safe to install. A 12 gauge structure with only necessary punch holes will resolve the wind issue. 12 gauge structure deforms approximately at 89 km/h and does not fracture at 120 km/h. whereas the 14 gauge structure that is being installed in Pakistan deforms at 79 km/h and fails at 120 km/h. The concerned authorities are not actively participating in efforts to eradicate these issues, which may result in disaster.

It has been observed that the solar PV mounting structures were damaged where more than 450 W-rated solar PV modules were installed on the rooftop. Most of the damaged solar PV mounting structures were installed with 530W to 550 W power ratings. The relevant authorities should allow solar PV modules with less area and more power that would bear the recommended wind load. For future

installations, the relevant government authorities should take strict action against those who are installing the solar panels on poorly fabricated, low gauge steel structures and impose a heavy penalty. As these mounting structures are installed in Gigawatts (GW), the wind cutter sheets should be placed behind the mounting structures to minimise the risk of failure. The solar PV mounting structure should be designed and installed according to an international standard approved by the American Society of Civil Engineers (ASCE).

Bibliography

[1] N. Alrikabi, "Renewable energy types," *Journal of Clean Energy Technologies*, vol. 2, no. 1, pp. 61–64, 2014.

[2] A. Tomar, L. Jain, and P. Batra, "Solar energy-finding new ways," *International Journal of Research*, vol. 1, no. 4, 2013.

[3] S. Mekhilef, R. Saidur, and A. Safari, "A review on solar energy use in industries," *Renewable and sustainable energy reviews*, vol. 15, no. 4, pp. 1777–1790, 2011.

[4] S. Adnan, A. Hayat Khan, S. Haider, and R. Mahmood, "Solar energy potential in pakistan," *Journal of renewable and Sustainable Energy*, vol. 4, no. 3, p. 032701, 2012.

[5] M. M. Rafique, S. Rehman, and L. M. Alhems, "Assessment of solar energy potential and its deployment for cleaner production in pakistan," *Journal of Mechanical Science and Technology*, vol. 34, pp. 3437–3443, 2020.

[6] F. U. H. Faiz, R. Shakoor, A. Raheem, F. Umer, N. Rasheed, and M. Farhan, "Modeling and analysis of 3 mw solar photovoltaic plant using pvsyst at islamia university of bahawalpur, pakistan," *International Journal of Photoenergy*, vol. 2021, pp. 1–14, 2021.

[7] M. Shahid, S. A. Kalhoro, D. Ara, N. Bano, and R. Perween, "Wind and solar energy potentials around southern sindh & southern baluchistan provinces, especially karachi of pakistan," *3c Tecnología: glosas de innovación aplicadas a la pyme*, vol. 8, no. 1, pp. 116–141, 2019.

[8] E. A. Franklin, "Mounting your solar photovoltaic (pv) system," pp. 1–4, 2017.

[9] A. Ashfaq and A. Ianakiev, "Features of fully integrated renewable energy atlas for pakistan; wind, solar and cooling," *Renewable and Sustainable Energy Reviews*, vol. 97, pp. 14–27, 2018.

[10] R. M. C. Lahore, "Historical Events." **Online:** https://rmcpunjab.pmd.gov.pk/P-historical.html, 2015.

[11] A. Rayyan, "Wind effect on solar panels," *AE Solar*, Sep 2022.

[12] NEPRA, "State of industry report," p. 20, 2021.

[13] M. Kamran, "Current status and future success of renewable energy in pakistan," *Renewable and Sustainable Energy Reviews*, vol. 82, pp. 609–617, 2018.

[14] A. Sadiqa, A. Gulagi, and C. Breyer, "Energy transition roadmap towards 100% renewable energy and role of storage technologies for pakistan by 2050," *Energy*, vol. 147, pp. 518–533, 2018.

[15] C. Roecker, "New mounting systems for pv on buildings," in *The 2nd World Solar Electric Buildings Conference*, pp. 1–3, 2000.

[16] J. Westin, "Wind actions on flat-roof-mounted photovoltaic panels," *Avdelningen for Konstruktionsteknik Lund's Tekniska Hogskola Lunds University*, pp. 1–3, 2011.

[17] W. Kessler, "Comparing energy payback and simple payback period for solar photovoltaic systems," in *E3S web of conferences*, vol. 22, p. 00080, EDP Sciences, 2017.

[18] H. Alrawashdeh and T. Stathopoulos, "Experimental investigation of the wind loading on solar panels: effects of clearance off flat roofs," *Journal of Structural Engineering*, vol. 148, no. 12, p. 04022202, 2022.

[19] J. Li, L. Tong, J. Wu, and Y. Pan, "Numerical investigation of wind influences on photovoltaic arrays mounted on roof," *Engineering Applications of Computational Fluid Mechanics*, vol. 13, no. 1, pp. 905–922, 2019.

[20] H. Alrawashdeh and T. Stathopoulos, "Critical considerations for modeling roof-mounted solar panels in atmospheric wind tunnels," *And Resilience*, p. 3, 2022.

[21] T. Stathopoulos and H. Alrawashdeh, "Wind loads on buildings: A code of practice perspective," *Journal of Wind Engineering and Industrial Aerodynamics*, vol. 206, pp. 10–38, 2020.

[22] Z. Zhang and T. Stathopoulos, "Wind loads on solar panels mounted on flat rooftops: Progress and limitations," in *Proceedings of the 2014 World Congress on Advance in Civil, Environmental, and Materials Research (ACEM 14), Busan, Korea*, pp. 59–69, 2014.

[23] G. A. Kopp, S. Farquhar, and M. J. Morrison, "Aerodynamic mechanisms for wind loads on tilted, roof-mounted, solar arrays," *Journal of Wind Engineering and Industrial Aerodynamics*, vol. 111, pp. 40–52, 2012.

[24] R. N. Pratt and G. A. Kopp, "Velocity measurements around low-profile, tilted, solar arrays mounted on large flat-roofs, for wall normal wind directions," *Journal of Wind Engineering and Industrial Aerodynamics*, vol. 123, pp. 226–238, 2013.

[25] S. E. Stenabaugh, Y. Iida, G. A. Kopp, and P. Karava, "Wind loads on photovoltaic arrays mounted parallel to sloped roofs on low-rise buildings," *Journal of Wind Engineering and Industrial Aerodynamics*, vol. 139, pp. 16–26, 2015.

[26] S. E. Stenabaugh, *Design Wind Loads for Solar Modules Mounted Parallel to the Roof of a Low-rise Building*. The University of Western Ontario (Canada), 2015.

[27] M. Sayana and M. Vijayan, "Buckling analysis of solar panel supporting structures," *International Journal of Civil Engineering*, vol. 3, pp. 31–39, 2016.

[28] NEPRA, "State of industry report," pp. 20–23, 2022.

[29] L. G. G. B. Ferreira, A. J. Alves, and J. L. Domingos, "Analysis of wind loading on photovoltaic panels mounting brackets," in *2018 IEEE International Conference on Environment and Electrical Engineering and 2018 IEEE Industrial and Commercial Power Systems Europe (EEEIC/I&CPS Europe)*, pp. 1–5, IEEE, 2018.

[30] E. Zuhal and S. Marangozoglu, "New design for solar panel tracking system based on solar calculations," in *2018 IEEE 61st International Midwest Symposium on Circuits and Systems (MWSCAS)*, pp. 2–3, IEEE, 2018.

[31] M. Boxwell, *Solar electricity handbook: A simple, practical guide to solar energy-designing and installing photovoltaic solar electric systems*, vol. 3. Greenstream publishing, 2010.

[32] K. Vidyanandan, "An overview of factors affecting the performance of solar pv systems," *Energy Scan*, vol. 27, no. 28, p. 216, 2017.

[33] B. V. Chikate, Y. Sadawarte, and B. Sewagram, "The factors affecting the performance of solar cell," *International journal of computer applications*, vol. 1, no. 1, pp. 0975–8887, 2015.

[34] M. Fouada, A. S. Lamia, and E. Morgan, "An integrated review of factors influencing the performance of photovoltaic panels," *Renew Sustain Energy Rev*, vol. 80, pp. 1499–1511, 2017.

[35] Y. Suchikova, "Provision of environmental safety through the use of porous semiconductors for solar energy sector," *Eastern-European Journal of Enterprise Technologies*, vol. 6, no. 5, pp. 26–33, 2016.

[36] G. G. Çelik and O. Celik, "A case study of structural failure of mounting systems for solar panels from south-eastern turkey: an investigation of design parameters under extreme weather events," 2019.

[37] J. Cao, A. Yoshida, P. K. Saha, and Y. Tamura, "Wind loading characteristics of solar arrays mounted on flat roofs," *Journal of Wind Engineering and Industrial Aerodynamics*, vol. 123, pp. 214–225, 2013.

[38] A. Abiola-Ogedengbe, H. Hangan, and K. Siddiqui, "Experimental investigation of wind effects on a standalone photovoltaic (pv) module," *Renewable Energy*, vol. 78, pp. 657–665, 2015.

[39] S. Li, D. Mao, S. Li, Q. Wang, Q. Yang, Y. Chen, and S. Zhou, "Wind load characteristics of photovoltaic panel arrays mounted on flat roof," *Engineering Research Express*, vol. 4, no. 1, p. 015027, 2022.

[40] H. Alrawashdeh and T. Stathopoulos, "Wind loads on solar panels mounted on flat roofs: Effect of geometric scale," *Journal of Wind Engineering and Industrial Aerodynamics*, vol. 206, p. 104339, 2020.

[41] A. C. SAuCA, T. MilCHiș, and F.-Z. Gobesz, "Wind loading on solar panels," *Műszaki Tudományos Közlemények*, vol. 10, no. 1, pp. 73–78, 2019.

[42] G. Baetu, C.-E. Teleman, E. Axinte, and V.-E. Rosca, "Numerical simulation of wind action on a solar panels array for different wind directions," *Buletinul Institutului Politehnic Din Lasi. Sectia Constructii, Arhitectura*, vol. 59, no. 4, p. 9, 2013.

[43] T. Stathopoulos, I. Zisis, and E. Xypnitou, "Local and overall wind pressure and force coefficients for solar panels," *Journal of wind engineering and industrial aerodynamics*, vol. 125, pp. 195–206, 2014.

[44] C. A. J. Pantua, J. K. Calautit, and Y. Wu, "A fluid-structure interaction (fsi) and energy generation modelling for roof mounted renewable energy installations in buildings for extreme weather and typhoon resilience," *Renewable Energy*, vol. 160, pp. 770–787, 2020.

[45] A. Abiola-Ogedengbe, *Experimental investigation of wind effect on solar panels*. The University of Western Ontario (Canada), 2013.

[46] W. P. Warsido, G. T. Bitsuamlak, J. Barata, and A. G. Chowdhury, "Influence of spacing parameters on the wind loading of solar array," *Journal of fluids and structures*, vol. 48, pp. 295–315, 2014.

[47] M. A. Sharif, "Numerical simulation of a ground-supported solar panel pv array subjected to periodic flow," *NTU Journal of Renewable Energy*, vol. 1, no. 1, pp. 50–55, 2021.

[48] R. Abdollahi, "Impact of wind on strength and deformation of solar photovoltaic modules," *Environmental Science and Pollution Research*, vol. 28, no. 17, pp. 21589–21598, 2021.

[49] N. D. Jackson and T. Gunda, "Evaluation of extreme weather impacts on utility-scale photovoltaic plant performance in the united states," *Applied Energy*, vol. 302, p. 117508, 2021.

[50] O. Yemenici and M. O. Aksoy, "An experimental and numerical study of wind effects on a ground-mounted solar panel at different panel tilt angles and wind directions," *Journal of Wind Engineering and Industrial Aerodynamics*, vol. 213, p. 104630, 2021.

[51] I. I. Sheikh, "Numerical investigation of drag and lift coefficient on a fixed tilt ground mounted photovoltaic module system over inclined terrain," *Int J Fluids Eng*, vol. 11, pp. 37–49, 2019.

[52] M. Waqas, D. A. Khan, W. Ahmad, A. Rouf, Rozeena Aslam, and S. Jamal, "Numerical investigation of impact of various wind loads on the structural stability and strength of solar panel supporting structure," pp. 70–84, 2020.

[53] M. Waqas, A. Khan, W. Ahmad, A. Rouf, R. Aslam, and S. Jamal, "Numerical investigation of impact of various wind loads on the structural stability and strength of solar panel supporting structure," vol. Volume 3, pp. 70–84, 05 2020.

[54] R. M. Gul, M. A. Kamran, F. U. Zafar, and M. Noman, "The impact of static wind load on the mechanical integrity of different commercially available mono-crystalline photovoltaic modules," *Engineering Reports*, vol. 2, no. 12, p. e12276, 2020.

[55] R. M. Gul, F. U. Zafar, M. A. Kamran, and M. Noman, "Effect of wind load on performance of photovoltaic (pv) modules available in pakistan," *Mehran University Research Journal Of Engineering & Technology*, vol. 40, no. 4, pp. 860–866, 2021.

[56] N. Shabbir, M. Usman, M. Jawad, M. H. Zafar, M. N. Iqbal, and L. Kütt, "Economic analysis and impact on national grid by domestic photovoltaic system installations in pakistan," *Renewable Energy*, vol. 153, pp. 509–521, 2020.

[57] M. Uzair, S. U. Hasan Kazmi, M. Uzair Yousuf, and A. Ali Zaidi, "Optimized performance of pv panels and site selection for a solar park in pakistan," *Transactions of the Canadian Society for Mechanical Engineering*, vol. 46, no. 2, pp. 412–426, 2022.

[58] L. L. LONGi Green Energy Technology Co., "Longi solar hi-mo5 hph 525-550w," 2020.

[59] A. Rezaeiha, H. Montazeri, and B. Blocken, "On the accuracy of turbulence models for cfd simulations of vertical axis wind turbines," *Energy*, vol. 180, pp. 838–857, 2019.

[60] F. R. Menter, "Two-equation eddy-viscosity turbulence models for engineering applications," *AIAA Journal*, vol. 32, pp. 1598–1605, Aug. 1994.

[61] K.-K. Chong, T.-K. Yew, C.-W. Wong, M.-H. Tan, W.-C. Tan, B.-H. Lim, and A.-C. Lai, "Prototype of dense-array concentrator photovoltaic system using non-imaging dish concentrators and cross compound parabolic concentrator," *Energy Procedia*, vol. 105, pp. 131–136, May 2017.

[62] D. C. Wilcox, "Formulation of the k-w turbulence model revisited," *AIAA Journal*, vol. 46, pp. 2823–2838, Nov. 2008.

[63] L. C. Team *et al.*, "Tips & tricks: Inflation layer meshing in ansys," *LEAP Aust. CFD blog [Online]. Available: http://www. computationalfluiddynamics. com. au/tips-tricks-inflation-layer-meshingin-ansys/.[Accessed: 25-Apr-2013]*, 2012.

[64] C. M. Jubayer and H. Hangan, "Numerical simulation of wind effects on a stand-alone ground mounted photovoltaic (pv) system," *Journal of Wind Engineering and Industrial Aerodynamics*, vol. 134, pp. 56–64, 2014.

[65] G. P. Reina and G. De Stefano, "Computational evaluation of wind loads on sun-tracking ground-mounted photovoltaic panel arrays," *Journal of Wind engineering and industrial Aerodynamics*, vol. 170, pp. 283–293, 2017.

[66] C. M. Jubayer and H. Hangan, "A numerical approach to the investigation of wind loading on an array of ground mounted solar photovoltaic (pv) panels,"

Journal of Wind Engineering and Industrial Aerodynamics, vol. 153, pp. 60–70, 2016.

[67] M. Shademan, R. Barron, R. Balachandar, and H. Hangan, "Numerical simulation of wind loading on ground-mounted solar panels at different flow configurations," *Canadian Journal of Civil Engineering*, vol. 41, no. 8, pp. 728–738, 2014.

[68] A. Fage and F. Johansen, "On the flow of air behind an inclined flat plate of infinite span," *Proceedings of the Royal Society of London. Series A, Containing Papers of a Mathematical and Physical Character*, vol. 116, no. 773, pp. 170–197, 1927.

[69] F. L. Water, "The beaufort wind scale," 2005.

[70] M. of Housing & Works (MOHW) Government of Pakistan (GOP), *Building Code of Pakistan - Seismic Provisions*, p. 44. Pakistan Engineering Council (PEC), 2007.

[71] R. C. Hibbeler and K. B. Yap, *Bending*, p. 317. Pearson Education, 10th ed., 2017.